ESD-TR-90-143

Technical Report
908

LWIR Stellar Calibration: Infrared Spectral Curves for 30 Standard Stars

C.W. Engelke

10 April 1991

Lincoln Laboratory

MASSACHUSETTS INSTITUTE OF TECHNOLOGY

LEXINGTON, MASSACHUSETTS

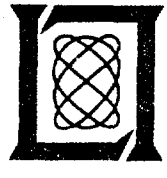

Prepared for the Department of the Army under Air Force Contract F19628-90-C-0002.

This report is based on studies performed at Lincoln Laboratory, a center for research operated by Massachusetts Institute of Technology. The work was sponsored by the U.S. Army Strategic Defense Command, Department of the Army under Air Force Contract F19628-90-C-0002.

The ESD Public Affairs Office has reviewed this report, and it is releasable to the National Technical Information Service, where it will be available to the general public, including foreign nationals.

This technical report has been reviewed and is approved for publication.

FOR THE COMMANDER

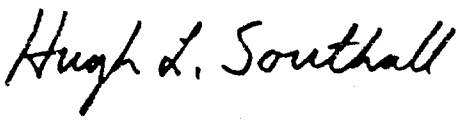

Hugh L. Southall, Lt. Col., USAF
Chief, ESD Lincoln Laboratory Project Office

MASSACHUSETTS INSTITUTE OF TECHNOLOGY
LINCOLN LABORATORY

LWIR STELLAR CALIBRATION: INFRARED SPECTRAL CURVES FOR 30 STANDARD STARS

C.W. ENGELKE
Group 51

TECHNICAL REPORT 908

10 APRIL 1991

LEXINGTON MASSACHUSETTS

ABSTRACT

Best estimate spectral energy distributions are created for approximately 30 stars by fitting theoretically expected spectral curves to the available empirical flux data on the stars at a variety of wavelengths. The curves can be integrated over the band response functions for a given sensor in order to produce broadband power predictions against which to calibrate.

TABLE OF CONTENTS

TABLE OF CONTENTS (Continued)

LIST OF ILLUSTRATIONS

LIST OF TABLES

LIST OF TABLES (Continued)

1. OVERVIEW

1.1 MOTIVATION

It is desirable to monitor and improve the calibration of infrared sensors using observations on well-known stellar sources. Such universally accessible standard sources can also ease comparison between different instruments. These goals can be met with minimal confusion if estimated spectral distributions of these stars are agreed upon by many researchers.

With this in view, the present work examines the available astronomical observations and uses these and stellar atmosphere theory to estimate the continuous spectral curves for about 30 stars in the wavelength range 2 μm < λ < 100 μm.

1.2 USE

Those interested in producing broadband power predictions for a sensor must integrate the continuous spectral curves over their particular bands. This report documents the origin and nature of these spectral curves and provides the information necessary to reproduce them. Section 2 reviews the available infrared data on stars of interest; Section 3 derives a two-parameter function describing theoretically expected spectra for stars of differing temperature and apparent angular size; Section 4 describes the process of fitting this function to the data and checking its plausibility as a correct representation of the spectra; and Section 5 and Appendix B contain the information needed to generate the continuous spectral distributions for individual members of a list of stars. In Section 5, Tables 32 to 35 list the parameters to be used in the function for specific stars. Appendix B contains information on CO bands for each, shows whether a CO absorption band in the stellar spectrum affects the result of an integration over some band of interest, and if so, how to modify the smooth spectrum to account for this.

1.3 SUMMARY

1.3.1 Stars

Only stars with smooth infrared spectra showing no evidence of excess emission from circumstellar dust clouds are fit directly. These have predictable spectral shapes. Measurements comparing stars of this sort also have the property that ratios of inband flux depend very little on the exact shape of the passband used and vary only gradually with changes in the effective wavelength of the observations.

1.3.2 Data

Relative measurements (i.e., $star_1 = b$; $star_2 = 1.2\ b$; etc., where we do not know b) are collected for more than 30 stars in 5 available wavebands. Measurements of absolute flux performed on a smaller subset of these stars are collected and reviewed. The combination of both these sets of measurements then allows the construction of a set of discrete flux values at a variety of wavelengths for each star.

1.3.3 Fitting Function

A simple two-parameter function is developed. The starting point is an analytic approximation to the semiempirical solar spectrum of Vernazza, et al. [1]. Theoretical arguments are used to predict how this shape would change for stars of lower effective temperatures. The final generalized spectral function of the parameters T_{eff} (the effective temperature of a star) and Ω is written as a modified Planck function:

$$\phi\lambda\left[\Omega, T_{eff}\right] = \Omega\, B\left[T\left(\lambda, T_{eff}\right), \lambda\right] = \frac{11910\Omega}{\lambda^5\left(\exp\left(\frac{14388}{\lambda T\left(\lambda, T_{eff}\right)}\right) - 1\right)}$$

where

$$T\left(T_{eff}, \lambda\right) = 0.738\lambda T_{eff}\left(1 + \frac{79450}{\lambda T_{eff}}\right)^{0.182}$$

defines the brightness temperature as a function of wavelength for a star with a given T_{eff} and Ω is the solid angle subtended by the star. The spectral flux is given in $Wcm^{-2}\,\mu^{-1}$; $T(\lambda, 5770\ K)$ gives the "whole disk" solar brightness temperatures from the model M in [1].

The assumptions made about stellar opacity in the process of deriving this function hold only for $1.6\ \mu m < \lambda < 100\ \mu m$, and $3500\ K < T_{eff} < 6000\ K$. The function can, however, be used to fit hotter stars if one ceases to consider T_{eff} and Ω to have their customary physical interpretation and regards them merely as mathematical conveniences (see Section 4, Table 30).

1.3.4 Quality of Fit

For stars with effective temperatures within the function's range of validity, values of T_{eff} and Ω found by optimizing the fit to the infrared data agree very well with values determined by independent means (to $\leq 5\%$ in most cases). This accuracy is high enough that the method may someday be of interest as a means of determining effective temperatures and angular diameters for stars. The excellent agreement provides supporting evidence that real stellar spectra behave as the fitting function supposes (or at least that all observations are consistent with that supposition).

The reduced χ^2 values calculated for the fits average about 0.3. Average residuals (data point minus fit) are about 3% for all stars. No evidence of systematic differences in the fits from one class of stars to another is apparent.

The overall calibration agrees well with previous calibrations. It is virtually identical to that of the infrared astronomical satellite (IRAS) at 12, 25, and 60 μm (Beichman et al. [2]), except for a 1.5%

upward correction. It also agrees within 1.5% with those of shorter wavelengths (Campins et al. [3]). The 20-μm calibration of Rieke, et al. [4] differs somewhat from both Campins et al. [3] and IRAS, but all agree within the stated uncertainties.

The infrared spectral distributions produced in this work, therefore, can be thought of as continuous curves smoothly merging the most widely used calibrations at discrete wavelengths. These continuous curves have the advantage, however, that any passband can use them and that the fitting procedure averages out random errors as all the discrete measurements on a star (at different wavelengths), in effect, enter into one weighted average.

Except for those stars with intrinsic variability, the uncertainty in flux values obtained from our curves should be 3% below 12 μm (with the exception of the regions containing CO bands where uncertainties rise to perhaps 8%), and about 0.25 λ% above 12 μm (i.e., a linearly growing uncertainty). It should be noted, however, that this uncertainty estimate is based on a priori assumptions about the quality of the data and validity of the fitting function. The actual residuals and comparisons of stellar band ratios with IRAS band ratios of asteroids are consistent with an uncertainty of 3% all the way out to 60 μm.

2. STAR DATA

2.1 CHOICE OF STARS

The stars reported in this document were chosen from lists that were included in Chambers and Bagnuolo [5] and Rieke [6] and recommended as standard calibrators. (See Appendix A for the star selection portion of the Rieke report.)

Rieke groups the recommended stars into two lists by criteria of brightness, predictability, and sky coverage. His primary list includes mostly main-sequence (Class V) and giant (Class III) stars of spectral types A, F, G, and K. His secondary list contains cooler, and some slightly variable, giant stars of type M. Supergiants (Class I) are rejected as standard stars because of more extreme variability and hard-to-model spectral shapes characterized by the strong, lumpy, excess emission of circumstellar dust. These spectral shapes differ even among stars of the same spectral type (with almost a 30% difference in the IRAS 12- to 25-μm flux ratios measured for α Ori and μ Cep even though both stars are classified as M2-I supergiants). Rieke does suggest that a program devoted to measuring the spectral shapes of individual supergiants and monitoring their variations against members of a network of primary standard stars would make them valuable as long wavelength calibrators because of their great brightness.

In this work, Class III-V stars are emphasized; however, the fluxes for several bright Class I supergiants (α Ori, α Her, α Sco, and μ Cep) are also evaluated in Appendix A in an indirect manner (by normalizing rough spectra to give integrated IRAS flux values correctly relative to the integrated IRAS fluxes of the more reliably modeled stars on the primary list).

Rieke estimates the infrared variability of several Class III stars that appeared in his secondary list; these spectra are modeled in this report. The values given in Table 1 assume that infrared variability is about 1/3 the measured visible light variability.

TABLE 1

Expected Infrared Variability of Selected Stars

Star	Type	Infrared Variability (%)
γ Dra	K5 III	2.5
α Cet	M1.5 III	2
μ Gem	M3 III	9
σ Lib	M3 III	5
β Gru	M5 III	11
β Peg	M2.5 II	16

The band ratios for these stars should remain relatively constant during changes in flux. The absolute flux values derived in this work, however, must have the expected variation added as an additional uncertainty.

2.2 RELATIVE PHOTOMETRY: 1.6 TO 60 μm

Astronomical measurements are typically relative. Comparison of the instrument response for an object of interest and its response for a nearby stellar standard (after applying an empirically determined correction for the difference in airmass along the two lines of sight) allows new observations to be introduced into a system of relative magnitudes used by the observer. The magnitude scale is logarithmic and designed so that, apart from a constant offset and unavoidable random errors, all researchers whose instruments are linear should get the same results for the same set of stars. In waveband i a magnitude scale would be defined:

$$m_i = -2.5 \log(P_i) + C_i,$$

where P_i essentially corresponds to the instrument response for a star at a given elevation on a given night. (Note: The brighter the object, the more negative the magnitude.)

A set of several stars and astronomical sources would typically be observed on a given night and their relative brightness represented using a magnitude scale. The constant C_i would then be adjusted to bring the magnitudes of previously known members of the set into line with their previously assigned magnitudes. Any new observations are now part of the same magnitude system. In addition, the random errors in the magnitudes of the repeated stars can be reduced by averaging in the new observations.

When a constant C_i has been chosen, it may be thought of as 2.5 log(Z_i), where Z_i is a new constant essentially describing the instrument response (corrected for the atmosphere) to an object with zero magnitude (i.e., it defines which intensity level is considered zero magnitude).

Relating instrument response to actual spectral flux units above the atmosphere is usually attempted by estimating the expected flux of one or more of the standard stars at the measured wavelength. For infrared photometry this estimate is often arrived at indirectly using theoretical spectral curves and flux measurements of the standards in the visible. Thus, the flux determination is not an integral part of the infrared measurements themselves, and unless two researchers have adopted their estimates from the same third source, their published flux values may disagree even though their actual relative measurements agree closely. For now, only a best estimate of the relative fluxes of the standard stars will be made, so all attempts at absolute calibrations made by the researchers cited will be ignored until a later section.

Tables 2 through 19 show the collected relative photometry of different researchers. Each set of magnitudes has had its constant offset adjusted separately so that all agree as well as possible with each other. The actual numerical value of the offset adopted in each waveband should at this point be considered arbitrary (and attention paid only to differences). However, for purposes of later reference the end results of the present work have been used to set the constants so that the zero magnitude flux in

each waveband is defined by a 10,000 K blackbody curve normalized to give magnitudes agreeing with those of IRAS at long wavelengths:

$$\text{zero magnitude} = \frac{1.89 \times 10^{-12}}{\lambda^5 (\exp[1.44/\lambda] - 1)}$$

(The uncertainty in this definition of the absolute scale is about 3% below 12 μm and 0.25 λμm% for λ > 12 μm). This absolute calibration is not based on the original papers and will be derived in subsequent chapters.

The effective wavelength attributed to the photometry in Tables 2 through 19 is an approximate average for all the researchers' wavebands. For stars on Rieke's lists of standards, the relative magnitudes change slowly with observing wavelength; as long as two researchers have used roughly corresponding wavebands, the exact effective wavelengths need not be the same to allow valid comparison.

2.3 NOTE ON SOURCES

Uncertainties were taken directly from the appropriate reference when available. If none was listed (or only a range indicated), a value was deduced by comparing the magnitudes of common stars with those obtained from the average of references for which reliable uncertainties were given.

The data sets included in the following tables are believed to be independent of each other. Johnson [10] is the source of the 2.2- and 3.5-μm photometry in Campins et al. [3] and Noguchi et al. [22]; thus these are not included separately. In the case of Gehrz [13], Gehrz and Woolf [12], and Gehrz, Hackwell, and Jones [14], it is not entirely clear how the photometry in any one study is related to that in the others. For this reason they are combined (averaging where differences existed) into one set of magnitudes in Tables 3 through 9 and 12 through 17.

TABLE 2

1.6-μm Relative Photometry

Star	Spectral Type	Engels et al. [7]	Thomas et al. [8]
α CMa	A1 V	−1.43 ±0.02	−1.45 ±0.02
α CMi	F5 IV	−0.68 ±0.02	
α Car	F0 Ib	−1.34 ±0.02	−1.35 ±0.02
α Cen A	G2 V	−1.46 ±0.05	−1.50 ±0.02
α Cen B	KI V	−0.57 ±0.05	−0.58 ±0.02
α Lyr	A0 V		−0.02 ±0.02

Region of second harmonic of CO absorption in cool stars. Entries for stars having no significant CO absorptions only.

TABLE 3

2.2-μm Relative Photometry of Nonvariable Stars (Class V-III)

Star	Spectral Type	Johnson et al. [10]	Engels et al. [7]	Thomas et al. [8]	Bergeat et al. [11]	Gehrz et al. [12-14]	Persi et al. [15]	Low and Rieke [16]	Frogel et al. [9]
α Boo	K2 III	−3.07		−3.06	−3.09	−3.06		−3.06	
		±0.02		±0.02	±0.03	±0.02		±0.04	
α Tau	K5 III	−2.88	−2.84	−2.86	−2.90	−2.88	−2.94	−2.96	
		±0.02	±0.02	±0.04	±0.03	±0.02	±0.05	±0.04	
α Aur	G8 III	−1.85			−1.82	−1.87	−1.83	−1.85	
		±0.03			±0.03	±0.02	±0.05	±0.04	
β Gem	K0 III	−1.16			−1.13	−1.16	−1.12		
		±0.02			±0.03	±0.03	±0.05		
α Hya	K4 III	−1.26	−1.30	−1.27					
		±0.03	±0.02	±0.01					
α Ari	K2 III	−0.70				−0.67		−0.72	
		±0.02				±0.03		±0.04	
γ Aql	K3 II	−0.66	−0.63		−0.68			−0.66	
		±0.02	±0.02		±0.03			±0.04	
α CMa	A1 V	−1.37	−1.45	−1.46		−1.46			
		±0.02	±0.02	±0.02		±0.03			
α CMi	F5 IV	−0.71	−0.75					−0.71	
		±0.02	±0.02	±0.04					
α Lyr	A0 V	−0.04				−0.04			−0.05
		±0.02				±0.03			±0.02
α Cen A	G2 V		−1.57	−1.57					
			±0.05	±0.02					
α Cen B	K1 V		−0.69	−0.66					
			±0.05	±0.02					
α UMa	K0 III								
β And	M0 III	−1.90			−1.92	−1.91		−1.92	
		±0.05			±0.03	±0.02		±0.04	
α Cet	M2 III	−1.74		−1.75					
		±0.04		±0.03					
γ And	K3 II	−0.88							
		±0.03							
μ UMa	M0 III	−0.92				−0.89			−0.89
		±0.03				±0.02			±0.02

TABLE 4

2.2-μm Photometry of Mildly Variable Stars (Class III-II)

Star	Spectral Type	Johnson et al. [10]	Engels et al. [7]	Thomas et al. [8]	Bergeat et al. [11]	Gehrz et al. [12-14]	Low and Rieke [16]	Frogel et al. [9]
γ Dra	K5 III	−1.40				−1.37	−1.36	
		±0.02				±0.03	±0.04	
β Gru	M3 II			−3.28				
				±0.02				
β Peg	M2.5	−2.28			−2.30	−2.28		
	II-III	±0.02			±0.03	±0.02		
γ Cru	M3 II		−3.13	−3.22				
			±0.02	±0.02				
ρ Per	M4	−2.00						
	II-III	±0.02						
μ Gem	M3 III	−1.96		−1.98				
		±0.02		±0.03				
2 Cen	M4 III	−1.71		−1.74				
		±0.02		±0.02				
η Gem	M3 III	−1.38						
		±0.05						
α Car	F0 I	−1.37	−1.40	−1.41				
		±0.05	±0.02	±0.02				
δ Vir	M3 III	−1.32		−1.27				−1.30
		±0.02		±0.02				±0.02
λ Vel	K5	−1.64	−1.62	−1.62				
	I-II	±0.03	±0.02	±0.02				
σ Lib	M4 III	−1.47		−1.49				
		±0.02		±0.02				
δ2 Cru	M3 III			−0.98				
				±0.02				

TABLE 5

2.2-μm Photometry of Variable Stars with Circumstellar Dust (Class I)

Star	Spectral Type	Johnson et al. [10]	Thomas et al. [8]	Gehrz et al. [12-14]
α Ori	M2 I	–4.19	–4.23	–4.37
		±0.05	±0.02	±0.03
μ Cep	M2 I	–1.82		–1.97
		±0.05		±0.03
α Her	M5	–3.58	–3.54	–3.57
	Ib-II	±0.05	±0.03	±0.03
α Sco	M1 I	–3.87	–3.98	
		±0.05	±0.02	

TABLE 6

3.5-μm Photometry of Stable Stars (Class V-III)

Star	Spectral Type	Johnson et al. [10]	Persi et al. [15]	Sinton et al. [17]	Engels et al. [7]	Thomas et al. [8]	Gerhz et al. [12-14]	Low and Rieke [16]
α Boo	K2 III	−3.15		−3.12		−3.10	−3.13	−3.14
		±0.02		±0.02		±0.02	±0.02	±0.05
α Tau	K5 III	−3.00	−3.03	−2.97	−2.93	−2.98	−2.99	−3.00
		±0.02	±0.05	±0.02	±0.03	±0.03	±0.02	±0.05
α Aur	G8 III	−1.88	−1.89	−1.91			−1.96	−1.86
		±0.03	±0.05	±0.02			±0.02	±0.05
β Gem	K0 III	−1.18	−1.18				−1.20	
		±0.02	±0.05				±0.02	
α Ari	K2 III	−0.75					−0.78	−0.75
		±0.02					±0.04	±0.05
α Hya	K4 III	−1.30			−1.40	−1.35		−1.36
		±0.05			±0.03	±0.02		±0.05
γ Aql	K3 II	−0.78			−0.74			−0.80
		±0.05			±0.03			±0.05
α CMa	A1 V	−1.30			−1.43	−1.44	−1.43	
		±0.05			±0.03	±0.02	±0.02	
α CMi	F5 IV	−0.70			−0.76		−0.73	−0.67
		±0.03			±0.03		±0.03	±0.05
α Lyr	A0 V	−0.04					−0.03	
α Cen A	G2 V				−1.62	−1.55		
					±0.05	±0.02		
α Cen B	K1 V				−0.72	−0.64		
					±0.05	±0.02		
α UMa	K0 II							
β And	M0 III			−2.06			−2.01	−2.10
				±0.02			±0.03	±0.05
α Cet	M2 III					−1.86	−1.84	
						±0.04	±0.03	
γ And	K3 II	−0.89						
		±0.02						
μ UMa	M0 III	−0.98		−1.04			−0.95	
		±0.04		±0.02			±0.03	

TABLE 7

3.5-μm Photometry of Mildly Variable Stars (Class III-II)

Star	Spectral Type	Johnson et al. [10]	Persi et al. [15]	Sinton et al. [17]	Engels et al. [7]	Thomas et al. [8]	Gerhz et al. [12-14]	Low and Rieke [16]
γ Dra	K5 III	−1.51 ±0.02					−1.41 ±0.02	−1.50 ±0.05
β Gru	M3 II	±0.02					−3.41	
β Peg	M2.5 II-III	−2.31 ±0.08		−2.42 ±0.02			−3.41 ±0.05	
γ Cru	M3 II				−3.31 ±0.03	−3.34 ±0.02		
ρ Per	M4 II-III	−2.18 ±0.05					−2.12 ±003	
μ Gem	M3 II!						−2.04 ±0.03	
ζ Cen	M4 III	−1.85 ±0.05				−1.86 ±0.02		
η Gem	M3 III						−1.63 ±0.03	
α Car	F0 I					±0.03	−1.43 ±0.02	−1.41
∂ Vir	M3 III	±0.03	−1.45			±0.03	−1.38 ±0.03	−1.37
λ Vel	K5 I-II					−1.80 ±0.03	−1.76 ±0.02	
σ Lib	M4 III	−1.60 ±0.02				−1.62 ±0.02		
∂2 Gru	M3 III					−1.07 ±0.02		

TABLE 8

3.5-μm Photometry of Stars with Circumstellar Dust (Class I)

Star	Spectral Type	Johnson et al. [10]	Sinton et al. [17]	Thomas et al. [8]	Gerhz et al. [12-14]
α Ori	M2 I	−4.45 ±0.02		−4.46 ±0.02	−4.47 ±0.03
μ Cep	M2 I	−2.06 ±0.02	−2.31 ±0.02		−2.20 ±0.08
α Sco	M1 I	−4.23 ±0.02		−4.23 ±0.02	−4.17 ±0.03
α Her	M5 Ib-II		−3.74 ±0.02	−3.76 ±0.03	−3.68 ±0.03

TABLE 9

4.8-μm Photometry (Class V-I)

Star	Spectral Type	Engels et al. [7]	Thomas et al. [8]	Sinton et al. [17]	Gehrz et al. [12-14]
α CMa	A1 V	−1.42 ±0.03	−1.38 ±0.03	−1.40 ±0.02	−1 40 ±0.02
α CMi	F5 IV	−0.77 ±0.03			−0.65 ±0.05
α Car	F0 I	−1.43 ±0.03	−1.44 ±0.03		
α Cen A	G2 V	−1.50 ±0.05	−1.53 ±0.03		
α Cen B	K1 V	−0.60 ±0.05	−0.60 ±0.03		
α Lyr	A0 V	−0.02 ±0.02	−0.03 ±0.02		

Region of fundamental CO absorption in cool stars.
For stars having no significant CO absorptions only.

TABLE 10

4.8-μm Photometry for Stable Stars with CO Absorptions (Class V-III)

Star	Spectral Type	Engels et al. [7]	Thomas et al. [8]	Sinton et al. [17]	Gerhz and Woolf [12]	Gillet et al. [18]
α Boo	K2 III		−2.96	−2.94	−3.01	−2.98
			±0.02	±0.02	±0.03	±0.05
α Tau	K5 III	−2.75	−2.74	−2.68	−2.67	−2.65
		±0.03	±0.04	±0.02	±0.03	±0.05
α Aur	G8 III				−1.82	−1.73
				±0.02	±0.03	
β Gem	K0 III			−1.11	−1.15	−1.10
				±0.02	±0.03	±0.05
α Ari	K2 III	−0.52				
		±0.05				
α Hya	K4 III	−1.24	−1.13			
	±0.03	±0.03				
γ Aql	K3 II	−0.70				
		±0.03				
β And	M0 III				−1.78	−1.61
				±0.02	±0.03	
α Cet	M2 III			−1.58		−1.42
			±0.03		±0.05	
μ UMa	M0 III			−0.66	−0.65	
				±0.02	±0.03	

TABLE 11

4.8-μm Photometry for Variable Stars (Class III-II)

Star	Spectral Type	Engels et al. [7]	Thomas et al. [8]	Sinton et al. [17]	Gerhz and Woolf [12]	Gillet et al. [18]
γ Dra	K5 III				−1.19 ±0.03	
β Gru	M3 II		−3.10 ±0.03			
β Peg	M2.5 II-III			−2.21 ±0.02	−2.06 ±0.06	−2.02 ±0.05
γ Cru	M3 II	−3.12 ±0.03	−3.08 ±0.03			
ρ Per	M4 II-III					−1.83 ±0.05
μ Gem	M3 III					
2 Cen	M4 III					
η Gem	M3 III				−1.10 ±0.03	−1.27 ±0.05
α Car	F0 I					
∂ Vir	M3 III		−1.12 ±0.03		−1.27 ±0.03	
λ Vel	K5 I-II	−1.49 ±0.03	−1.42 ±0.03			
σ Lib	M4 III		−1.41 ±0.03			
∂2 Gru	M3 III		−0.77 ±0.03			

TABLE 12

11-μm Photometry of Stable Stars
(Class V-III)

Star	Spectral Type	IRAS 12 μ Pointed	IRAS 12 μ Survey	Tokunaga 10.1 μ [19]	Thomas et al. 10 to 11 μ [8]	Gerhz et al. [12-14]	Low and Rieke [16]
α Boo	K2 III	−3.15	−3.22	−3.13	−3.21	−3.17	−3.10
		±0.02	±0.05	±0.02	±0.06	±0.05	±0.08
α Tau	K5 III	−3.00	−3.08	2.99	−2.97	−2.95	−3.04
		±0.02	±0.05	±0.02	±0.08	±0.05	±0.08
α Aur	G8 III	−1.91	−1.90	−1.90		−1.92	−1.93
		±0.02	±0.02	±0.02		±0.06	±0.08
β Gem	K0 III	−1.20	−1.21	−1.20		−1.18	
		±0.02	±0.05	±0.02		±0.05	
α Ari	K2 III		−0.70			−0.70	−0.83
			±0.10			±0.08	±0.08
α Hya	K4 III		−1.47		−1.41		−1.35
			±0.05		±0.04		±0.08
γ Aql	K3 II		−0.68	−0.74			
			±0.05	±0.02			
α CMa	A1 V	−1.36	−1.36	−1.38	−1.45	−1.43	
		±0.02	±0.02	±0.02	±0.06	±0.07	
α CMi	F5 IV	−0.74	−0.72	−0.72		−0.78	
		±0.02	±0.05	±0.02		±0.08	
α Lyr	A0 V	0.02	−0.02	0.04		0.05	
		±0.02	±0.05	±0.02		±0.05	
α Cen A	G2 V		−1.45		−1.68		
			±0.02		±0.05		
α Cen B	K1 V		−0.55		−0.77		
			±0.02		±0.05		
α UMa	K0 III		−0.81			−0.83	
			±0.05			±0.05	
β And	M0 III		−2.12	−2.00		−2.01	−2.13
			±0.10	±0.02		±0.05	±0.08
α Cet	M2 III		−1.90		−1.83	−1.89	
			±0.02		±0.04	±0.08	
γ And	K3 II						
μ UMa	M0 III		−0.98	−0.99		−0.99	
			±0.05	±0.04		±0.05	

TABLE 13

11-μm Photometry for Variable Stars (Class III-II)

Star	Spectral Type	IRAS 12 μ Pointed	IRAS 12 μ Survey	Tokunaga 10.1 μ [19]	Thomas et al. 10 to 11 μ [8]	Gerhz et al. [12-14]	Low and Rieke [16]
γ Dra	K5 III	−1.43	−1.45			−1.42	−1.41
		±0.02	±0.02			±0.06	±0.08
β Cru	M3 II	−3.42	−3.41		−3.54		
		±0.02	±0.05		±0.05		
β Peg	2.5		−2.44	-2.41		−2.49	
	II-III		±0.05	(-2.50)		±0.05	
				±0.02			
γ Cru	M3 II		−3.31		−3.51		
			±0.05		±0.05		
ρ Per	M4		−2.20			−2.15	
	II-III		±0.05			±0.08	
μ Gem	M3 III		−2.18			−2.06	
				±0.10			±0.08
2 Cen	M4 III		−1.99		−2.01		
			±0.10		±0.05		
η Gem	M3 III		−1.67			−1.68	
			±0.02			±0.08	
α Car	F0 I	−1.40	−1.45		−1.61		
		±0.02	±0.05		±0.06		
∂ Vir	M3 III		−1.50		−1.42	−1.55	
			±0.05		±0.08	±0.08	
λ Vel	K5 I-II						
σ Lib	M4 III		−1.73		−1.75		
			±0.05		±0.05		
∂2 Cru	M3 III		−1.08				
			±0.02				

TABLE 14

11-μm Photometry of Stars with Circumstellar Dust (Class I)

Star	Spectral Type	IRAS 12 μ Survey	Tokunaga 10.1 μ [19]	Thomas et al. 10 to 11 μ [8]	Gehrz et al. [12-14]
α Ori	M2 I	−5.15		−5.36	−5.44
		±0.05		±0.05	±0.06
μ Cep	M2 I	−3.75	−3.80		−4.04
		±0.05	±0.02		±0.06
α Sco	M1 I	−4.73		−4.76	−4.74
		±0.05		±0 05	±0.08
α Her	M5 I	−3.92	−3.90	−4.04	−3.99
		±0.02	±0.02	±0.08	±0.06

TABLE 15

22-μm Photometry of Stable Stars
(Class V-II)

Star	Spectral Type	IRAS 25 μ Pointed	IRAS 25 μ Survey	Tokunaga 20 μ [19]	Morrison et al. [20,21]	Gerhz et al. [12-14]	Low and Rieke [16]
α Boo	K2 III	−3.10 ±0.025	−3.06 ±0.03	−3.09 ±0.025	−3.15 ±0.05	−3.11 ±0.08	−3.20 ±0.08
α Tau	K5 III	−2.97 ±0.025	−2.99 ±0.03	−3.05 ±0.025	−3.06 ±0.05	−3.07 ±0.08	−3.02 ±0.06
α Aur	G8 III	−1.91 ±0.025	−1.91 ±0.03	−1.89 ±0.025	−1.88 ±0.05		−1.83 ±0.08
β Gem	K0 III	−1.18 ±0.025	−1.16 ±0.03	−1.17 ±0.025	−1.13 ±0.05	−1.15 ±0.08	
α Ari	K2 III	−0.79 ±0.03					−0.75 ±0.08
α Hya	K4 III	−1.34 ±0.03					
γ Aql	K3 II		−0.78 ±0.03	−0.78 ±0.025			
α CMa	A1 V	−1.32 ±0.025	−1.35 ±0.03	−1.32 ±0.025	−1.32 ±0.05		
α CMi	F5 IV	−0.72 ±0.025	−0.69 ±0.03	−0.69 ±0.025			
α Lyr	A0 V	−0.18 ±0.025	−0.13 ±0.03		−0.14 ±0.05		
α Cen A	G2 V		−1.41 ±0.03				
α Cen B	K1 V		−0.51 ±0.03				
α UMa	K0 III		−0.78 ±0.03				
β And	M0 III			−2.05 ±0.025	−2.09 ±0.05	−2.02 ±0.08	−2.13 ±0.08
α Cet	M2 III		−1.89 ±0.03				
γ And	K3 II						
μ UMa	M0 III		−1.03 ±0.03	−1.04 ±0.03		−0.92 ±0.08	

TABLE 16

22-μm Photometry of Variable Stars (Class III-II)

Star	Spectral Type	IRAS 25 μ Pointed	IRAS 25 μ Survey	Morrison et al. [20,21]	Gerhz et al. [12-14]	Low and Rieke [16]
γ Dra	K5 III	−1.47 ±0.025	−1.47 ±0.03			−1.42 ±0.08
β Gru	M3 II	−3.45 ±0.025	−3.47 0.03			
β Peg	M2.5 II-III		−2.50 ±0.03	−2.56 ±0.025	−2.71 ±0.07	
γ Cru	M3 II		−3.39 ±0.03			
ρ Per	M4 II-III		−2.27 ±0.03			
μ Gem	M3 III		−2.19 ±0.03			
2 Cen	M4 III		−1.94 ±0.03			
η Gem	M3 III		−1.71 ±0.03			
α Car	F0 I	−1.38 ±0.025	−1.41 ±0.03			
∂ Vir	M3 III		−1.54 ±0.03			
λ Vel	K5 I-II					
σ Lib	M4 III		−1.61 ±0.03			
∂2 Gru	M3 III		−1.14 ±0.03			

TABLE 17

22-μm Photometry of Stars with Circumstellar Dust (Class I)

Star	Spectral Type	IRAS 25 μ Survey	Tokunaga [19]	Morrison et al. [20,21]
α Ori	M2 I	-5.63 ±0.03		−5.57 ±0.05
μ Cep	M2 I	−4.49 ±0.03	−4.55 ±0.03	−4.59 ±0.05 (−4.65)
α Sco	M1 I	−4.62 ±0.03		−4.70 ±0.05 (−4.63)
α Her	M5 I	−4.11 ±0.03	−4.13 ±0.04	−4.09 ±0.05

TABLE 18

60-μm Photometry of Stable Stars (Class V-II)

Star	Spectral Type	IRAS 60 μ Pointed	IRAS 60 μ Survey
α Boo	K2 III	-3.11 ±0.03	-3.02 ±0.15
α Tau	K5 III	-2.95 ±0.03	-3.02 ±0.10
α Aur	G8 III	-1.86	-1.85 ±0.10
β Gem	K0 III	-1.17 ±0.03	-1.22 ±0.10
α Ari	K2 III		-0.77 ±0.10
α Hya	K4 III		-1.34 ±0.10
γ Aql	K3 II		-0.66 ±0.10
α CMa	A1 V	-1.27 ±0.03	-1.23 ±0.10
α CMi	F5 IV	-0.70 ±0.03	-0.72 ±0.10
α Lyr	A0 V	-1.95 ±0.03	-1.94 ±0.10
α Cen A + B	G2 V + K1 V		-1.62 ±0.10
α UMa	K0 III		
γ And	M0 III		-2.07 ±0.15
α Cet	M2 III		-2.47 ±0.10
γ And	K3 II		
μ UMa	M0 III		-0.97 ±0.10

TABLE 19

60-μm Photometry of Variable Stars (Class III-II)

Star	Spectral Type	IRAS 60 μ Pointed	IRAS 60 μ Survey
γ Dra	K5 III	−1.48	−1.42
		±0.03	±0.10
β Gru	M3 II	−3.50	−3.52
		±0.04	±0.15
β Peg	M2.5		−2.47
	II-III		±0.10
γ Cru	M3 II		−3.38
			±0.18
ρ Per	M4		−2.33
	II-III		±0.10
μ Gem	M3 III		−2.10
			±0.10
2 Cen	M4 III		−2.02
			±0.10
η Gem	M3 III		−1.70
			±0.15
α Car	F0 I	−1.33	
		±0.04	
∂ Vir	M3 III		−1.42
			±0.15
λ Vel	K5		
	I-II		
σ Lib	M4 III		−1.73
			±0.08
∂2 Gru	M3 III		−1.17
			±0.06

2.4 RELATIVE FLUX LEVELS

For each waveband with available photometry, the weighted average of all the magnitude estimates for each star was taken. The difference of the resulting average magnitude from that of α Boo was then used to calculate each star's relative flux in units of α Boo.

If the absolute flux of any of the nonvariable stars listed in Tables 20 through 22 could be determined experimentally at one of these wavelengths, the table of relative values could then be used to determine the flux of the other stars at this same wavelength (within the limits set by the uncertainties in the original determination and in the transfer ratios).

TABLE 20

Relative Flux Values for A- to K-Type Stars
(α BOO = 1)

Star	2.2 μ (± %)	3.5 μ (± %)	11 μ (± %)	22 μ (± %)	60 μ (± %)
α Boo	1.00 ±1	1.00 ±1	1.00 ±1.3	1.00 ±1.5	1.00 ±3
α Tau	0.842 ±1	0.876 ±1	0.870 ±1.3	0.926 ±1.5	0.870 ±3
α Aur	0 325 ±1 5	0 327 ±1.5	0.318 ±1.1	0.332 ±1.5	0 317 ±3
β Gem	0.171 ±1.5	0.168 ±1.5	0.166 ±1.3	0.169 ±1.5	0.169 ±3
γ Dra	0.213 ±1.5	0.216 ±1.5	0.207 ±1.4	0.223 ±2	0.223 ±3
α Hya	0.192 ±1	0.196 ±1.5	0.203 ±3	0.198 ±3	0.197 ±8
α Ari	0.113 ±1.5	0.113 ±2	0.110 ±5	0.119 ±2	0.116 ±8
γ Aql	0.108 ±1.5	0.113 ±2.5	0.108 ±2	0.118 ±2	0.105 ±8
α CMa	0.225 ±1.5	0.209 ±1.5	0.194 ±1.2	0.196 ±1.5	0.184 ±3
α CMi	0.116 ±1.5	0.109 ±1.5	0.108 ±1.3	0.110 ±1.5	0.110 ±3
α Lyr	0.0619 ±1.3	0.0578 ±1.5	0.0536 ±1.3	0.067 ±02	0.346 ±3
α Cen A	0.252 ±2	0.236 ±2	0.221 ±2	0.211 ±3	0.177 ±10
α Cen B	0.109 ±2	0.102 ±2	0.095 ±2	0.091 ±3	0.077 ±10

TABLE 21

Relative Flux Values for M-Type Stars
(α Boo = 1)

Star	2.2 μ (± %)	3.5 μ (± %)	11 μ (± %)	22 μ (± %)	60 μ (± %)
β And	0.346 ±1.5	0.371 ±1.5	0.365 ±2	0.385 ±2	0.386 ±10
α Cet	0.296 ±2.5	0.308 ±2.5	0.313 ±2	0.332 ±2.5	0.318 ±8
μ Uma	0.136 ±2	0.142 ±1.5	0.137 ±3	0.149 ±2	0.140 ±8
β Peg	0.486 ±1.5	0.518 ±2	0.528 ±2	0.595 ±2	0.558 ±8
β Gru	1.22 ±2	1.30 ±2	1.30 ±2	1.40 ±2	1.44 ±3
α Car	0.216 ±1.5	0.207 ±2	0.206 ±1.5	0.208 ±2	0.195 ±3
γ Cru	1.11 ±2	1.21 ±2	1.27 ±3.5	1.31 ±3	1.29 ±15
μ Gem	0.363 ±2	0.368 ±3	0.383 ±6	0.430 ±2.5	0.397 ±8
η Gem	0.211 ±5	0.252 ±3	0.256 ±2	0.279 ±3	0.275 ±10
ρ Per	0.374 ±2	0.402 ±2.5	0.412 ±4	0.474 ±2.5	0.491 ±d
∂ Vir	0.196 ±1.5	0.204 ±2	0.218 ±4	0.239 ±3	0.212 ±10
2 Cen	0.291 ±1.5	0.310 ±1.5	0.349 ±4	0.345 ±3	0.369 ±8
σ Lib	0.232 ±2	0.248 ±2	0.273 ±3	0.254 ±3	0.281 ±8

TABLE 22

Relative Flux Values in the Vicinity of CO Bands for Stars with No Expected Absorption
(α Lyr = 1)

Star	1.6 μ (± %)	4.8 μ (± %)
α Lyr	1.00 ±2	1.00 ±2
α CMa	3.70 ±1.5	3.54 ±1.5
α CMi	1.84 ±2	1.92 ±2
α Car	3.40 ±2	3.65 ±1.5
α Cen A	3.87 ±2	3.98 ±2
α Cen B	1.67 ±2	1.69 ±2

2.5 DETERMINATIONS OF ABSOLUTE FLUX

The following absolute flux measurements (Tables 23 through 27) for 10 to 20 μm and 1 to 5 μm were reviewed in Rieke et al. [4] and Campins et al. [3], respectively. They constitute only those determinations classified by Rieke as direct calibrations. The uncertainties estimated by the experimenters are here assumed to be at the 1-σ level whether or not this has been explicitly stated.

Only direct calibrations are included because these are the more fundamental flux determinations based on measurement rather than theory. It is the intention of this report to introduce theory only at a later stage so that it can be clearly seen how well independent measurements and theoretical expectations agree. Two categories of direct calibration are mentioned in Rieke et al. [4] and Campins et al. [3]: blackbody comparison and solar analog.

2.5.1 Absolute Calibration by Blackbody Comparison

Flux measurements of α Lyr at 1.24, 2.20, and 3.76 μm [23], shown in Table 23, were calibrated by direct comparison to a telescope-mounted standard blackbody observed in a narrow atmospheric window (a window in which total atmospheric extinction to infinity was estimated to be only a few percent).

TABLE 23

Alpha Lyrae (Vega)
Blackbody Comparisons

Wavelength (μm)	Flux ($Wcm^{-2}\mu^{-1}$)	Uncertainty (%)
1.24	30.6×10^{-14}	3
2.20	4.19×10^{-14}	3
3.76	5.44×10^{-15}	3

Calibrations of β Gem at 10.6 and 21 μm and of α Tau and α Aur at 11.34 μm [4] are shown in Tables 24 and 25, respectively. These calibrations involve comparing a blackbody standard to the planet Mars and then Mars to the star with a separate instrument, thus working around the problem of dynamic range.

In the case of the α Tau and α Aur measurements, the blackbody standard was placed on a nearby mountain and compared with the planet Mars while it was low in the sky. To minimize problems with corrections for the differing atmospheric absorptions along the line of sight to the mountain, to Mars, and to the star, a very narrow (0.8-μm) passband centered at 11.34 μm was selected. Under the favorable atmospheric conditions encountered at the observing site, it was estimated that the total atmospheric absorption in this band amounted to only 2%. The narrow band also minimized problems caused by the very different spectra emitted by a planet and by a star.

TABLE 24

Beta Geminorum (Pollux)
Blackbody Comparisons by Way of Mars

Wavelength (μm)	Flux ($Wcm^{-2}\mu^{-1}$)	Uncertainty (%)
10.6	2.99×10^{-16}	3.3
21	1.95×10^{-17}	10

TABLE 25

Alpha Aurigae (Capella)
Blackbody Comparison by Way of Mars

Wavelength (μm)	Flux ($Wcm^{-2}\mu^{-1}$)	Uncertainty (%)
11.34	4.47×10^{-16}	8

In the case of the β Gem, the simultaneous flux measurement of Mars was performed at close range by apparatus on board the Viking orbiter, which in turn had been calibrated before launch by comparing two blackbodies of differing temperatures in a vacuum chamber on Earth. During this procedure the temperature of one blackbody was varied from 140 to 330 K, while the other was held at liquid nitrogen temperature. The calibrated radiometry then provided temperature estimates that agreed with those of a thermister to ±0.5 K (Chase et al. [24]). Rieke's observations took place at a time when, as viewed from Earth, Mars was within 5° of the star being calibrated, thus minimizing errors in atmospheric correction when comparing them.

2.5.2 Calibration by Solar Analog Method

Solar analog calibrations of the photometry at 2.22 and 3.54 μm [10] and of new photometry at 1.6 and 4.8 μm, shown in Tables 26 and 27, respectively, were taken from Campins et al. [3]. A solar analog calibration of the photometry at 10.6 μm [16] was taken from Rieke et al. [4].

The solar analog method of direct calibration utilizes relative photometry including stars of solar type, which on average can be extrapolated from their known visible flux along a spectral curve with the same shape as that of the sun. This curve has been well determined using direct measurements of the sun against terrestrial blackbody standards; thus, ultimately solar analog calibration is again a comparison with blackbody standards, only now using a more indirect route.

While it is clear that all solar-type stars have almost the same flux ratios between the visible and infrared, there is a residual 2% scatter that appears to be intrinsic to the stars rather than due to observational error [3]. It is not clear where in this range the sun falls (it may not be an average solar-type star), and this uncertainty in the above method has been added to the error estimates given.

TABLE 26

Alpha Boo Flux Constants by Which to Scale Relative Fluxes in Tables 20 and 21

Solar Analog Method

Wavelength (μm)	Flux ($Wcm^{-2}\mu^{-1}$)	Uncertainty (%)
2.22	6.33×10^{-13}	3
3.54	1.18×10^{-13}	3.3
10.6	1.84×10^{-15}	7

TABLE 27

Alpha Lyr Flux Constants by Which to Scale Relative Fluxes in Table 22

Solar Analog Method

Wavelength (μm)	Flux ($Wcm^{-2}\mu^{-1}$)	Uncertainty (%)
1.6	1.24×10^{-13}	3
4.8	2.19×10^{-13}	5

3. THEORETICAL SPECTRAL ENERGY DISTRIBUTION

3.1 ANALYTIC EXPRESSIONS FOR STELLAR SPECTRA

If one is to work with many stellar spectra in both the fitting and band integration processes, it would be preferable to have these spectra in the form of easily written and manipulated mathematical functions rather than long arrays of discrete values or complicated computer subroutines.

The IRAS low-resolution spectrometer (LRS) stellar spectra shows that the stars on Rieke's primary and secondary lists resemble Planck functions. The formulas developed in this section are, therefore, based on a modification to the Planck function involving an apparent brightness temperature that is a function of wavelength. There are physical reasons why this is a natural form in which to express a stellar spectrum.

3.1.1 Wavelength Dependence of Brightness

The effective temperature of a star T_{eff} is defined as *the temperature required for a blackbody with equivalent surface area to emit the same total power as the star integrated over all wavelengths.*

$$L^{*} = 4\pi R^{*2} \sigma T_{eff}^{4} \quad .$$

It is sometimes assumed that a star spectrum can be taken as that of a blackbody having the star's effective temperature. This is not true for all stars (for the sun, deviations from a blackbody shape of about 25% are encountered over the wavelength interval from 2 to 30 μm). In general, a star's brightness temperature (the temperature of a blackbody with the same irradiance at a specific wavelength) is not independent of wavelength.

Radiation from a star originates some distance down into the stellar atmosphere. In the case of stars with solar temperature or less, the infrared opacity in the atmosphere is proportional to λ^2. This implies that at short infrared wavelengths radiation can travel a comparatively long distance through the stellar atmosphere, allowing radiation reaching an observer to escape from a deeper, hotter layer of the star. As the observing wavelength gets longer, the radiation reaching the observer comes predominantly from outer cooler layers of the stellar atmosphere (Figure 1). Because of this, a star like the sun, which has a 6000-K brightness temperature near 2 μm, is observed to drop to only a 4500-K brightness temperature in the 20-μm region. Thus, the spectral curve has to drop more steeply with increasing wavelength than a 6000-K blackbody curve.

3.2 SOLAR SPECTRUM

Before attempting a general formula to fit the spectra of the standard stars, it is useful to examine the sun's infrared spectrum as a prototype. Because it is close, the sun provides a unique source of meas-

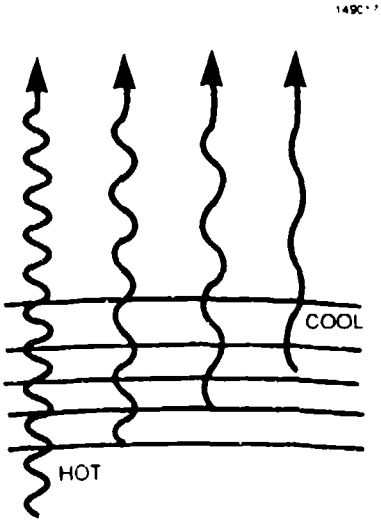

Figure 1. Cross section of stellar atmosphere

urements on a star at very high spatial and spectral resolution over a very wide range of energies. Information gathered from semiempirical analyses of such solar data has, in the past, been a major guide in extending and correcting theory. As a result, it can be assumed that the sun has the most thoroughly understood stellar spectrum.

As far as theory and computation are concerned, the infrared is the simplest part of the solar spectrum. The radiation is continuous and originates in regions of local thermodynamic equilibrium (LTE). The source of opacity H_f is known, and its functional behavior is easy to represent.

If the distribution of temperature, pressure, etc., in the solar atmosphere were known, it would be a simple matter to calculate the infrared radiation emitted by each layer: merely use the Planck function as a consequence of LTE, figure out how much is absorbed in the process of traversing the atmosphere, and then sum the contributions from all layers to obtain the infrared spectrum.

If, as is in fact the case, the exact structure of the atmosphere is not known in advance, measurements of the actual spectrum can be used to deduce one that is plausible. This semiempirical method in the case of the sun uses all data ranging from ultraviolet to extreme infrared to constrain models of atmospheric structure.

One commonly used representation of the solar spectrum is that calculated from the semiempirical model M [1]. The brightness temperature predictions of model M, along with the available measurements over the subject wavelength range, are plotted in Figure 11 of Vernazza et al.[1], reproduced here as Figure 2.

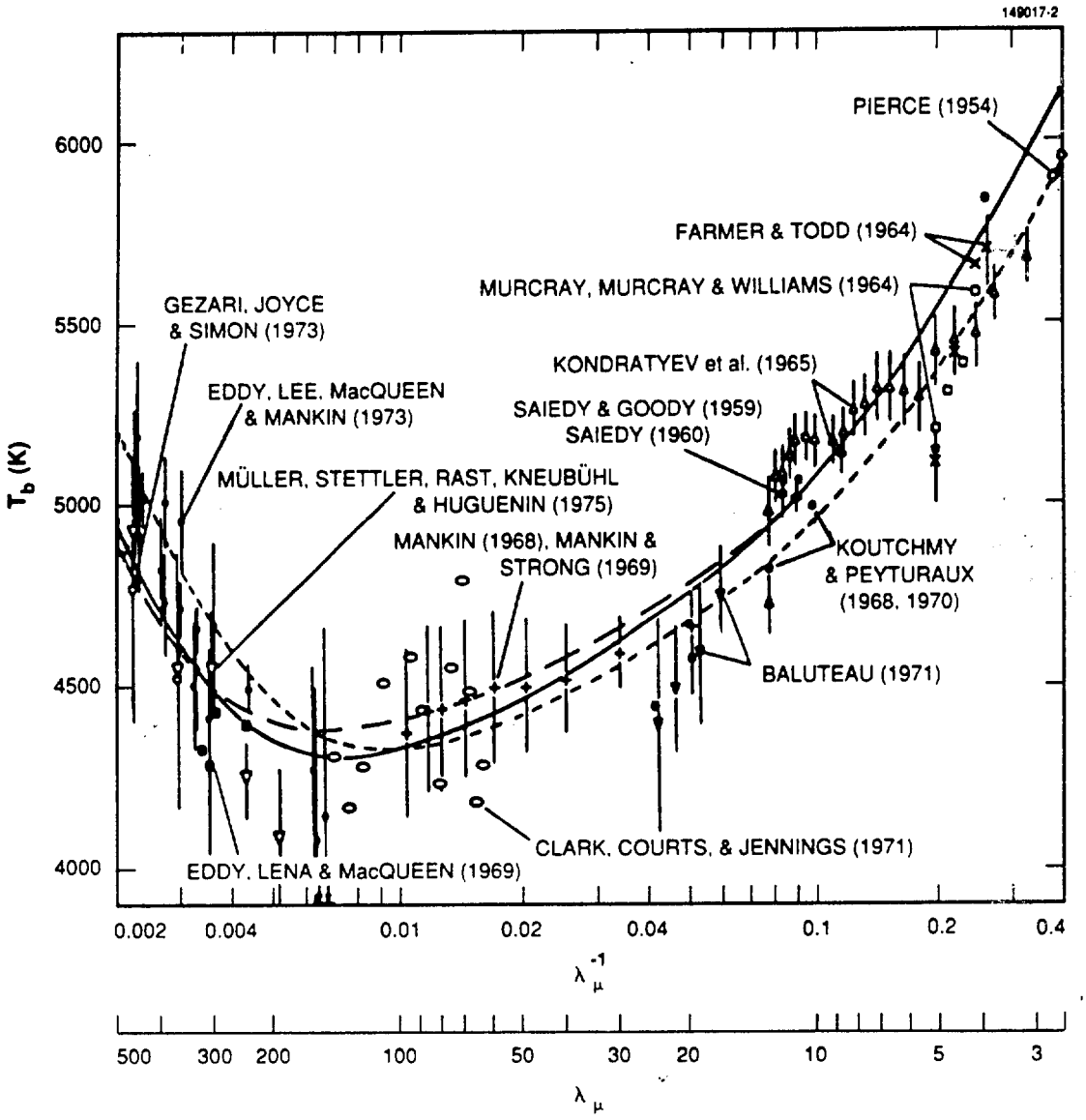

Figure 2. Vernazza et al. combined plot of the observed brightness temperatures T_b^{center} and T_b^{disk} in the range 2.5–500 μm. The solid curve and the short dashed curve represent T_b^{center} and T_b^{disk}, respectively, calculated from model M. The short dashed curve is used to obtain flux estimates and has been approximated by the equation $T_b(\lambda) = 4260(1 + 13.77/\lambda)^{0.182}$. The long dashed curve represents T_b^{center} calculated from an older semiempirical model solar atmosphere (the HSRA model).

Trial and error and some least square fitting were used to arrive at an analytic approximation to the brightness temperature predictions of model M:

$$T_{disk}(\lambda) = 4260\left(1+\frac{13.77}{\lambda}\right)^{0.182}.$$

This expression gives results consistent to within 0.25% with those of model M between 2 and 25 μm, and to within 0.5% out to 100 μm.

Combined uncertainties in measured solar flux as estimated in Mankin [25] are listed in Table 28 for several wavelengths.

TABLE 28

Uncertainty in Determination of Solar Spectrum Beyond 10 μm

10 μm	15 μm	20 μm	30 μm	50 μm	75 μm	100 μm
±2%	±3%	±4%	±5%	±5.5%	±5.5%	±5.5%

3.3 H^- FREE-FREE ABSORPTION

The source of infrared opacity beyond 1.6 μm in the solar atmosphere (and for stars moderately cooler than the sun) is described as "almost exclusively free-free transitions of negative hydrogen ions, and to a lesser extent negative helium ions. In such transitions a free electron accelerated in the field of a neutral hydrogen or helium atom absorbs or emits radiation. The free-free absorption coefficient of negative hydrogen has been computed by numerous authors . . . and is found to be proportional to the electron pressure and to the square of the wavelength for wavelengths greater than a few microns." [25]

The simple nature of this relation and the wide class of stars for which it is the main source of opacity make it easy to produce a general spectral function that scales in a simple way for changes in effective temperature between about 3300 and 6000 K.

3.4 SCALING OF SOLAR SPECTRUM TO OTHER T_{eff}

3.4.1 Temperature-Opacity Relations in Stellar Atmospheres

In simple models of stellar atmospheres it is found that the temperature distribution, when written in terms of the mean optical depth τ (rather than physical depth) into a star's atmosphere, has the same functional form regardless of stellar type:

$$T(\tau) = T_{eff} f(\tau).$$

More detailed theoretical treatments apparently bear this out for wide classes of stars having the same dominant opacity mechanisms, and this provides a way to transfer some of what is known about the sun to other stars. On this subject, Carbon and Gingerich [6] write:

> "A common technique . . . for producing the temperature distributions of intermediate spectral-type stars consists of scaling an empirical solar $T(\tau)$ relation by the ratio T_{eff}(star) / T_{eff}(solar).
>
> "Some estimate of the validity of this approach can be obtained by use of the models in the grid. . . . we compare the temperature distributions determined by directly calculating blanketed models and by scaling a (6000,4) model in this manner. The scaling relation fails in going to higher values of T_{eff} because of the shift from H^- to H as the dominant continuous opacity and the increased importance of the hydrogen line blocking. Scaling to cooler temperatures involves appreciably less error since H^- remains the principal opacity source. These results suggest that a solar model scaled to 4000 K effective temperature will differ comparatively little from the explicitly calculated grid models. Hence, the scaling technique, which has commonly been used without thorough examination, has been validated . . . ."[26]

3.4.2 Derivation of Spectrum from Temperature Distribution

Computing a stellar spectrum starting from a given $T(\tau)$ requires writing the temperature distribution as $T(\tau_\lambda)$, a function of the monochromatic optical depth, and then integrating the contributions of the thermal emission that reach an observer from each level of the atmosphere at any given wavelength.

$$\phi(\lambda) \approx 11910\Omega \int_0^\infty \frac{e^{-\tau_\lambda}}{\lambda^5 \left(\exp\left(\frac{14388}{\lambda T(\tau_\lambda)} \right) - 1 \right)} d\tau_\lambda .$$

In order to convert τ_λ to τ, one must first find $d\tau_\lambda/d\tau = \kappa_\lambda/\kappa$, the ratio of the coefficient of monochromatic absorption to the Rosseland mean absorption coefficient. In general, this could be very complicated; however as mentioned previously, for stars with temperatures equal to or cooler than the sun, and for wavelengths longer than about 1.6 μm, the dominant source of opacity is free-free absorption by the H^- ion, and this has a coefficient of absorption with a smooth and simple wavelength dependence ($\approx\lambda^2$). There are also temperature and pressure dependences to both the mean and the monochromatic absorption coefficients. Nevertheless, when the ratio is taken, the simple relation $d\tau_\lambda/d\tau = \alpha\lambda^2 T^2$ is found to hold to a very good degree of approximation over the range of pressures, temperatures, and wavelengths with which this report deals. This is demonstrated in Figure 3, which shows a plot of log $(\kappa_\lambda/\lambda^2\kappa)$ versus log(T), for points calculated using a variety of temperature and pressure conditions typical of those encountered in stars of solar temperature or cooler. The conditions are taken from the model M solar atmosphere, and the model α Boo atmosphere of Johnson et al. [27]. The Rosseland mean absorption coefficients for the model M and the H^- free-free absorption coefficients for the α Boo model [27] were calculated from the formulas and tables in Allen [28].

The fact that points (Figure 3) generated from conditions in a giant star and in a dwarf fall basically on the same line is an encouraging sign that differences in gravity may not have much effect on the scaling of spectra with temperature; however, the further we deviate from solar conditions, the more suspect the scaling. The best fit line to the data in Figure 3 has a slope of 2.04.

Thus, we can approximate

$$d\tau_\lambda = \frac{\kappa_\lambda}{\kappa} d\tau \propto \lambda^2 T^2 d\tau \approx \alpha\lambda^2 T_{eff}^2 \; f^2(\tau)\, d\tau,$$

$$\tau_\lambda \approx \alpha\lambda^2 T_{eff}^2 \int_0^\tau f^2(\tau')\, d\tau' = \alpha\lambda^2 T_{eff}^2 \, F(\tau).$$

$$\phi\left(\lambda, T_{eff}\right) \approx \frac{11910\Omega}{\lambda^5} \int_0^\infty \frac{\exp^{-(\alpha\lambda^2 T_{eff}^2 F(\tau))}}{\left(\exp\left(\frac{14388}{\lambda T_{eff} f(\tau)}\right) - 1\right)} \alpha\lambda^2 T_{eff}^2 \, f^2(\tau) d\tau \,.$$

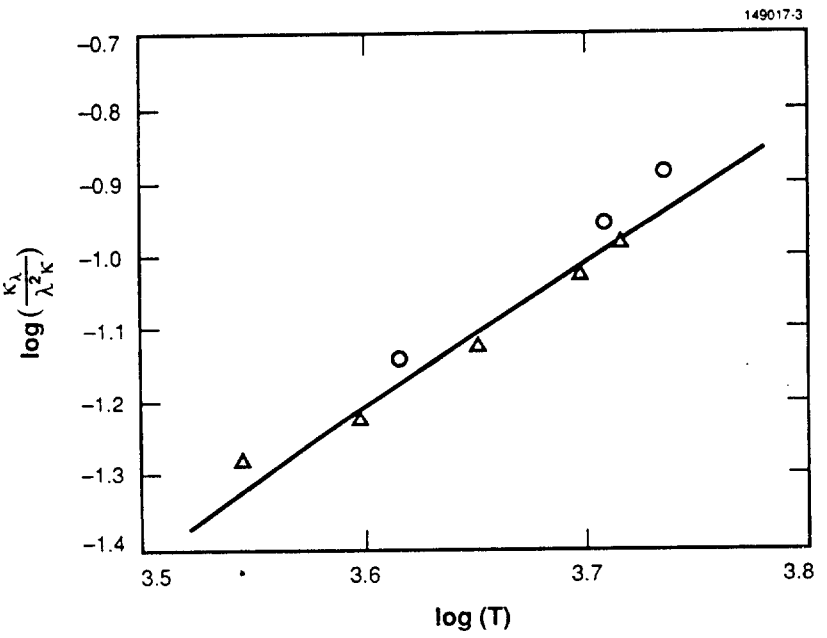

Figure 3. Logarithmic plot of the ratio of the monochromatic absorption coefficient to Rosseland mean absorption coefficient divided by λ^2 versus the temperature at the same point in the stellar atmosphere. The circular data points were calculated using atmospheric parameters taken from the Vernazza et al. model solar atmosphere, and the triangular points were calculated using the model atmosphere of Johnson et al. for the star α Boo.

Using this expression, stellar spectrum solutions are possible for all T_{eff} (< 6000 K), without actually integrating or determining the explicit forms of $f(\tau)$ and $F(\tau)$. The form of $\phi(\lambda,T_{eff})$ is already known for the special case of T_{eff} = 5770 K: it is the solar spectrum $\phi_{sun}(\lambda)$. Because the integrand involved depends only on the combination λT_{eff}, the form of $\phi(\lambda)$ for other T_{eff} can be obtained by substituting $\lambda T_{eff}/5770$ for the variable λ wherever it appears in the analytic expression for $\lambda^5\,\phi_{sun}(\lambda)$.

Employing this substitution in the analytic approximation to the model M solar spectrum previously introduced gives a generalized $\phi(\lambda, T_{eff})$:

$$\phi\left(\lambda,T_{eff}\right)=\frac{11910\Omega}{\lambda^5\left(\exp\left(\frac{14388}{0.738\lambda T_{eff}\left(1+\frac{79450}{\lambda T_{eff}}\right)^{0.182}}\right)-1\right)}.$$

In the wavelength region between 2 and 100 μm, this two-parameter function then scales the semiempirical solar spectrum [1] to stars for which $d\tau_\lambda/d\tau \propto \lambda^2 T^2$ (i.e., giant and main-sequence stars with T_{eff} < 6000 K). The parameter T_{eff} adjusts the shape of the curve, and the parameter Ω adjusts the solid angle subtended by the star and, thus, the overall normalization of the curve. This formula can also be written as $\Omega\, B[T(T_{eff}, \lambda), \lambda]$, where

$$T\left(T_{eff},\lambda\right)=0.738\,T_{eff}\left(1+\frac{79450}{\lambda T_{eff}}\right)^{0.182}$$

defines the dependence of brightness temperature on wavelength, and B[T,λ] represents the Planck function. Figure 4 shows a graph of the brightness temperature dependence for several values of T_{eff}.

In the case of stars sufficiently cooler than the sun, more molecules are expected to form, and new sources of opacity become influential. This should cause departures from the fitting function. It is assumed that this departure does not occur until stars later than type M5 III, since it is not until M7 III that H_2O absorptions are noticed in stellar infrared spectra (Baldwin, et al. [29]). If this assumption is wrong (which would not be too surprising – see Manduca et al. [30] on the possible effect of H_2O opacity on the continuum flux of late-type stars), the fact should become evident when comparing the predicted relative fluxes of different types of stars (obtained using the fits) with those actually measured.

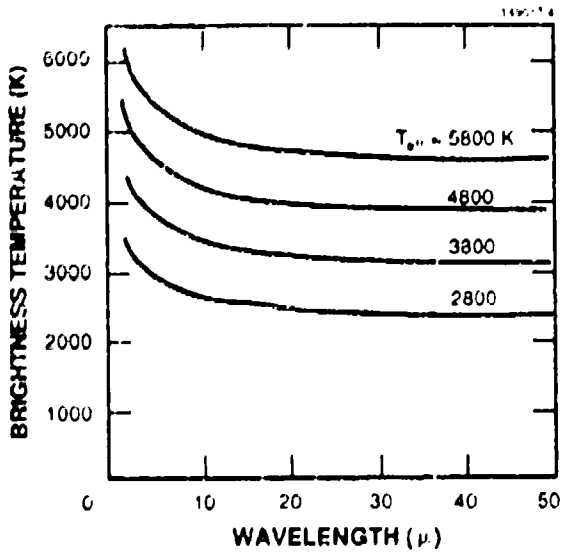

Figure 4 Stellar brightness temperature versus wavelength for several values of effective temperature

4. TWO-PARAMETER CURVE FITTING

A two-stage attempt was made to get the best overall fit of the set of spectral functions for all the standard stars to the absolute flux measurements on individual members while holding the relative fluxes of all the stars in correct relation to each other.

4.1 FITTING PROCEDURE, FIRST ROUND: FITS TO RAW ABSOLUTE DATA

First, the table of relative flux values was used to transfer all the absolute flux measurements to their equivalent values for a single star. A two-parameter fit was then performed to the eight data points, each weighted by an uncertainty composed of the original measurement error and the error in the stellar ratio. This was repeated for all the stable stars with well-measured ratios.

The resulting smooth fits for each star were evaluated at 2.2, 3.5, 11, 22, and 60 μm. These flux values and the table of relative fluxes were then used for each star to find the corresponding α Boo fluxes. At each wavelength all the predicted α Boo flux values were then averaged, producing the smoothed flux distribution to which the final fittings would be performed.

First round fits for stars that are believed to have no significant CO absorptions were also evaluated at 1.6 and 4.8 μm (typically the location of CO bands), as well as 2.2, 3.5, 11, 22, and 60 μm. The fluxes at these extra wavelengths were transferred back to a single star, this time α Lyr rather than α Boo, and averaged as before.

4.2 FITTING PROCEDURE, SECOND ROUND: FITS RELATIVE TO SMOOTHED ALPHA BOO AND ALPHA LYR

All subsequent two-parameter fits for cool giant stars were performed against the f[illegible]ed α Boo data points transferred to the star of interest using the ratios in Tables 20 and 21 and w[illegible]i only by the small uncertainty (about 2% at 20 μm rather than 10%) in these flux ratios.

Two-parameter fits for relatively hot main-sequence stars with no CO bands, such [illegible]Cen, α CMa, and α CMi, were performed relative to seven data points, including two transferred from the smoothed α Lyr spectrum, again weighted only by the uncertainties in the flux ratios used to transfer them.

4.3 RESULTS OF TWO-PARAMETER FITTING

To check the validity of the data and the theory, the reduced χ^2 (sometimes called goodness of fit) for the final fits can be examined for clues.

$$\chi^2_{N-n} = \sum_i \frac{(D_i - \Phi[\lambda_i])^2}{(N-n)\sigma_i^2}$$

where

N = the number of data points being fit;
n = the number of parameters in the fit;
$\phi[\lambda]$ = the fitting function evaluated using the best fit parameters;
D_i = the data points ($D_1 \ldots D_N$);
λ_i = the wavelength at which data point i is located;
σ_i = the uncertainty by which data point i is weighted.

This number is generally expected to be around 1 if the errors are random and are not over or underestimated. For large enough N values and accurate σ estimates, there is about a 50-50 chance of χ^2 being larger or smaller than 1 (but not by much). The range of values about 1 that have a reasonable probability can be found for a given value of $N - n$ in common references (Bevington [31]).

4.3.1 Goodness of Fit to Raw Absolute Data

The average value of reduced χ^2, obtained using the final fits and the data points transferred from the original eight (unsmoothed) absolute flux measurements, comes out about 0.30 (or 0.25 if only nonvariable stars are included). If the errors were estimated correctly and were random, there would be a less than 5% chance that a value less than or equal to this could be obtained because of chance alignments. Therefore, it is likely either that most of the error estimates were conservative or that the errors are primarily not random.

It is hard to see what could cause a systematic error that seemingly "knows" about the shape of the fitting function (hard at least for the data obtained by blackbody comparisons; the three solar analog data points might be expected to behave this way). Nevertheless, in the remainder of this report it is assumed that a systematic uncertainty in shape shared by all the fits exists, causing an uncertainty in flux that ranges from about 3% below 10 μm to perhaps 6% at 25 μm. Approximately this same estimated uncertainty can be derived either from the uncertainties cited by Rieke [4] based on the stellar direct calibration measurements or those given in Mankin [25] based on the estimated quality in measurements of the solar spectrum (and thus the shape of our fitting function). Since this is apparently not a random effect and is the same for all the stars, no averaging of calibrations based on different stars can reduce the resulting uncertainty in flux and band ratios.

4.3.2 Goodness of Fit Relative to Alpha Boo

The average value of reduced χ^2, obtained in fits against the five smoothed α Boo absolute flux values transferred using Tables 20 through 22, is about 1.3. The probability that by chance a two-parameter fit would give a value smaller than or equal to this is about 75%. That is reasonable, indicating that the random errors estimated in the relative fluxes are about right at the 1-σ level.

If one averages the relative fit χ^2 values only for stars included in Rieke's primary and secondary lists for which no variability is noted, an even more encouraging average value of 0.8 is obtained. The

probability that the reduced χ^2 would be less than or equal to this is about 50%, indicating that the estimated 1-σ measurement errors are very accurate when the effect of variability is discounted.

This excellent fit indicates nothing about our knowledge of the absolute shape of the function used to fit the stars but only that the way the two-parameter fits for different stars behave relative to each other can mimic the actual relative measurements. It also does not say whether there is much systematic behavior to mimic or whether these stars just have constant ratios to each other within the expected errors at all wavelengths; however, one can also examine the values of the parameters (T_{eff} and Ω) obtained in the fits for different stars and compare them with those found using independent means. As shown below, such a comparison offers much to encourage the idea that the elaborate fitting function with its dependence on T_{eff} has something to do with the way the spectra of actual stars with differing temperatures relate to each other and that the measurements are sensitive enough to demonstrate this.

4.4 COMPARISON OF BEST-FIT PARAMETERS AND INDEPENDENT MEASUREMENTS

Both parameters used in the fitting function have been determined by independent means for at least some of the stars we are fitting (see Table 29). Effective temperatures (with uncertainties less than 5%) for stars of a given spectral type are available in Gray [32].

Angular diameters have been determined for some stars by means of interferometry, lunar occultation, and indirect means involving the modeling of visible light spectra. A compilation of such measurements is available in Augason et al. [33] for the stars α Boo and α Tau.

TABLE 29

Comparison of Best-Fit and Measured Parameters for Sample of Important Stars

Star	Spectral Type	Best-Fit T_{eff} (K)	Best-Fit $Ø_D$ (mas)	T_{eff} Gray [32]	$Ø_D$ (expt) (mas)
α Boo	K2 III	4265	21.5	4200	21.9[a*]
α Tau	K5 III	3840	21.4	3800	21.6[a*]
β Gem	K0 III	4420	8.62	4400	. . .
α Cen A	G2 V	5760	8.52	5870	8.40†

* Weighted average of all determinations [33]
† Derived from listed radius and distance (closest star) [27]

For this select group of stars the agreement in the best-fit parameters and the independently measured values is better than 2% in all cases. Note, as well, that a wide range of stellar types is represented (virtually the entire range for which we a priori expected the fitting function to be valid). It thus appears, at least from this limited sample, that the behavior of the fitting function models the behavior of the real world and that the infrared measurements available are accurate enough to discriminate between stars of different temperature on this basis.

The fact that α Cen, a solar-type star, comes out with approximately the same temperature as the sun is a particularly good sign. It implies that if one started with just the relative photometry and performed a solar analog calibration using α Cen as the solar analog star, the calibration would be essentially the same. This is a nice check of internal consistency.

4.4.1 Behavior of Best Fit T_{eff} versus Spectral Type

There are actually about a dozen stars with $T_{eff} < 6000$ K on which two-parameter fits have been performed and for which Gray [32] has given temperatures (though angular sizes are unavailable). If the ratio of the best-fit T_{eff} to the value in Gray is taken for each, the average result is 0.999 and the standard deviation is 0.04. This is very good agreement given that uncertainties of 5% were cited.

There are also about 10 stars of spectral type later than M2 (cooler than 3600 K) for which Gray provides no temperatures. If the best-fit T_{eff} for all 20 plus G to M type, Class III-II stars are plotted versus spectral type, an approximately linear relation is found (Figure 5) both in the region where Gray has given values and beyond. The lack of any discontinuity encourages us to use the same fitting function for stars as late as M5 III or so.

4.5 STARS FOR WHICH $T_{eff} > 6000$ K

For a star with an effective temperature higher than that of the sun, a discrepancy between Gray's value of T_{eff} and the best-fit value is evident. This discrepancy is to be expected since the theory behind the derivation of the fitting function applied only to stars cooler than 6000 K. However, when viewed just as a mathematical curve, the function provides a reasonable fit to the data (with the same sorts of χ^2 values as before) when used with the best-fit (but unphysical) parameters listed in Table 30. Because there is no discontinuity in the opacity of these stars at 1.6 μm, the fits in this section have the same level of pseudovalidity at least back to 1.2 μm.

4.6 DEPTH AND SHAPE OF CO ABSORPTION BANDS: CLASS III-II STARS

The fundamental ($\Delta v = 1$) vibration-rotation band of CO is centered near 4.7 μm, a first overtone ($\Delta v = 2$) band is centered near 2.5 μm, and a second overtone at about 1.6 μm, just at the edge of the range of validity for the reported fits. The work of Strecker et al. [35], Hackwell and Gehrz [36], and others indicates that these molecular absorption bands account for significant deviations from smooth spectra for giant and supergiant stars of 6000 K and cooler (the extended atmospheres of which allow molecules to form). The primary concern here is the 4.7-μm band.

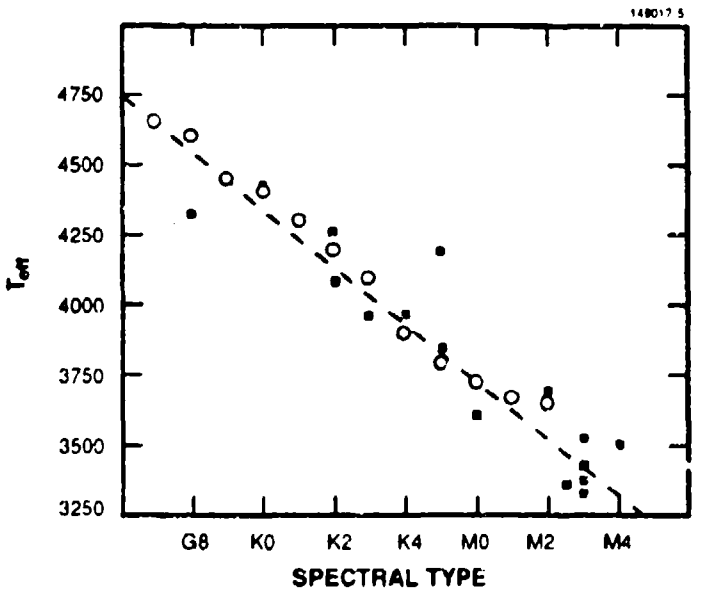

Figure 5. Effective temperature versus spectral type (Class III stars). Circles give temperatures listed in Gray for stars of the given spectral type. The squares are T_{eff} values from 2-parameter fits done in present work. The dashed line gives the best fit through the data points and is used to predict temperatures for stars of spectral types cooler than those for which Gray has tabulated values.

TABLE 30
Using Best-Fit Parameters

Star	Spectral Type	t* (K)	ω* (10-15 sr)	χ^2_ν Absolute	χ^2_ν Relative
α CMa	A1 V	6104	1.147	0.3	0.7
α CMi	F5 IV	4869	0.807	0.5	1.6
α Car	F0 Ib	4766	1.559	0.4	1.0
α Lyr	A0 V	5881	0.332	0.4	0.1†

*Use t and ω in place of T_{eff} and Ω in fitting function.

†Note that the χ^2 given for α Lyr refers only to flux below 12 μm, since it is well established that an orbiting debris cloud contributes significant extra flux at 20 μm and beyond (Leggett [34]).

4.6.1 CO Absorption Depth at 4.8 μm from Fits and Relative Photometry

Since it is expected that certain stars being fit have no significant CO bands (i.e., the Class V stars α Cen A, α CMa, α Lyr, the Class IV star α CMi; and the hot Class I star α Car), these can be used as standards against which to measure the depth of the absorption in those stars that do have CO bands. In particular, the relative photometry at 4.8 μm can be used to find the measured ratios of stars with absorptions to those without. The smooth two-parameter fits can then be used to find the expected ratios in the absence of CO bands in any of the stars. The difference reveals the percent absorption. This procedure was done for 15 stars and the results plotted against spectral type. There seems to be approximately a linear relationship between percent absorption and spectral type (and thus effective temperature) of the particular star (Figure 6).

4.6.2 CO Absorption Bands, Shape, and Depth from Spectrophotometry

Strecker et al. [35] reports the results of airborne stellar spectrophotometry on 13 stars earlier than type M3, giving relatively continuous spectral curves for the stars in the wavelength range 1.2 μm < λ < 5.5 μm. Spectra were calibrated by scaling the data so that α Lyr has the spectral curve predicted by the theoretical modeling of Schild et al. [37]. Theoretical models for this class of star have been found to be suspect in the infrared portion of the spectrum [3]. It is, however, possible to recalibrate the curves by dividing out the assumed α Lyr curve and then multiplying by the α Lyr fit obtained in the present work. Doing this and then dividing each star's spectrum by its own fit should give flat distributions about equal to 1, except in regions of absorption. This is indeed the result obtained, as shown in Figure 7(a) and in the Appendices.

Profiles of CO absorption can be extracted in this way for six of the stars that have been fit (α Boo, α Tau, β Gem, β And, α Cet, and β Peg). The absorption depths read off these plots at the 4.8-μm point correlate very well with those obtained in the previous section using photometry; however, the new values seem to be systematically 3% deeper. The slope of a linear fit to the plot of depth versus spectral type is essentially identical (see Table 31).

The profile of the absorption band obtained from the data in Strecker et al. [35] extends only to 5.5 μm (and not even this far in some cases). No published data seem to be available that show what happens beyond this point, yet the issue is important because here the band has just barely passed the region of maximum absorption. Rather than project straight-line trends, this report uses the same star's first overtone band at 2.7 μm as a model of the complete band shape. An affine transformation is performed on the 2.7-μm profile in order to map the region at the beginning of the band (up to just after the maximum absorption) onto the corresponding part of the 4.8-μm fundamental band. The transformed continuation of the 2.7-μm band up to the region of zero absorption is then assumed to give the best guess for how the real 4.8-μm absorption profile would continue [see Figure 7(b)].

4.6.3 Stars with No Direct Spectrophotometry

Two things that are apparent from the Strecker data are that the same basic absorption profile seems to repeat in cool stars of types K2 to M3 and that the depth of this absorption at its maximum

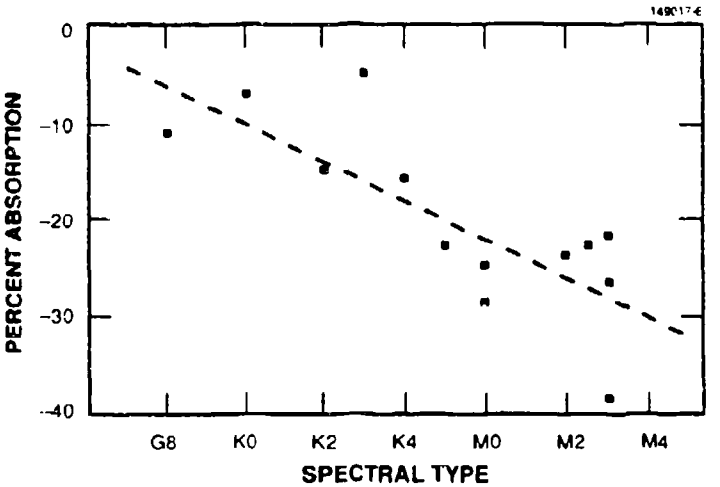

Figure 6. CO absorption depth at 4.8 μm versus spectral type (Class III stars); determination from relative photometry.

TABLE 31

Absorption Depths at 4.8 μm

Star	CO Absorption (Photometry) %	CO Absorption (Spectroscopy) [35]
α Boo	−15	
α Tau	−24	−26
α Aur	−11	
β Gem	−7	−11
α Hya	−16	
γ Aql	−5	
γ Dra	−23	
α Cet	−24	−28
β And	−25	−26
β Peg	−23	−28
γ Cru	−22	
β Gru	−27	
μ UMa	−29	
η Gem	−39	

increases approximately linearly with a star's spectral type. This implies that a good way to approximate the spectra of a star for which no information is provided would be to take an average CO absorption profile normalized to depth 1 at 4.8 μm, multiply by a scaling factor based on the star's spectral type, and subtract the percent absorption thus determined from the continuous curve generated by our fitting function.

To generate such an average profile, the normalized absorptions found in α Tau, β And, and β Peg were averaged: the result is shown in Figure 8. A tabulated version of this profile is given in Appendix B. The expected depth can be read in Table 32, as can the expected T_{eff} (provided in Gray [32] where appropriate and from a linear fit beyond M2).

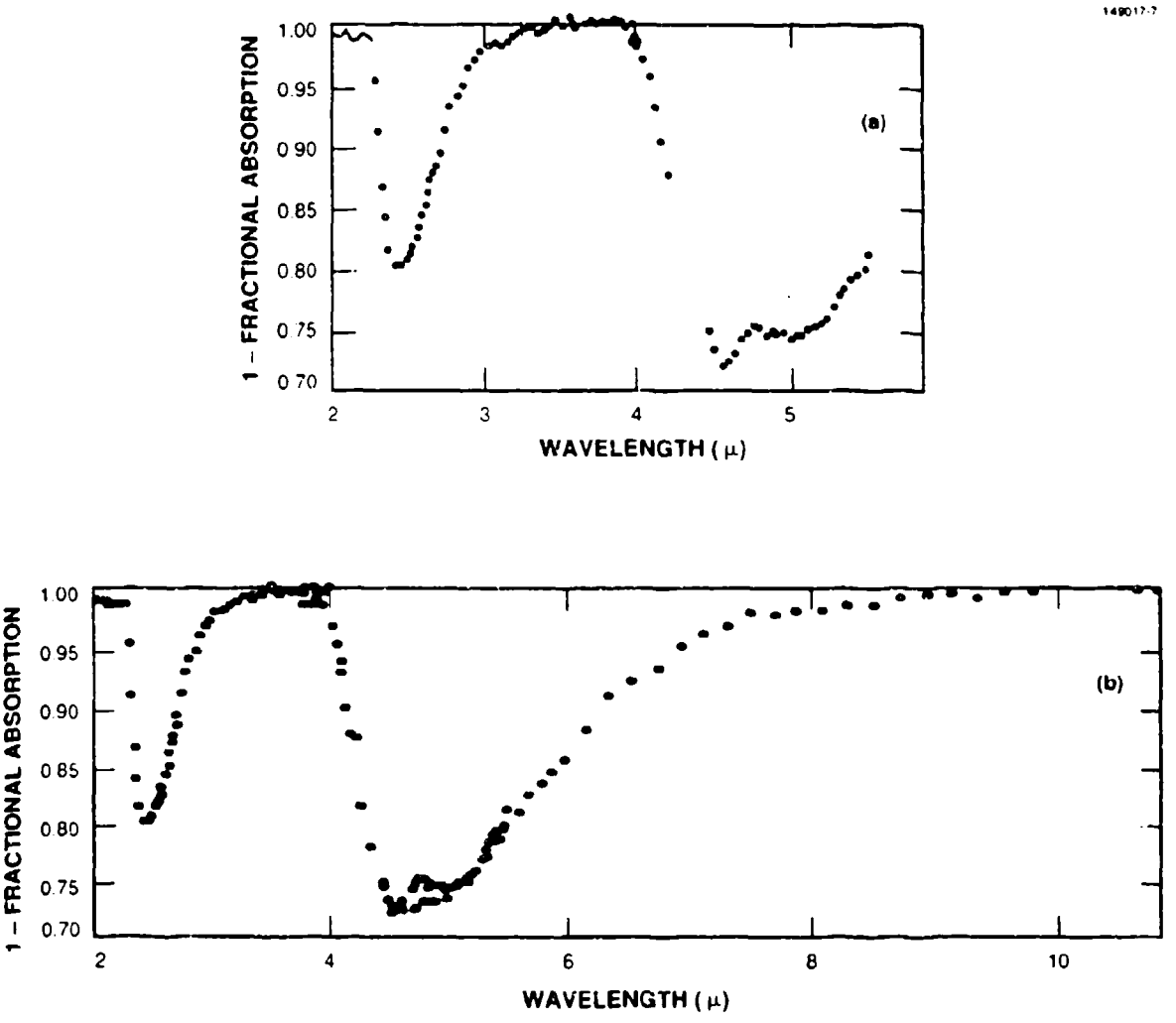

Figure 7. Alpha Tauri CO bands: (a) Raw data from Strecker et al., (b) same data with postulated extension beyond 5.5 μm based on affine transformation of 2.5-μm band.

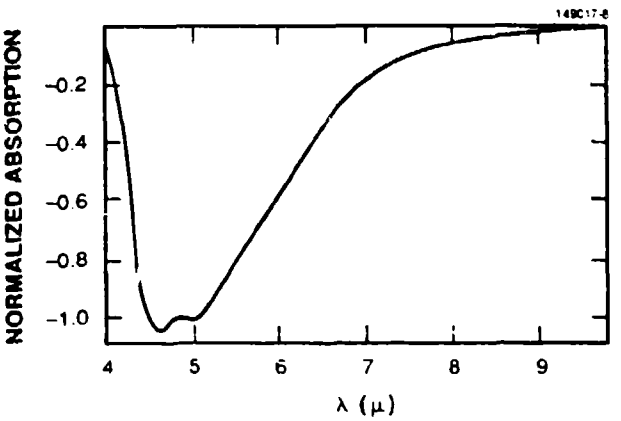

Figure 8. Average CO absorption profile at 5 μm.

TABLE 32

Depth of Absorption and T_{eff} of Star by Spectral Type

Index	Spectral Type	Teff Gray [32]	CO Absorption Depth (%)
1	G7 III	4650	–5.3
2	G8 III	4600	–7.3
3	G9 III	4450	–9.4
4	K0 III	4400	–11.4
5	K1 III	4300	–13.5
6	K2 III	4200	–15.5
7	K3 III	4100	–17.5
8	K4 III	3900	–19.6
9	K5 III	3800	–21.6
10	M0 III	3730	–23.7
11	M1 III	3670	–25.7
12	M2 III	3650	–27.7
13	M3 III	3410*	–29.8
14	M4 III	3310*	–31.8
15	M5 III	3210*	–33.9
16	M6 III	3110*	–35.9

* From linear fit to two-parameter T_{eff} values determined in this work.

Actual absorption data for specific stars scatter from a linear fit with a standard deviation of 5.5%. Most of this is probably real variation in stars. Furthermore, the shape of the CO profile causes uncertainties of about 5%. Thus, the uncertainty near the center of the band for predictions on a star having no spectral observations of its own are about 7 to 8%.

5. SPECTRA USED FOR PREDICTIONS

5.1 METHOD

Because of the good agreement between the best fit values obtained for T_{eff} and those listed in [32], it was decided to use one-parameter fits for the broadband predictions. The same function was used as before, but this time the effective temperature parameter was preset according to the stars' spectral type (Table 32) and only Ω was optimized during the fitting process.

The resulting curves were then multiplied by arrays which modify the star's spectra to account for the CO bands. If the star was one of the six with measurements presented in [35], these data were used directly (with the projection beyond 5.5 μm performed as in Section 4.5.2). When no direct measurements were available, the average CO profile was used with a depth set for the stars' specific spectral type according to Table 32.

The parameters used are shown for the whole group of stars discussed in Section 5.2. Plugging the parameters into the two-parameter function gives the star's spectral flux density outside the Earth's atmosphere in units of Watts cm^{-2} μ^{-1}. Appendix B contains the expanded form of the spectra, CO absorptions, and residuals for specific stars.

Once the spectral flux density is found for a given star as described above, it is multiplied by an array representing the transmission and response function for the band of interest and integrated numerically. This result is then multiplied by the light-gathering area of the sensor. Figure 9 shows the resulting spectrum of α Tau plotted versus wavelength.

5.2 PARAMETERS TO BE USED IN SPECTRAL ESTIMATION

5.2.1 Spectral Type G to K

The stars in Table 33 are nonvariable (except γ Dra) and are the stars for which the theory in this report was designed (H^-_{ff} absorption is the only major infrared opacity source). It is not surprising, therefore, that in general they have values of reduced χ^2 of 1 or less. The exceptions are α Cen (Table 34), which is in the southern hemisphere and as a result, probably not tied in as accurately to the flux ratio network of northern stars; and γ Dra, which is variable in the visible, and judging from its fit, in the infrared as well.

5.2.2 Spectral Type M

Table 35 lists some of the stars that are variable by 5 to 10% in the infrared (the larger the number following M in the spectral designation, the more likely is significant variability). However, the photometry from which these fits were derived was collected over a long time period and one may hope that the fits represent the average flux over several cycles.

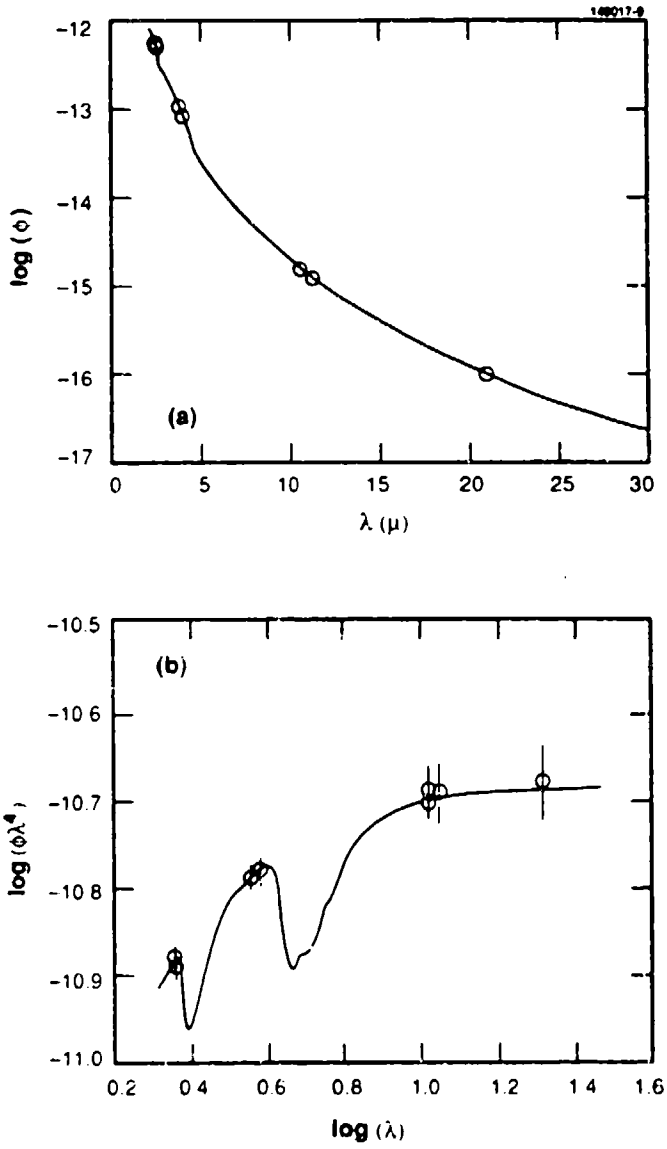

Figure 9. Alpha Tauri spectrum, best fit with CO bands superimposed (displayed two ways).

TABLE 33

Class III Stars: Types G to K

Star	T_{eff} (K)	Ω (10^{-15} sr)	χ^2_ν Absolute	χ^2_ν Relative
α Boo (K2 III)	4200	8.71	0.3	1.6
α Tau (K5 III)	3800	8.60	0.1	0.5
β Gem (K0 III)	4400	1.380	0.3	0.7
α Aur (G8 III)	4600	2.53	0.3	0.7
α Hya (K4 III)	3900	1.875	0.3	0.9
α Ari (K2 III)	4200	0.987	0.2	0.2
γ Aql (K3 II)	4100	0.989	0.1	1.1
γ Dra (K5 III)	3800	2.10	0.6	3.5

TABLE 34
Class V Stars

Star	T_{eff} (K)	Ω (10^{-15} sr)	χ^2_ν Absolute	χ^2_ν Relative
α Cen A (G2 V)	5870	1.324	0.7	2.3
α CEN B	5060	0.688	0.6	3

TABLE 35

Class II-III Stars: Type M

Star	T_{eff} (K)	Ω (10^{-15} sr)	χ^2_ν Absolute	χ^2_ν Relative
μ Uma (M0 III)	3730	1.444	0.3	2
β And (M0 III)	3730	3.69	0.1	0.9
α Cet (M2 III)	3650	3.28	0.3	0.02
β Peg (M2.5 II-III)	3470	5.82	0.3	1.4
μ Gem (M3 III)	3410	4.38	0.6	0.7
η Gem (M3 III)	3410	2.82	0.6	1.4
β Gru (M3 II)	3410	14.74	0.2	1.7
γ Cru (M3 II)	3410	13.74	0.2	0.3
∂ Vir (M3 III)	3410	2.36	0.	0.9
2 Cen (M4 III)	3310	1.75	0.8	0.8
σ Lib (M4 III)	3310	2.96	0.7	2.3
ρ Per (M4 II-III)	3310	4.88	0.4	1.8

5.3 RELATIVE BEHAVIOR OF FITS WITH WAVELENGTH

It is easy to divide the fit obtained for each star by the fit obtained for α Boo and evaluate the predicted relative flux at wavelengths close to those at which measurements of relative flux were taken. Tables 36 and 37 give the relative flux values predicted using the fits and the corresponding measured values taken from Tables 20 and 21.

If the fitting functions indeed represent the true spectral shape, the ratio of the predictions to the measurements should come out close to 1 with a standard deviation that is a measure of the average random error in the group of measurements. The average number will not be exactly 1 if there is also an error in the measured value of α Boo, but will differ by about the error (e.g., at 11 μm the average of the photometric magnitudes listed for α Boo was −3.15 ± 0.013, but perhaps −3.14 is the true magnitude).

TABLE 36

Predicted and Measured Relative Flux Values
Primary Standards
(α BOO = 1)

Star	2.2 μm	3.5 μm	11 μm	22 μm	60 μm
α Tau	**0.842**	**0.864**	**0.889**	**0.893**	**0.894**
	0.842	0.876	0.870	0.926	0.870
α Aur	**0.334**	**0.327**	**0.320**	**0.318**	**0.318**
	0.325	0.327	0.318	0.332	0.317
β Gem	**0.170**	**0.168**	**0.166**	**0.166**	**0.166**
	0.171	0.168	0.166	0.169	0.169
α Hya	**0.191**	**0.195**	**0.199**	**0.200**	**0.200**
	0.192	0.196	0.203	0.198	0.197
α Ari	**0.113**	**0.113**	**0.113**	**0.113**	**0.113**
	0.113	0.113	0.110	0.119	0.116
γ Aql	**0.109**	**0.110**	**0.111**	**0.111**	**0.111**
	0.108	0.113	0.108	0.118	0.105
γ Dra	**0.206**	**0.211**	**0.217**	**0.218**	**0.219**
	0.213	0.216	0.207	0.223	0.223
α CMa	**0.226**	**0.209**	**0.194**	**0.191**	**0.191**
	0.225	0.209	0.194	0.196	0.184
α CMi	**0.116**	**0.112**	**0.108**	**0.107**	**0.107**
	0.116	0.109	0.108	0.110	0.110
α Lyr	**0.0621**	**0.0580**	**0.0540**	**0.0533**	**0.0532**
	0.0619	0.0578	0.0536	0.067	0.346

Note: **Bold Face** numbers use the fits; medium face numbers are measured.

Average: Fit Value Divided By Measured Value and the 1-σ Deviation

1.0001	**0.9962**	**1.0119**	**0.9700**	**1.0058**
±0.015	**±0.015**	**±0.019**	**±0.02**	**±0.03**

TABLE 37

Predicted and Measured Relative Flux Values
Secondary Standards
(α BOO = 1)

Star	2.2 μm	3.5 μm	11 μm	22 μm	60 μm
β And	**0.350**	**0.361**	**0.373**	**0.375**	**0.376**
	0.346	0.371	0.365	0.385	0.386
α Cet	**0.310**	**0.312**	**0.325**	**0.327**	**0.328**
	0.296	0.308	0.313	0.332	0.318
μ UMa	**0.134**	**0.138**	**0.143**	**0.143**	**0.144**
	0.136	0.142	0.137	0.149	0.140
β Peg	**0.492**	**0.518**	**0.548**	**0.553**	**0.555**
	0.486	0.518	0.528	0.595	0.558
β Gru	**1.21**	**1.28**	**1.36**	**1.38**	**1.38**
	1.22	1.30	1.30	1.40	1.44
γ Cru	**1.12**	**1.19**	**1.26**	**1.28**	**1.28**
	1.11	1.21	1.27	1.31	1.29
μ Gem	**0.355**	**0.376**	**0.399**	**0.404**	**0.405**
	0.363	0.368	0.383	0.430	0.397
η Gem	**0.232**	**0.246**	**0.261**	**0.264**	**0.265**
	0.211	0.252	0.256	0.279	0.275
ρ Per	**0.380**	**0.406**	**0.436**	**0.441**	**0.443**
	0.374	0.402	0.412	0.474	0.491
∂ Vir	**0.193**	**0.205**	**0.217**	**0.220**	**0.221**
	0.196	0.204	0.218	0.239	0.212
2 Cen	**0.291**	**0.311**	**0.334**	**0.339**	**0.340**
	0.291	0.310	0.349	0.345	0.369
σ Lib	**0.230**	**0.246**	**0.264**	**0.268**	**0.269**
	0.232	0.248	0.273	0.254	0.281

Note: **Bold Face** numbers use the fits; medium face numbers are measured.

Average: Fit Value Divided By Measured Value and the 1σ Deviation

1.008	**0.9945**	**1.018**	**0.9654**	**0.9822**
±0.03	**±0.017**	**±0.033**	**±0.037**	**±0.044**

The results using fits to A- to K-type stars (Table 36) and those using fits to the cooler, less stable, M-type stars (Table 37) are completely consistent, and they seem to indicate that it was valid to extend the use of the fitting function to the cooler stars despite any fears about the effects of molecular opacity and significantly different pressure regimes.

The apparent errors in the relative α Boo flux values obtained from photometry are about 0.2% at 2.2 μm, 0.5% at 3.5 μm, 1.3% at 11 μm, 3.1% at 22 μm, and 0.2% at 60 μm. Except for the 22-μm result, these errors are all in keeping with the average random errors deduced from the standard deviations or with the estimated errors in the α Boo photometry.

5.3.1 Depression in Alpha Boo Spectrum

At 22 μm the deviation of prediction from measurement is larger than can be explained by chance errors in photometry (and an examination of the original photometry shows the effect in several independent data sets). The most likely explanation is that the actual α Boo spectrum deviates from that predicted in this region. However, the small standard deviation in the prediction-measurement ratios shows essentially only that α Boo acts differently from the predictions here, possibly because α Boo is unique among these stars in having an abnormally low proportion of heavy elements in its atmosphere. To take into account the depression, the integrated broadband powers in the 20-μm region can be lowered by 3% for α Boo.

5.4 COMPARISON WITH PREVIOUS CALIBRATIONS

Standard star fluxes reconstructed from previously published calibrated photometric systems can easily be compared with the present predictions at the same wavelength for all the stars in common. The good agreement of these predictions with the short wavelength calibration of Campins et al. [3] is clear from Table 38.

TABLE 38

Percent Difference in Average Stellar Flux Obtained Using Previous Calibrations

	2.2 μm (%)	3.5 μm (%)	11 μm (%)	22 μm (%)	60 μm (%)
IRAS			−1.5	−1.5	−1.5
Rieke [4]			−1.5	+4	
Campins [3]	+0.5	−1.5			
Aerospace [5]			+4	+10	

As far as band ratios are concerned, using our model M fits (including the adjustment for α Boo at 20 μm) is essentially equivalent to using the IRAS calibration. The IRAS researchers extrapolated a 12-μm calibration (obtained from Rieke's 10-μm) to 25 and 60 μm, by assuming that the average of band ratios for a group of standard stars (some hotter than the sun and some cooler) should be the same as the solar band ratios calculated from the Vernazza et al. [1] spectrum, a method reminiscent of solar analog calibration (but having a somewhat more speculative basis, since solar-type stars were not used). The agreement between their band ratios and those in this report is due to the use of the model M solar spectrum as the basis for both. The use of this spectrum has now, however, been justified on a somewhat more rigorous basis.

Since the methods of extrapolation used were not independent, the 60-μm agreement between IRAS and this report does not in itself say anything about the accuracy in the 60-μm calibration. However, the IRAS researchers performed an independent check by extrapolating their 25-μm calibration using asteroids. The 60-μm calibration obtained using observations of three asteroids (the expected spectral emission curves of which were predicted using the standard asteroid model) differed by −4% from the calibration obtained using stars [2]). If one uses a more realistic Saari-Shorthill-type temperature distribution ([38], and the Johnson et al. [39] for the asteroids, the asteroid-based 60-μm calibration differs from the stellar-based by only −1% (Engelke [40]). Thus, there is some reason to think that the calibration curves reported here may be useful out to 60-μm with high accuracy.

The difference between the Vernazza et al.-type and the Rieke calibrations at 20 μm (and the large difference in 10- to 20-μm band ratios) appears to be due to the indirectly extrapolated photometry Rieke uses to transfer the 20-μm β Gem flux to other stars in the system.

5.5 FINAL RESULTS IN THE FORM OF MAGNITUDES

To ease comparison with the astronomical literature, Table 39 displays the results of this work in the form of magnitudes. Once again the absolute scale is defined by

$$\text{zero magnitude} = \frac{1.89 \times 10^{-12}}{\lambda^5(\exp[1.44/\lambda]-1)},$$

Uncertainties in this absolute scale are again 3% below 12 μm, increasing to 6% at 25 μm. The 22-μm α Boo magnitude has been raised by 0.03 to account for the apparent depression mentioned earlier.

TABLE 39

Theoretical Relative Magnitudes

Star	2.2 μm	3.5 μm	4.8 μm	11.0 μm	22.0 μm	60.0 μm
			(± .05)			
α Boo	−3.05	−3.12	−2.96	−3.15	−3.10	−3.10
α Tau	−2.87	−2.96	−2.68	−3.02	−3.01	−2.98
α Aur	−1.86	−1.91	−1.83	−1.91	−1.89	−1.86
β Gem	−1.13	−1.19	−1.07	−1.20	−1.18	−1.15
α Hya	−1.26	−1.35	−1.14	−1.40	−1.38	−1.36
α Ari	−0.69	−0.76	−0.59	−0.79	−0.77	−0.74
γ Aql	−0 65	−0.72	−0.53	−0.76	−0.74	−0.72
α Cen A	−1.54	−1.53	−1.52	−1.48	−1.45	−1.42
α Cen B	−0.60	−0.62	−0.63	−0.60	−0.58	−0.55
α [illegible]Ma	−1.44	−1.42	−1.41	−1.37	−1 34	−1.31
[illegible]CMi	−0.71	−0.74	−0.75	−0.73	−0.71	−0.68
[illegible]Lyr	−0.04	−0.03	−0 02	+0.02	excess	excess
α Car	−1.39	−1.43	−1.44	−1.43	−1.40	−1.37
γ Dra	−1.34	−1.43	−1.20	−1.49	−1 48	−1.45
	±0.03	±0.03	±0.03	±0.06	±0.03	±0.03
β And	−1.91	−2.02	−1 69	−2.08	−2.07	−2.04
μ UMa	−0.90	−1.00	−0.71	−1.06	−1.05	−1.03
σ Cet	−1.75	−1.86	−1.55	−1.93	−1.92	−1.89
	±0.02	±0.02		±0.02	±0.02	±0.02
β Peg	−2.28	−2.40	−2.09	−2.49	−2.48	−2.46
	±0.16	±0.16	±0.17	±0.16	±0.16	±0.16
γ Cru	−3.18	−3.31	−2.97	−3.40	−3.40	−3.37
β Gru	−3.23	−3.39	−3.05	−3.48	−3.47	−3.45
	±0.11	±0.11	±0.12	±0.11	±0.11	±0.11
ρ Per	−2.00	−2.14	−1.77	−2.25	−2.24	−2.22
	±0.15	±0.15	±0.16	±0.15	±0.15	±0.15
μ Gem	−1.94	−2.07	−1.73	−2.16	−2.16	−2.13
	±0.09	±0.09	±0.10	±0.09	±0.09	±0.09
η Gem	−1.46	−1.59	−1.25	−1.69	−1.68	−1.66
	±0.15	±0.15	±0.1	±0.15	±0.15	±0.15
2 Cen	−1.71	−1.85	−1.49	−1.96	−1.96	−1.93
	±0.15	±0.15	±0.15	±0.15	±0.15	±0.15
∂ Vir	−1.27	−1.40	−1.06	−1.49	−1.49	−1.46
σ Lib	−1.46	−1.60	−1.23	−1.70	−1.70	−1.68
	±0.05	±0.05	±0.07	±0.05	±0.05	±0.05
α Her	−3.56	−3.75	−3.43	−3.91	excess	excess
	±0.15	±0.15	±0.15	±0.15		

Note: Uncertainties of 0.01 unless otherwise specified.

APPENDIX A

SELECTION OF POSSIBLE STARS STANDARD STAR NETWORK

G. H. Rieke

27 June 1988

I. Introduction

A network of standard "stars" needs to satisfy the following requirements:

1. They must be of a brightness that can be measured at high accuracy without danger of saturation – i.e., neither too faint nor too bright.
2. They should be distributed well over the sky.
3. They should preferably be non-variable, or at least their brightness should be predictable accurately with a minimum of additional observation or modeling.
4. They should be point-like, so instruments with different fields of view will obtain the same calibration.
5. They should be at well-determined, preferably fixed, positions.
6. Although not essential, it is useful if their spectral energy distributions have a close similarity so that transfers from one standard to another will be comparable without complex spectral modeling.

Some subsets of these requirements can be met by a variety of astronomical objects – e.g., stars, asteroids, compact nebulae. Stars are the most satisfactory solution in terms of meeting all of them. Comparison of the IRAS data with visible photometry in Waters, Cote, and Aumann (1987) [41] shows that the optical to infrared colors are particularly well behaved for stars of spectral types between A0 and K5, it is known from optical photometry that stars over this range of spectral type tend to be non-variable, and stellar atmospheres are best understood over this range (particularly A through G types). Thus, the most satisfactory standard networks will be based on stars of types between A and K.

From the brightness ranges desired at the various wavelengths (requirement 1), it is apparent that there is a more than adequate number of satisfactory stars for standard networks shortward of 10 μm, assuming reasonably state-of-the-art detection systems. 10 and 20 μm are on the Rayleigh Jeans tail of the stellar blackbodies, so stellar fluxes are lower than at the shorter wavelengths; in addition, the thermal background degrades detection limits. Thus, the critical question is how good a standard network can be obtained at these wavelengths. This question has been addressed by drawing up a proposed network and examining its characteristics.

II. Proposed Standard Star Network

The proposed network contains 48 prime stars, with an additional 18 secondary stars of somewhat lower quality. The prime list was selected according to the following criteria:

1. IRAS band 2 (25 μm) magnitude ≤ 0
2. Spectral type between A0 and K7
3. No variability
4. No infrared excess.

The secondary list includes stars with

1. IRAS band 2 (25 μm) magnitude ≤ -1
2. Spectral type between A0 and M5
3. Variability at V (0.56 μm) ≤ 0.4 magnitudes
4. No strong infrared excess.

The secondary list is nearly all M stars with small amplitude variability. It is expected that the variations will be less in the infrared, because of the reduced temperature dependence of flux on the Rayleigh Jeans tail. As a rule of thumb, IR amplitudes may be about 1/3 the visible ones. In addition, the M stars can be expected to have larger mass loss and hence may have infrared features due to dust in circumstellar shells, and their photospheric absorption features will be very strong, making correction to arbitrary bands more difficult than for members of the prime list. Many of these questions can be removed if these stars are observed thoroughly as part of setting up the network. However, the variability is unlikely to be perfectly regular, so it will not be feasible to elevate these stars to the status of prime standards.

These lists are attached as Tables 1a and 1b. The distribution of the proposed network on the sky is illustrated in Figure 1. Particularly with the addition of the secondary list, this network is well distributed on the sky and it would provide a greatly improved basis for all photometry at these wavelengths.

III. The 20 μm Problem

For some experiments, it is desired at 20 μm to have calibrators that are at magnitude -3 or brighter. The proposed network has only four stars this bright, two from the prime list and two from the secondary one. There are at least three forms of tertiary network that could be used to address this problem.

Asteroids have the advantage of smooth spectra that are relatively easy to model to adjust measurements to other bands. They are also point-like. Their positions are not fixed, but they can be obtained accurately with sufficient effort – however, they cannot provide all-sky coverage because they are grouped along the ecliptic, and at any given time even a significant zone of ecliptic can be free of bright asteroids. Moreover, they have variability with earth-asteroid-sun phase angle and many vary with rotation (hence on short time scales) because of albedo variations over their surfaces.

Compact HII regions and planetary nebulae are non-variable and fixed on the sky. However, their spectra are complex and will vary strongly from one to the other. In addition, they are extended at some level. HII regions will tend to be distributed only along the Galactic plane.

Bright infrared stars are fixed on the sky and point-like. They are variable, but with long timescales (~ 200 days or more). Their spectra will bear some family resemblances to each other, but will have much more variety than is desirable to trace measurements to other spectral bands.

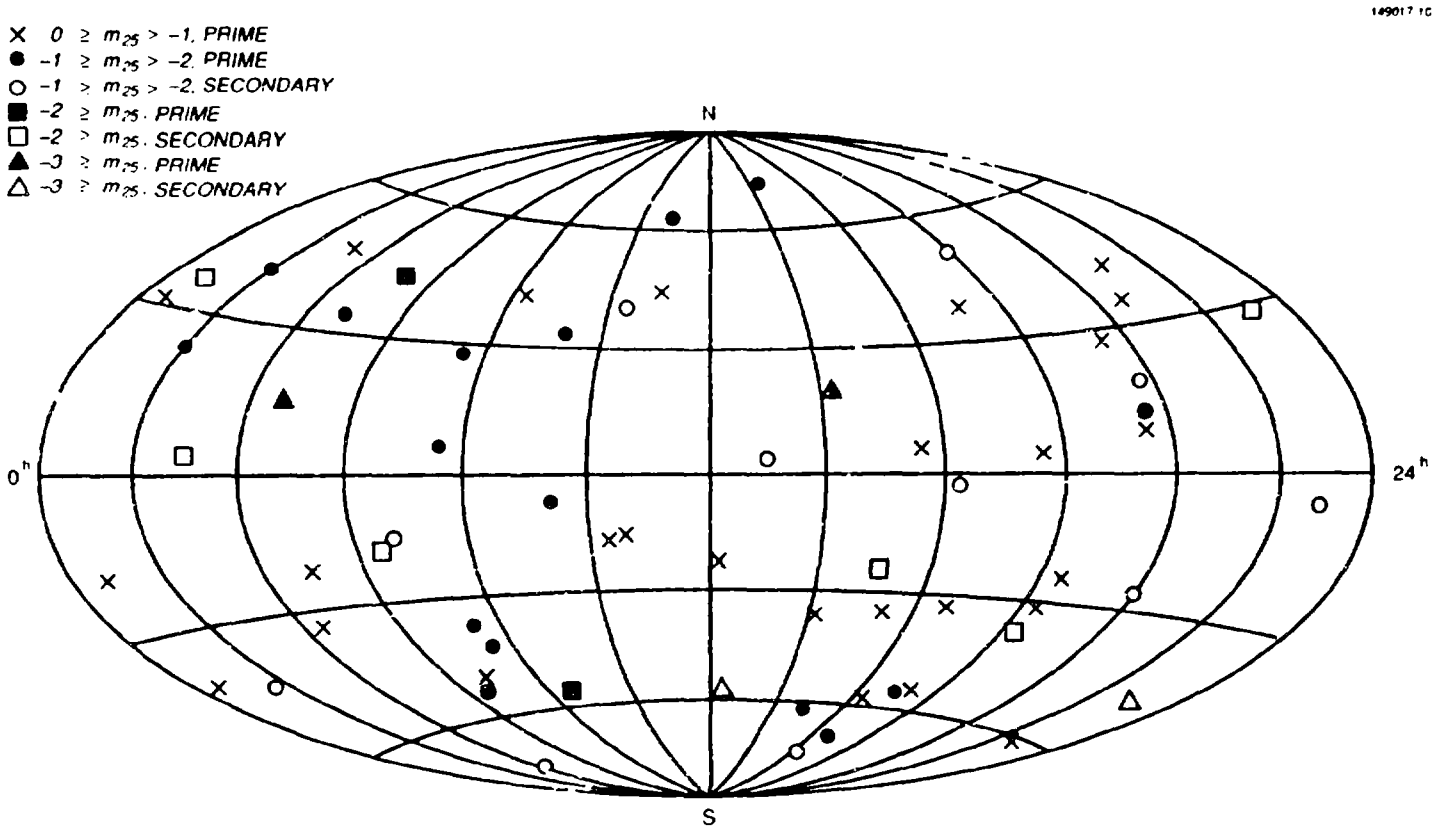

Figure 1. Distribution of proposed standard star network.

Of these choices, the most satisfactory appears to be the bright infrared stars. A check of 25% of the sky shows that there should be 80 to 100 of these objects brighter than −3 at 20 μm, well distributed over the whole sky. Three steps need to be taken to use these objects as calibrators:

1. The standard star network needs to be established to permit accurate measurements of the IR stars.
2. The IR stars need to be observed thoroughly over a variation cycle, so the changes in spectral characteristics can be derived. These changes should repeat fairly closely over future cycles.
3. Close to the time the star is used as a calibrator (preferably within one week), it should be compared with a member of the standard network to establish its current brightness level.

IV. Summary

It appears that a satisfactory calibration strategy can be based on networks of standard stars. For wavelengths out through 10 μm, a conventional standard star network can be established that has enough bright members distributed over the sky to meet foreseen requirements. At 20 μm, experiments requiring very bright calibrators will need to use variable stars. Because the timescale of variability is long, an accurate calibration can still be achieved if the calibrator star is referred to a member of the standard network within one week of the measurement, and if the spectral properties of the calibrator during its variability cycle have been determined either in advance or as part of the measurement series.

TABLE 1a

Prime Standard List

B.S.	Name	α_{2000}	∂_{2000}	Type	m_v	m_{12}	m_{25}
99	a Phe	00 26 17.0	−42 22	18 KO III	2.4	−0.7	−0.7
165	∂ And	00 39 19.6	+30 40	51 K3 III	3.3	−0.1	−0.1
188	β Cet	00 43 35.3	−17 12	59 KO III	2.0	−0.8	−0.8
603	γ^1 And	02 03 53.9	+42 47	19 K3 IIb	2.3	−1.3	−1.4
617	a Ari	02 07 10.3	+23 45	27 K2 IIIb	2.0	−1.1	−1.2
1017	α Per	03 24 19.3	+49 41	51 F5 Ib	1.8	0.0	0.0
1393	43 Eri	04 24 02.1	−34 01	01 K4 III	4.0	0.0	−0.1
1457	α Tau	04 35 55.2	+16 33	30 K5 III	0.8	−3.5	−3.4
1577	i Aur	04 56 59.6	+33 58	09 K3 II	2.7	−1.2	−1.2
1654	ε Lep	05 05 27.6	−22 16	22 K5 III	3.2	−0.7	−0.9
1708	α Aur	05 16 41.3	+45 53	59 G5 III	0.1	−2.3	−2.3
2326	α Car	06 23 57.2	−52 44	41 FO II	−0.7	−1.8	−1.8
2491	α CMa	06 45 08.9	−16 58	42 A1 V	−1.5	−1.7	−1.7
2553	τ Pup	06 49 56.1	−50 53	36 K1 III	2.9	−0.2	−0.2
2773	π Pup	07 17 08.5	−37 51	05 K3 Ib	2.7	−1.6	−1.7
2878	σ Pup	07 29 13.8	−43 05	18 K5 III	3.2	−0.9	−1.0
2943	α CMi	07 39 18 1	+05 30	13 F5 IV	0.4	−1.1	−1.1
2990	β Gem	07 45 18.9	+28 34	01 KO IIIb	1.1	−1.6	−1.6
3275	31 Lyn	08 22 50.1	+43 17	11 K4 III	4.2	0.0	0.0
3307	ε Car	08 22 30.8	−59 34	30 K3 III	1.9	−2.3	−2.4
3705	α Lyn	09 21 03.2	+34 33	23 K7 III	3.1	−1.2	−1.2
3748	α Hya	09 27 35.2	−08 31	39 K3 II	2.0	−1.8	−1.7
4094	μ Hya	10 26 0-5.4	−16 37	50 K4 III	3.8	−0.1	−0.1
4232	ν Hya	10 49 37.4	−16 37	11 K2 III	3.1	−0.2	−0.2

TABLE 1a (Continued)

Prime Standard List

B.S.	Name	α_{2000}	∂_{2000}	Type	m_v	m_{12}	m_{25}
4301	α UMa	11 03 43.6	+61 03	45 KO III	1.8	–1.2	–1.2
4335	ψ UMa	11 09 39.7	+44 54	29 K1 III	3.0	–0.1	–0.1
4630	ε Cru	12 10 07.4	–22 11	37 K2 III	3.0	–0.4	–0.4
5288	θ Cen	14 06 40.8	–36 12	22 KO III	2.1	–0.7	–0.7
5340	α Boo	14 15 39.6	+19 57	10 K1 III	0.0	–3.6	–3.5
5459	α Cen[1]	14 39 36.2	–60 07	50 G2 V/K1 V	0.0	–2.2	–2.2
5563	β UMa	14 50 42.2	+74 20	09 K4 III	2.1	–1.9	–1.9
5705	ϕ^1 Lup	15 21 48.3	–36 41	15 K5 III	3.6	–0.6	–0.6
5854	α Ser	15 44 16.0	+06 32	25 K2 III	2.6	–0.4	–0.4
6217	α TrA	16 48 39.9	–69 40	01 K2 IIb	1.9	–1.7	–1.7
6229	η Ara	16 49 47.0	–59 29	02 K5 III	3.8	–0.6	–0.6
6241	ε Sco	16 50 09.7	–34 36	17 K2 III	2.3	–0.6	–0.7
6285	ζ Ara	16 58 37.1	–55 24	59 K3 III	3.1	–1.1	–1.1
6418	π Her	17 15 02.7	+36 33	48 K3 II	3.2	–0.5	–0.6
6461	β Ara	17 25 17.9	–55 47	31 K3 Ib	2.8	–0.8	–0.9
6603	β Oph	17 43 28.3	+04 02	34 K2 III	2.8	–0.3	–0.3
6859	∂ Sgr	18 20 59.6	–29 41	49 K3 III	2.7	–0.8	–0.9
6913	λ Sgr	18 27 58.1	–25 18	25 K1 III	2.8	–0.1	–0.1
7417	β^1 Cyg	19 30 43.2	+27 35	57 K3 II	3.1	–0.3	–0.4
7525	γ Aql	19 46 15.5	+10 48	36 K3 II	2.7	–1.1	–1.2
7557	α Aql	19 50 46.9	+08 06	52 A7 V	0.8	–0.1	–0.2
7949	ε Cyg	20 46 12.6	+33 13	58 KO III	2.5	–0.4	–0.4
8079	ξ Cyg	21 04 55.8	+43 40	55 K4 Ib	3.7		
8502	α Tuc	22 18 30.1	–60 35	15 K3 III	2.9	–0.8	–0.8

TABLE 1b

Secondary Standard List

B.S.	Name	α_{2000}	∂_{2000}	Type	m_v	m_{12}	m_{25}
337	β And	01 09 43.9	+35 14	37 MO III	2.1	−2.5	−2.5
555	ψ Phe[2]	01 53 38.7	−46 10	18 M4 III	4.4	−1.2	−1.3
911	α Cet[3]	03 02 16.7	+04 23	05 M1.5 III	2.5	−2.3	−2.3
1208	γ Hyi	03 47 14.5	−74 21	14 M2 III	3.2	−1.5	−1.5
2286	μ Gem[4]	06 22 57.6	+22 49	30 M3 III	2.9	−2.6	−2.6
4069	μ UMa	10 22 19.7	+41 58	29 MO III	3.0		
4763	γ Cru	12 31 19.7	−57 47	06 M3.5	1.6	−3.7	−3.8
4910	∂ Vir	12 55 36.1	+03 51	23 M3 III	3.4	−1.9	−1.9
5603	σ Lib[5]	15 04 04.1	−25 55	16 M3 III	3.3	−2.1	−2.0
6056	∂ Oph	16 14 20.6	−03 40	41 MO III	2.7	−1.8	−1.8
6020	∂^1 Aps[6]	16 20 20.7	−78 45	41 M5 III	4.7	−1.3	−1.4
6705	γ Dra[7]	17 56 36 3	+51 20	29 K5 III	2.2	−1 8	−1.9
6832	η Sgr[8]	18 17 37.5	−36 42	45 M3.5 III	3.1	−2.2	−2.2
7536	∂ Sgr[9]	19 47 23.2	+18 03	32 M2 II	3.8	−1.4	−1.4
7650	62 Sgr[10]	20 02 39.4	−27 36	42 M4 III	4.6	−1.3	−1.5
8636	β Gru[11]	22 42 40.0	−46 05	53 M5 III	2.1	−3.8	−3.9
8698	λ Aqr[12]	22 52 36.8	−07 47	34 M2 III	3.7		
8775	β Peg[13]	23 03 46.4	+28 58	04 M2.5 II	2.4		

NOTES TO TABLE 1

1 α Cen is a double with separation 21"; both components contribute to IR flux.

2 ΔV = 0.20 mag

3 ΔV = 0.06 mag

4 ΔV = 0.26 mag

5 ΔV = 0.16 mag

6 ΔV = 0.21 mag

7 ΔV = 0.08 mag

8 ΔV = 0.04 mag

9 ΔV = 0.09 mag

10 ΔV = 0.16 mag

11 ΔV = 0.30 mag

12 ΔV = 0.10 mag

13 ΔV = 0.43 mag

APPENDIX B

INFORMATION FOR INDIVIDUAL STARS

IN ALPHABETIC ORDER

CO Absorption for Stars Without Published Spectra

Generalized CO profile obtained by averaging the normalized absorption depth as a function of wavelength for α Tau, β Peg, and β And:

λ (μm)	Profile (λ)	λ (μm)	Profile (λ)
3.90	–0.01 ±0.01	6.4	–0.41 ±0.14
4.0	–0.04 ±0.02	6.5	–0.37 ±0.13
4.1	–0.21 ±0.05	6.6	–0.34 ±0.13
4.2	–0.38 ±0.1	6.7	–0.30 ±0.12
4.3	–0.70 ±0.07	6.8	–0.27 ±0.11
4.4	–0.91 ±0.08	6.9	–0.24 ±0.10
4.5	–1.02 ±0.04	7.0	–0.22 ±0.09
4.6	–1.05 ±0.03	7.1	–0.18 ±0.09
4.7	–1.02 ±0.05	7.2	–0.19 ±0.08
4.8	–1.00 ±0.02	7.3	–0.13 ±0.07
4.9	–1.00 ±0.02	7.4	–0.11 ±0.07
5.0	–1.01 ±0.02	7.5	–0.09 ±0.06
5.1	–0.99 ±0.02	7.6	–0.07 ±0.06
5.2	–0.96 ±0.02	7.7	–0.06 ±0.05
5.3	–0.90 ±0.04	7.8	–0.06 ±0.05
5.4	–0.85 ±0.07	8.0	–0.05 ±0.05
5.5	–0.81 ±0.09	8.2	–0.04 ±0.04
5.6	–0.77 ±0.06	8.4	–0.03 ±0.03
5.7	–0.74 ±0.06	8.6	–0.03 ±0.03
5.8	–0.70 ±0.07	8.8	–0.02 ±0.02
5.9	–0.65 ±0.09	9.0	–0.02 ±0.02
6.0	–0.59 ±0.11	9.2	–0.01 ±0.01
6.1	–0.55 ±0.13	9.4	0.0
6.2	–0.49 ±0.13	9.6	
6.3	–0.45 ±0.13	9.8	

This profile is normalized so that the depth is 1 at 4.85 μm. To use, one needs the characteristic absorption depth A_{co} for stars of the type of interest. Then create a new spectrum:

$\phi_{new}(\lambda) = \{1 + A_{co} PROF(\lambda)\} \phi_{old}(\lambda)$.

CO Absorption for Stars Without Published Specra

CO profile at 2.5 μm obtained by averaging the normalized absorption depth as a function of wavelength for α Tau, β Peg, and α Boo (See Figure B-1):

λ (μm)	Profile (λ)	λ (μm)	Profile (λ)
2.24	–0.04 ±0.03	2.74	0.45 ±0.18
2.26		2.78	–0.38 ±0.20
2.28	–0.11 ±0.08	2.82	–0.32 ±0.20
2.30	–0.33 ±0.02	2.86	–0.28 ±0.20
2.32	–0.48 ±0.04	2.90	–0.24 ±0.19
2.34	–0.61 ±0.04	2.94	0.19 ±0.14
2.36	–0.71 ±0.04	2.98	–0.15 ±0.15
2.38	–0.75 ±0.04	3.02	–0.13 ±0.13
2.40	–0.78 ±0.03	3.06	–0.12 ±0.12
2.42	–0.80 ±0.02	3.10	–0.11 ±0.11
2.44	–0.79 ±0.02	3.14	–0.10 ±0.10
2.46	–0.79 ±0.01	3.18	–0.10 ±0.10
2.48	–0.78 ±0.01	3.22	–0.09 ±0.09
2.50	–0.77 ±0.03	3.26	–0.07 ±0.07
2.52	–0.76 ±0.05	3.30	–0.06 ±0.06
2.54	–0.74 ±0.05	3.34	–0.05 ±0.05
2.56	–0.70 ±0.07	3.38	–0.06 +0.05
2.58	–0.67 ±0.07	3.42	–0.04 ±0.05
2.60	–0.65 ±0.10	3.46	–0.04 ±0.04
2.62	–0.62 ±0.11	3.50	–0.02 ±0.02
2.64	–0.59 ±0.13	3.54	–0.02 ±0.02
2.66	–0.57 ±0.14	3.58	–0.01 ±0.01
2.68	–0.55 ±0.12	2.70	–0.52 ±0.15

This profile is normalized to correspond to the depth at 2.5 μm when the depth at 4.85 μm is 1. To use, one needs the characteristic absorption depth A_{CO} for stars of the type of interest.

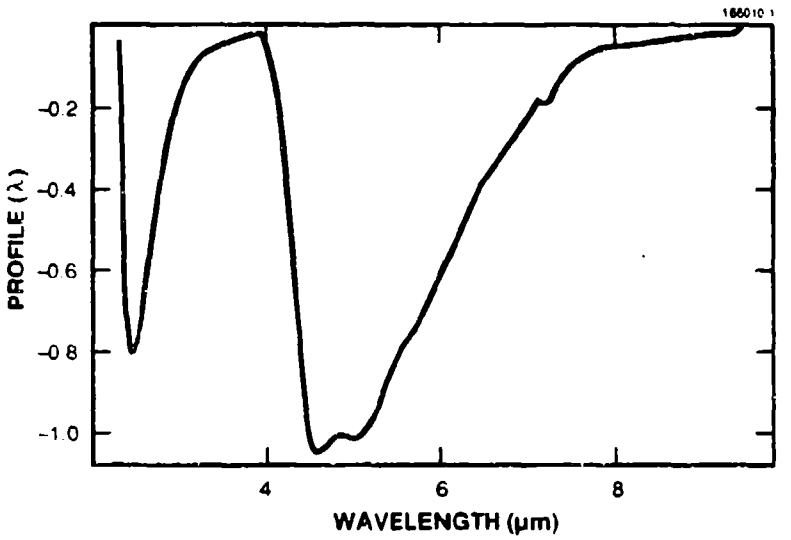

Figure B-1. Average CO absorption profile.

Alpha Arietis (Hamal)
Spectral Type: K2 III
T_{eff}: 4200 K

$$\phi(\lambda) = \frac{1.176 \times 10^{-11}}{\lambda^5 \left(\exp\left(\frac{4.641}{\lambda(1+18.92/\lambda)^{0.182}} \right) - 1 \right)}$$

Data, Fit, and Residuals for α Ari

Wavelength (μm)	Data 10^{-14} $Wcm^{-2}\,\mu^{-1}$	Fit 10^{-14} $Wcm^{-2}\,\mu^{-1}$	Residuals (%)
2.20	7.65 ±3.5%	7.486	+2.2
2.22	7.15 ±3.4%	7.255	−1.4
3.54	1.333 ±3.9%	1.363	−2.2
3.76	1.06 ±3.9%	1.090	−2.8
10.6	0.0198 ±6%	0.02004	−1.2
10.6	0.0202 ±9%	0.02004	+0.8
11.34	0.0155 ±9%	0.01535	+1.0
21.0	0.00137 ±10%	0.00132	+3.8

$\chi^2 = 1.6$, reduced $\chi^2_\nu = 0.23$

Apparent 1σ random error = 2.2%

CO band at 4.7 and 2.5 μm
Average profile scaled by $A_{CO} = 0.16$

Beta Andromedae (Mirach)
Spectral Type: M0 III
T_{eff}: 3730 K

$$\phi(\lambda) = \frac{4.395 \times 10^{-11}}{\lambda^5 \left(\exp\left(\frac{5.226}{\lambda(1 + 21.30/\lambda)^{0.182}} \right) - 1 \right)}$$

Data, Fit, and Residuals for α Ari

Wavelength (μm)	Data 10^{-14} $Wcm^{-2}\ \mu^{-1}$	Fit 10^{-14} $Wcm^{-2}\ \mu^{-1}$	Residuals (%)
2.20	23.4 ±3.6%	23.16	+1.0
2.22	21.9 ±3.4%	22.46	–2.5
3.54	4.38 ±3.9%	4.351	+0.7
3.76	3.49 ±3.9%	3.489	0.0
10.6	0.0657 ±4.0%	0.06607	–0.6
10.6	0.0672 ±7%	0.06607	+1.7
11.34	0.0513 ±8%	0.05066	+1.3
21.0	0.00444 ±10%	0.004393	+1.1

$\chi^2 = 0.77$, reduced $\chi^2_\nu = 0.11$
Apparent 1σ random error = 1.3%

CO band at 4.7 and 2.5 μm
Strecker et al. [35]

Discrete Tabulation of CO Bands for Use in Integration Over Bands

Beta and CO band absorption at 2.5 μm

l (μm)	1 - CO	l (μm)	1-CO
2.26	1.00	2.74	0 .886
2.28	0.972	2.78	0.900
2.30	0.932	2.82	0.913
2.32	0.893	2.86	0.929
2.34	0.861	2.90	0.943
2.36	0.838	2.94	0.957
2.38	0.823	2.98	0.968
2.40	0.818	3.02	0.977
2.42	0.818	3.06	0.984
2.44	0.811	3.10	0.989
2.46	0.815	3.14	0.992
2.48	0.819	3.18	0.992
2.50	0.822	3.22	0.989
2.52	0.824	3.26	0.997
2.54	0.833	3.30	0.998
2.56	0.834	3.34	0.998
2.58	0.842	3.38	1.00
2.60	0.849	3.42	
2.62	0.848	3.46	
2.64	0.855	3.50	
2.66	0.861	3.66	
2.68	0.867	3.70	
2.70	0.872	3.74	
		3.78	

Beta and CO band absorption at 5 μm

3.90	0.990	6.4	0.851
4.0	0.985	6.5	0.865
4.1	0.946	6.6	0.873
4.2	0.869	6.7	0.886
4.3	0.845	6.8	0.897
4.4	0.810	6.9	0.907
4.5	0.773	7.0	0.918
4.6	0.721	7.1	0.929
4.7	0.722	7.2	0.937
4.8	0.737	7.3	0.947
4.9	0.734	7.4	0.953
5.0	0.733	7.5	0.963
5.1	0.739	7.6	0.967
5.2	0.743	7.7	0.972
5.3	0.754	7.8	0.976
5.4	0.756	7.9	0.982
5.5	0.762	8.0	0.986
5.6	0.780	8.2	0.986
5.7	0.790	8.3	0.990
5.8	0.798	8.4	0.990
5.9	0.806	8.6	0.992
6.0	0.815	8.8	0.995
6.1	0.820	9.0	0.996
6.2	0.834	9.3	0.998
6.3	0.843	9.6	1.00

See Figure B-2.

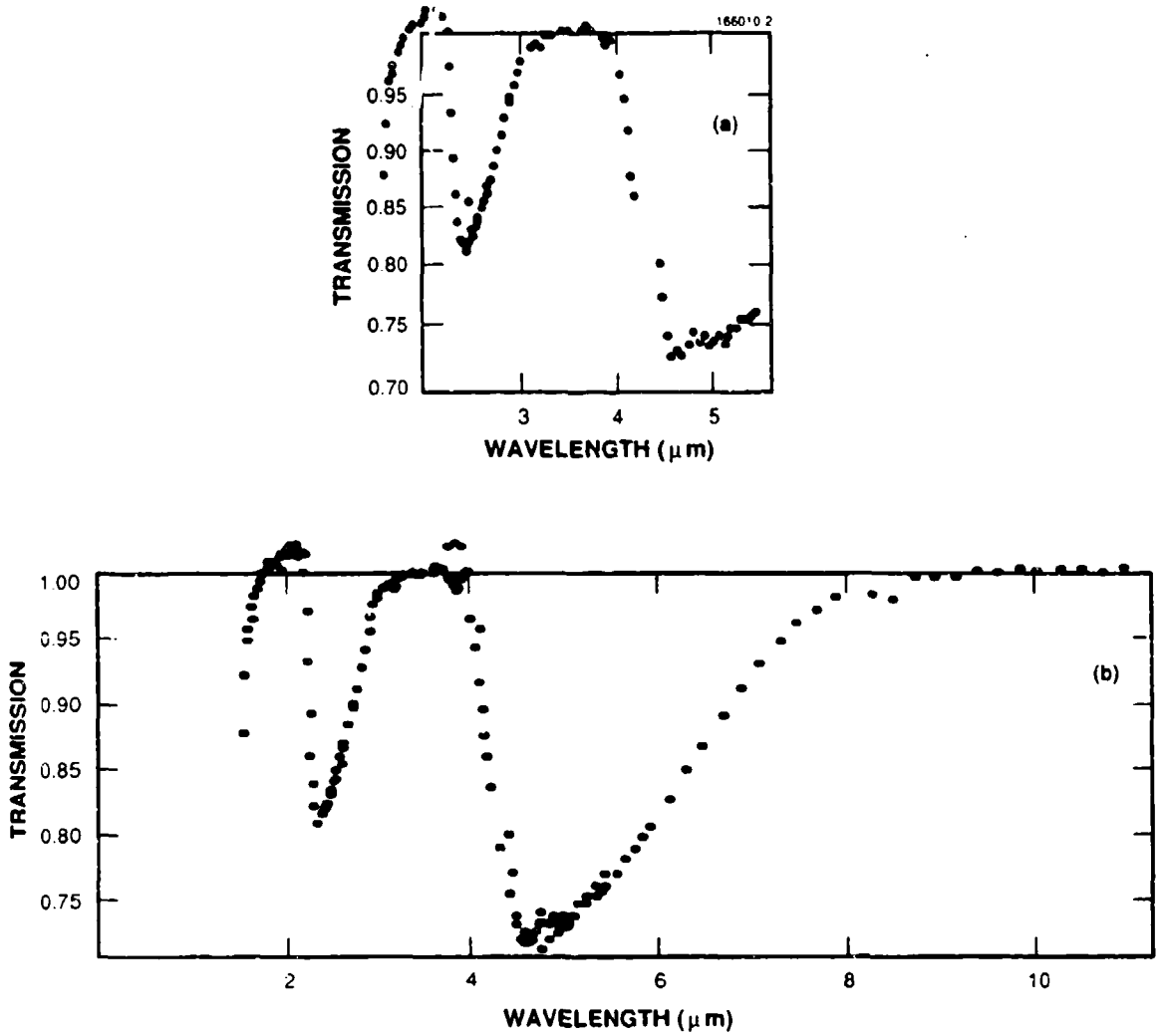

Figure B-2. Beta And CO bands at 2.5 and 5μm: (a) Strecker et al. data and (b) same data with projection beyond 5.5μm superimposed.

Gamma Aquilae (Tarazed)

Spectral Type: K3 II

T_{eff}: 4100 K

$$\phi(\lambda) = \frac{1.178 \times 10^{-11}}{\lambda^5 \left(\exp\left(\frac{4.755}{\lambda(1+19.38/\lambda)^{0.182}} \right) - 1 \right)}$$

Data, Fit, and Residuals for γ Aql

Wavelength (μm)	Data 10^{-14} $Wcm^{-2}\,\mu^{-1}$	Fit 10^{-14} $Wcm^{-2}\,\mu^{-1}$	Residuals (%)
2.20	7.31 ±3.5%	7.224	+1.2
2.22	6.84 ±3.4%	7.003	–2.3
3.54	1.33 ±4%	1.323	+0.5
3.76	1.06 ±4.4%	1.059	+0.1
10.6	0.0195 ±4%	0.01958	–0.4
10.6	0.0199 ±7%	0.01958	+1.6
11.34	0.0152 ±8%	0.01500	+1.3
21.0	0.00136 ± 10%	0.001295	+5

$\chi^2 = 0.93$, reduced $\chi^2_\nu = 0.13$

Apparent 1σ random error = 2.1%

CO band at 4.7 and 2.5 μm
Average profile scaled by $A_{CO} = 0.18$

Alpha Aurigae (Capella)

Spectral Type: G8 III

T_{eff}: 4600 K

$$\phi(\lambda) = \frac{3.016 \times 10^{-11}}{\lambda^5 \left(\exp\left(\frac{4.238}{\lambda(1+17.27/\lambda)^{0.182}} \right) - 1 \right)}$$

Data, Fit, and Residuals for α Aur

Wavelength (μm)	Data 10^{-14} $Wcm^{-2}\,\mu^{-1}$	Fit 10^{-14} $Wcm^{-2}\,\mu^{-1}$	Residuals (%)
2.20	22.0 ±3.5%	22.06	–0.3
2.22	20.6 ±3.5%	21.37	–3.6
3.54	3.86 ±3.7%	3.929	–1.8
3.76	3.08 ±3.7%	3.136	–1.8
10.6	0.0573 ±3.4%	0.05656	+1.3
10.6	0.0585 ±7%	0.05656	+3.4
11.34	0.0447 ±8%	0.04330	+3.2
21.0	0.00383 ±10%	0.003723	+2.9

$\chi^2 = 2.2$, reduced $\chi^2_\nu = 0.31$

Apparent 1σ random error = 2.5%

CO band at 4.7 and 2.5 μm

Average profile scaled by $A_{CO} = 0.08$

Alpha Bootis (Arcturus)

Spectral Type: K2 III

T_{eff}: 4200 K

$$\phi(\lambda) = \frac{1.038 \times 10^{-10}}{\lambda^5 \left(\exp\left(\frac{4.642}{\lambda(1+18.9/\lambda)^{0.182}} \right) - 1 \right)}$$

Data, Fit, and Residuals for α Boo

Wavelength (μm)	Data 10^{-14} $Wcm^{-2}\,\mu^{-1}$	Fit 10^{-14} $Wcm^{-2}\,\mu^{-1}$	Residuals (%)
2.20	67.70 ±3.2%	66.1	+2.4
2.22	63.3 ±3.2%	64.0	−1.1
3.54	11.80 ±3.5%	12.03	−1.9
3.76	9.41 ±3.5%	9.62	−2.2
10.6	0.1801 ±3.5%	0.1769	+1.8
10.6	0.184 ±7%	0.1769	+4
11.34	0.1406 ±8%	0.1355	+3.8
21.0	0.01154 ±10%	0.01169	−1.3

$\chi^2 = 2.2$, reduced $\chi^2_\nu = 0.31$

Apparent 1σ random error = 2.5%

CO band at 4.7 μm
Average profile scaled by $A_{CO} = 0.16$

CO band at 2.5 μm
Strecker et al. [35]

Discrete Tabulation of CO Bands for Use Integration Over Bands

Alpha Boo CO band absorption at 2.5 μm

l (μm)	1 - CO	l (μm)	1-CO
2.22	1.00	2.70	0 .920
2.24	1.00	2.74	0.938
2.26	0.995	2.78	0.951
2.28	0.969	2.82	0.967
2.30	0.943	2.86	0.976
2.32	0.911	2.90	0.980
2.34	0.883	2.94	0.988
2.36	0.867	2.98	0.999
2.38	0.857	3.02	0.998
2.40	0.851	3.06	0.994
2.42	0.847	3.10	0.997
2.44	0.848	3.14	0.997
2.46	0.850	3.18	0.994
2.48	0.853	3.22	0.994
2.50	0.856	3.26	0.997
2.52	0.864	3.30	1.00
2.54	0.868	3.34	0.996
2.56	0.876	3.38	0.999
2.58	0.882	3.42	1.00
2.60	0.890	3.46	
2.62	0.895	3.5	
2.64	0.902	3.54	
2.66	0.908	3.58	

Alpha Boo CO band absorption at 5 μm

3.90	0.998	6.4	0.934
4.0	0.994	6.5	0.941
4.1	0.966	6.6	0.946
4.2	0.939	6.7	0.952
4.3	0.888	6.8	0.957
4.4	0.854	6.9	0.962
4.5	0.837	7.0	0.965
4.6	0.832	7.1	0.971
4.7	0.837	7.2	0.970
4.8	0.840	7.3	0.979
4.9	0.840	7.4	0.982
5.0	0.838	7.5	0.986
5.1	0.842	7.6	0.989
5.2	0.846	7.7	0.990
5.3	0.856	7.8	0.990
5.4	0.864	8.0	0.992
5.5	0.870	8.2	0.994
5.6	0.877	8.4	0.995
5.7	0.882	8.6	0.995
5.8	0.888	8 8	0.997
5.9	0.896	9.0	0.997
6.0	0.906	9.2	0.998
6.1	0.912	9.4	1.00
6.2	0.922	9.6	1.00
6.3	0.928	9.8	1.00

See Figure B-3.

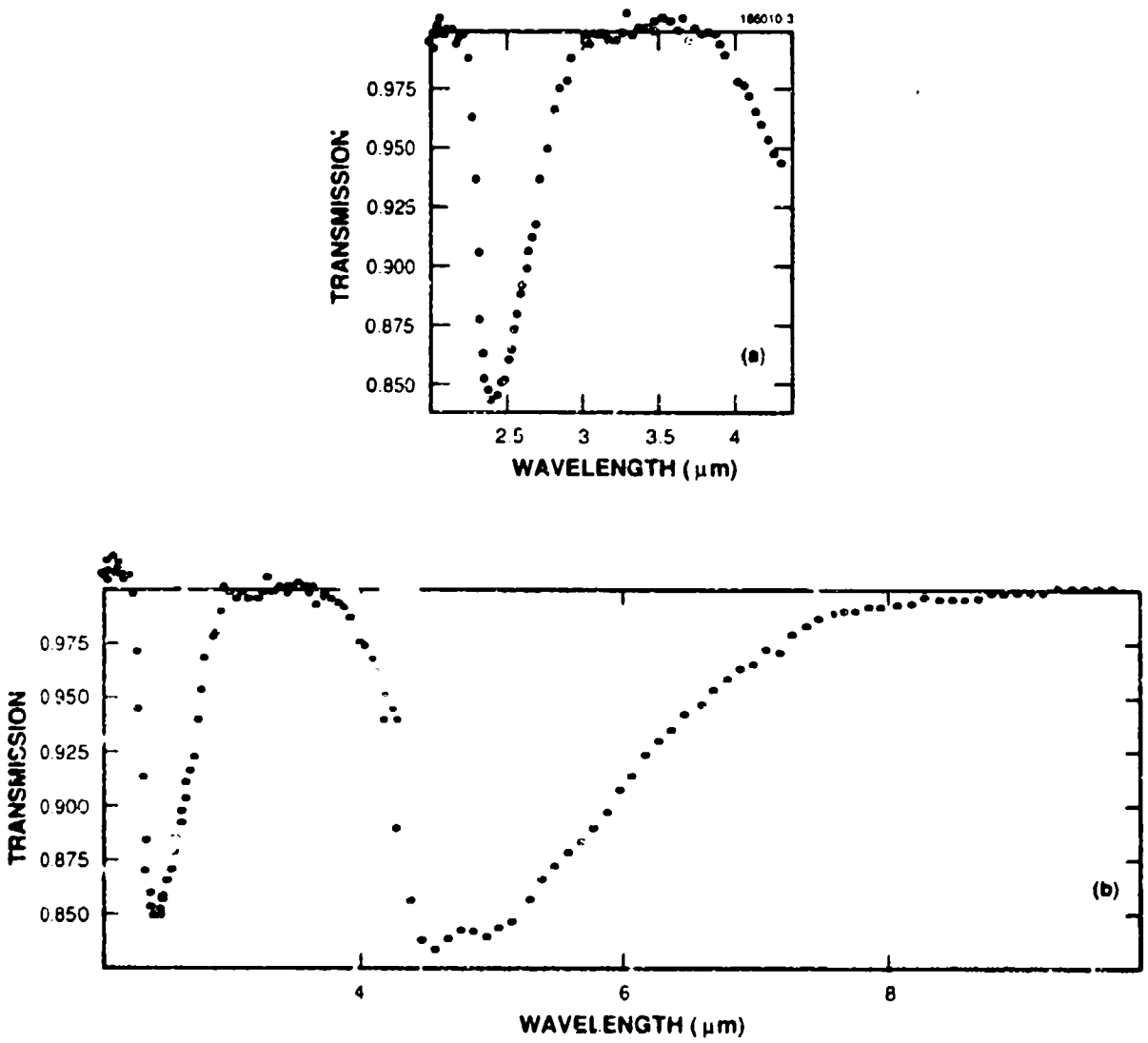

Figure B-3. Alpha Boo CO bands. (a) Strecker et al. data and (b) extension of data for α Boo using the average CO profile scaled to a depth of 16% at 4.8μm.

Alpha Canis Majoris (Sirius)

Spectral Type: A1 V

T_{eff}: 9330 K

t: 6104 K

$$\phi(\lambda) = \frac{1.366 \times 10^{-11}}{\lambda^5 \left(\exp\left(\frac{3.19}{\lambda(1+13.02/\lambda)^{0.182}} \right) - 1 \right)}$$

Data, Fit, and Residuals for α CMa

Wavelength (μm)	Data 10^{-14} $Wcm^{-2}\,\mu^{-1}$	Fit 10^{-14} $Wcm^{-2}\,\mu^{-1}$	Residuals (%)
1.60	45.7 ±3.5%	46.55	−1.8
2.20	15.2 ±3.6%	14.92	+1.9
2.22	14.2 ±3.4%	14.44	−1.7
3.54	2.47 ±3.6%	2.516	−1.8
3.76	1.967 ±3.6%	1.998	−1.6
4.80	0.775 ±5.2%	0.7782	−0.4
10.6	0.0349 ±3.7%	0.03431	+1.7
10.6	0.0357 ±7%	0.03431	+4
11.34	0.0273 ±8%	0.02623	+4.1
21.0	0.00226 ±10%	0.002238	+1.0

$\chi^2 = 2.1$, reduced $\chi^2_\nu = 0.26$

Apparent 1σ random error = 2.3%

No CO bands

Alpha Canis Minoris (Procyon)
Spectral Type: F5 IV
T_{eff}: 6700 K
t: 4869 K

$$\phi(\lambda) = \frac{9.611 \times 10^{-12}}{\lambda^5 \left(\exp\left(\frac{4}{\lambda (1 + 16.32/\lambda)^{0.182}} \right) - 1 \right)}$$

Data, Fit, and Residuals for α CMi

Wavelength (μm)	Data 10^{-14} $Wcm^{-2}\,\mu^{-1}$	Fit 10^{-14} $Wcm^{-2}\,\mu^{-1}$	Residuals (%)
1.60	22.7 ±3.6%	22.83	–0.6
2.20	7.85 ±3.6%	7.647	+2.7
2.22	7.34 ±3.4%	7.406	–0.9
3.54	1.286 ±3.6%	1.345	–4.4
3.76	1.026 ±3.9%	1.072	–4.3
4.80	0.420 ±5.4%	0.4234	–0.8
10.6	0.0195 ±3.9%	0.01913	+1.9
10.6	0.0199 ±7%	0.01913	+4.0
11.34	0.0152 ±8%	0.01464	+3.8
21.0	0.0127 ±10%	0.00125	+1.1

$\chi^2 = 4.2$, reduced $\chi^2_\nu = 0.52$

Apparent 1σ random error = 2.9%

No CO bands

Alpha Carinae (Canopus)

Spectral Type: F0 I

T_{eff}: 7500 K

t: 4766 K

$$\phi(\lambda) = \frac{1.857 \times 10^{-11}}{\lambda^5 \left(\exp\left(\frac{4.09}{\lambda(1+16.67/\lambda)^{0.182}} \right) - 1 \right)}$$

Data, Fit, and Residuals for α Car

Wavelength (μm)	Data 10^{-14} $Wcm^{-2}\ \mu^{-1}$	Fit 10^{-14} $Wcm^{-2}\ \mu^{-1}$	Residuals (%)
1.60	42.0 ±3.6%	42.54	−1.3
2.20	14.6 ±3.6%	14.32	+2.0
2.22	13.7 ±3.6%	13.87	−1.2
3.54	2.44 ±3.9%	2.530	−3.6
3.76	1.95 ±3.9%	2.018	−3.4
4.80	0.799 ±5.4%	0.7979	+0.1
10.6	0.0371 ±3.8%	0.03614	+2.7
10.6	0.0379 ±7%	0.03614	+4.9
11.34	0.0290 ±8%	0.02766	+4.8
21.0	0.00240 ±10%	0.002375	+1.1

$\chi^2 = 3$, reduced $\chi^2_\nu = 0.38$

Apparent 1σ random error = 3%

No CO bands

Alpha Centauri A (Rigel Kent)

Spectral Type: G2 V

T_{eff}: 5870 K

$$\phi(\lambda) = \frac{1.577 \times 10^{-11}}{\lambda^5 \left(\exp\left(\frac{3.321}{\lambda(1+13.54/\lambda)^{0.182}} \right) - 1 \right)}$$

Data, Fit, and Residuals for α Cen A

Wavelength (μm)	Data 10^{-14} $Wcm^{-2}\,\mu^{-1}$	Fit 10^{-14} $Wcm^{-2}\,\mu^{-1}$	Residuals (%)
1.60	47.8 ±4%	50.62	−5.5
2.20	17.06 ±3.8%	16.34	+4.4
2.22	15.9[illegible] ±3.6%	15.81	+0.9
3.54	2.78 ±3.9%	2.773	+0.3
3.76	2.22 ±3.9%	2.203	+0.8
4.80	0.871 ±5.3%	0.860	+1.3
10.6	0.0398 ±4%	0.03806	+4.6
10.6	0.0407 ±7%	0.03806	+6.9
11.34	0.0311 ±[illegible]%	0.02910	+6.9
21.0	0.00244 ±10%	0.000248	−1.6

$\chi^2 = 6.5$, reduced $\chi^2_\nu = 0.72$

Apparent 1σ random error = 4.1%

[illegible] CO bands

Alpha Centauri B

Spectral Type: K1 V

T_{eff}: 5060 K

$$\phi(\lambda) = \frac{8.194 \times 10^{-12}}{\lambda^5 \left(\exp\left(\frac{3.853}{\lambda (1 + 15.70/\lambda)^{0.182}} \right) - 1 \right)}$$

Data, Fit, and Residuals for α Cen B

Wavelength (μm)	Data 10^{-14} $Wcm^{-2}\ \mu^{-1}$	Fit 10^{-14} $Wcm^{-2}\ \mu^{-1}$	Residuals (%)
1.60	20.7 ±4%	20.76	–0.3
2.20	7.38 ±3.8%	6.894	+7.0
2.22	6.90 ±3.6%	6.675	+3.4
3.54	1.204 ±3.9%	1.203	+0.1
3.76	0.960 ±3.9%	0.9584	+0.2
4.80	0.370 ±5%	0.3774	–2.0
10.6	0.0171 ±4%	0.01697	+0.8
10.6	0.0175 ±7%	0.01697	+3.1
11.34	0.0134 ±8%	0.01299	+3.2
21.0	0.00105 ±10%	0.001113	–5.7

$\chi^2 = 5.2$, reduced $\chi^2_\nu = 0.58$

Apparent 1σ random error = 3.4%

No CO bands

2 Centauri

Spectral Type: M4III

T_{eff}: 3310 K

$$\phi(\lambda) = \frac{4.466 \times 10^{-11}}{\lambda^5 \left(\exp\left(\frac{5.890}{\lambda(1 + 24.00/\lambda)^{0.182}} \right) - 1 \right)}$$

Data, Fit, and Residuals for 2 Cen

Wavelength (μm)	Data 10^{-14} $Wcm^{-2}\,\mu^{-1}$	Fit: 10^{-14} $Wcm^{-2}\,\mu^{-1}$	Residuals (%)
2.20	19.7 ±3.6%	19.24	+2.4
2.22	18.4 ±3.4%	18.68	−1.5
3.54	3.66 ±3.6%	3.748	−2.3
3.76	2.92 ±3.7%	3.016	−3.2
10.6	0.0629 ±5.3%	0.05904	+6.6
10.6	0.0642 ±8%	0.05904	+8.7
11.34	0.0495 ±9%	0.04532	+9.2
21.0	0.00398 ±10%	0.003954	+0.7

$\chi^2 = 5.6$, reduced $\chi^2_\nu = 0.80$

Apparent 1σ random error = 5.3%

CO bands at 4.7 and 2.5 μm
Average profile scaled by $A_{CO} = 0.32$

Muu Cephi (Erakis)

Spectral Type: M2 I

Variable with Circumstellar Dust

Below 4.5 μm,

$$\phi(\lambda) = \frac{1.53 \times 10^{-10}}{\lambda^5 \left(\exp\left(\frac{9.75}{\lambda(1+39.7/\lambda)^{0.182}} \right) - 1 \right)}$$

4.5- to 14-μm portion of Muu Cephi spectrum

λ	Log(ϕ)	λ	Log(ϕ)	λ	Log(ϕ)
4.5	−13.729	6.9	−14.231	9.3	−14.252
4.6	−13.777	7.0	−14.273	9.4	−14.251
4.7	−13.762	7.1	−14.304	9.5	−14.239
4.8	−13.791	7.2	−14.323	9.6	−14.242
4.9	−13.802	7.3	−14.365	9.7	−14.246
5.0	−13.813	7.4	−14.371		
5.1	−13.870	7.5	−14.392	10.00	−14.225
5.2	−13.854	7.6	−14.413	10.25	−14.246
5.3	−13.863	7.7	−14.412	10.50	−14.291
5.4	−13.871	7.8	−14.441	10.75	−14.351
5.5	−13.879	7.9	−14.447	11.00	−14.400
5.6	−13.911	8.0	−14.457	11.25	−14.456
5.7	−13.930	8.1	−14.461	11.50	−14.513
5.8	−13.938	8.2	−14.463	11.75	−14.583
5.9	−13.957	8.3	−14.444	12.00	−14.629
6.0	−13.987	8.4	−14.450	12.25	−14.691
6.1	−14.021	8.5	−14.436	12.50	−14.751
6.2	−14.016	8.6	−14.436	12.75	−14.809
6.3	−14.059	8.7	−14.436	13.00	−14.843
6.4	−14.090	8.8	−14.437	13.25	−14.873
6.5	−14.120	8.9	−14.366	13.50	−14.902
6.6	−14.151	9.0	−14.330	13.75	−14.940
6.7	−14.170	9.1	−14.290	14.00	−14.959
6.8	−14.213	9.2	−14.247		

A_{λ} = 0.4

16- to 32-μm portion of Muu Cephi spectrum

		21.50	−15.418	27.25	−15.824
16.00	−15.144	21.75	−15.436	27.50	−15.838
16.25	−15.127	22.00	−15.455	27.75	−15.857
16.50	−15.126	22.25	−15.475	28.00	−15.876
16.75	−15.126	22.50	−15.495	28.25	−15.896
17.00	−15.126	22.75	−15.519	28.50	−15.915
17.25	−15.127	23.00	−15.542	28.75	−15.929
17.50	−15.142	23.25	−15.557	29.00	−15.943
17.75	−15.138	23.50	−15.571	29.25	−15.961
18.00	−15.142	23.75	−15.593	29.50	−15.978
18.25	−15.169	24.00	−15.615	29.75	−15.993
18.50	−15.180	24.25	−15.631	30.00	−16.008
18.75	−15.210	24.50	−15.647	30.25	−16.028
19.00	−15.218	24.75	−15.667	30.50	−16.048
19.25	−15.237	25.00	−15.686	30.75	−16.062
19.50	−15.256	25.25	−15.700	31.00	−16.077
19.75	−15.272	25.50	−15.714	31.25	−16.096
20.00	−15.289	25.75	−15.729	31.50	−16.115
20.25	−15.311	26.00	−15.743	31.75	−16.134
20.50	−15.332	26.25	−15.762	32.00	−16.153
20.75	−15.352	26.50	−15.781		
21.00	−15.371	26.75	−15.795		
21.25	−15.394	27.00	−15.810		

See Figure B-4.

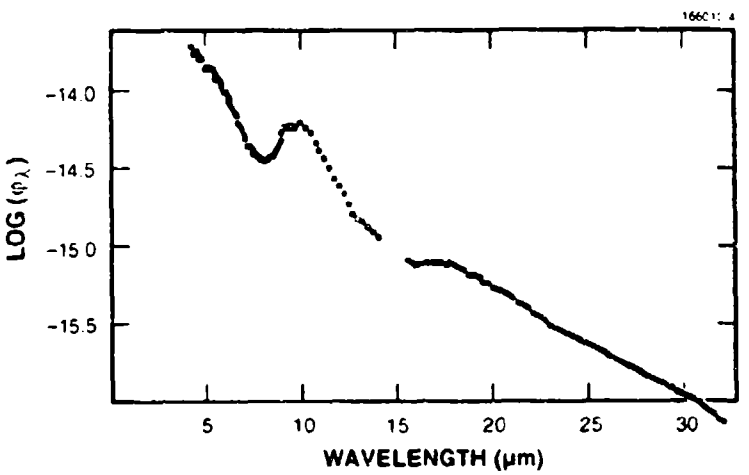

Notes.

The 4.5- to 14-μm portion of the spectrum is calibrated by making comparison observations of the moon (Russell et al. [42]). The emissivity of moon rock has a complicated wavelength dependence between about 5 and 10 μm (Murkray et al. [43]), therefore one should be somewhat skeptical of this part of the above μ Cep spectrum.

The 2.2- to 4.5-μm portion was estimated by fitting the two-parameter spectral function derived in this work (with a $T_{eff} \approx 2000$ to the 2- to 4-μm work of Russell et al.). If one wishes to minimize the use of the lunar calibrated part of the spectrum, one can use the fitted curve out to 7.5 μm or so.

The 16- to 32-μm portion is taken from Forrest et al. [44])

The normalization of the two spectral segments, 2.2 to 14 μm and 16 to 30 μm, were set so that when integrated over the 12- and 25-μm IRAS bands, respectively (the shape of which is available in Beichmann et al.), and compared to the standard stars integrated over these bands, one gets the same relative magnitudes obtained in the IRAS survey.

Figure B-4. Spectrum of Muu Cephi (Erakis), M2-I supergiant with circumstellar dust.

Alpha Ceti (Menkar)

Spectral Type: M2 III

T_{eff} : 3650 K

$$\phi(\lambda) = \frac{3.906 \times 10^{-11}}{\lambda^5 \left(\exp\left(\frac{5.341}{\lambda(1+21.77/\lambda)^{0.182}} \right) - 1 \right)}$$

Data, Fit, and Residuals for α Cet

Wavelength (μm)	Data 10^{-14} Wcm^{-2} μ^{-1}	Fit 10^{-14} Wcm^{-2} μ^{-1}	Residuals (%)
2.20	20.07 ±4.0%	19.86	+0.7
2.22	18.74 ±3.9%	19.27	−2.8
3.54	3.63 ±4.1%	3.755	−3.3
3.76	2.90 ±4.2%	3.013	−3.8
10.6	0.0564 ±4%	0.05738	−1.7
10.6	0.0576 ±7%	0.05738	+0.4
11.34	0.0440 ±8%	0.04400	0.0
21.0	0.00383 ±10%	0.003820	+0.3

$\chi^2 = 2.2$, reduced $\chi^2_\nu = 0.31$

Apparent 1σ random error = 2.1%

CO bands at 4.7 and 2.5 μm
Strecker et al. [35]

Discrete Tabulation of CO Bands for Use in Integration Over Bands

Alpha Cet CO band absorption at 2.5 μm

λ (μm)	1 – CO	λ (μm)	1–CO
2.26	0.988		
2.28	0.963		
2.30	0.912		
2.32	0.876		
2.34	0.841		
2.36	0.798	2.94	0.937
2.38	0.796	2.98	0.940
2.40	0.799	3.02	0.945
2.42		3.06	0.948
2.44		3.10	0.954
2.46		3.14	0.954
2.48		3.18	0.956
2.50		3.22	0.956
2.52		3.26	0.954
2.54		3.30	0.948
2.56		3.34	0.953
2.58		3.38	0.959
2.60		3.42	0.965
2.62		3.46	0.968
2.64		3.50	0.972
2.66		3.66	0.990
2.68		3.70	0.990
2.70		3.74	0.994
		3.78	0.997

Alpha Cet CO band absorption at 5 μm

3.90	1.00	6.4	0.928
4.0	0.996	6.5	0.933
4.1	0.920	6.6	0.933
4.2	0.856	6.7	0.931
4.3	0.770	6.8	0.923
4.4	0.694	6.9	0.928
4.5	0.686	7.0	0.940
4.6	0.695	7.1	0.950
4.7	0.712	7.2	0.960
4.8	0.722	7.3	0.967
4.9	0.756	7.4	0.976
5.0	0.757	7.5	0.984
5.1	0.767	7.6	0.993
5.2	0.770	7.7	1.00
5.3	0.783	7.8	1.00
5.4	0.790		
5.5	0.827		
5.6	0.849		
5.7	0.865		
5.8	0.875		
5.9	0.887		
6.0	0.897		
6.1	0.907		
6.2	0.914		
6.3	0.921		

See Figure B-5.

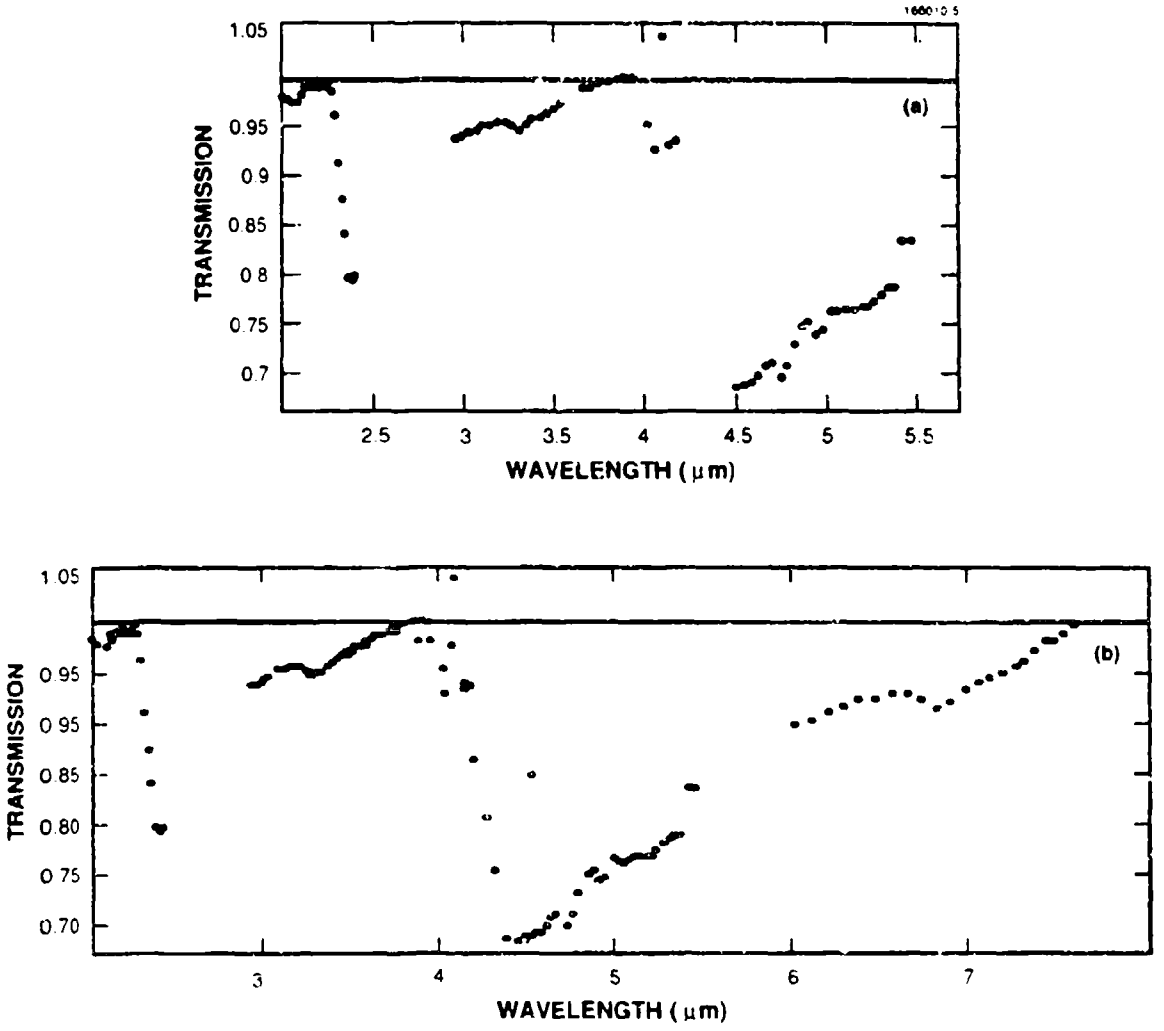

Figure B-5. Alpha Ceti CO bands: (a) Strecker et al. data and (b) same data with postulated extension beyond 5.5 μm based on affine transformation of 2.5-μm band.

Gamma Crucis

Spectral Type: M3 II - III

T_{eff}: 4200 K

$$\phi(\lambda) = \frac{1.636 \times 10^{-10}}{\lambda^5 \left(\exp\left(\frac{5.717}{\lambda(1+23.30/\lambda)^{0.182}} \right) - 1 \right)}$$

Data, Fit, and Residuals for γ Cru

Wavelength (μm)	Data 10^{-14} $Wcm^{-2}\,\mu^{-1}$	Fit 10^{-14} $Wcm^{-2}\,\mu^{-1}$	Residuals (%)
2.20	75.1 ±3.8%	74.20	+1.2
2.22	70.3 ±3.6%	72.02	–2.4
3.54	14.28 ±3.9%	14.32	–0.3
3.76	11.39 ±3.9%	11.51	–1.0
10.6	0.229 ±5%	0.2234	+2.5
10.6	0.234 ±8%	0.2234	+4.7
11.34	0.179 ±9%	0.1714	+4.4
21.0	0.0151 ±10%	0.01494	+1.1

$\chi^2 = 1.5$, reduced $\chi^2_\nu = 0.21$

Apparent 1σ random error = 2.7%

CO bands at 4.7 and 2.5 μm

Average profile scaled by $A_{CO} = 0.30$

Gamma Draconis (Etanin)

Spectral Type: K5 III

T_{eff}: 3800 K

$$\phi(\lambda) = \frac{2.501 \times 10^{-11}}{\lambda^5 \left(\exp\left(\frac{5.13}{\lambda (1 + 20.91/\lambda)^{0.182}} \right) - 1 \right)}$$

Data, Fit, and Residuals for γ Dra

Wavelength (μm)	Data 10^{-14} Wcm^{-2} μ^{-1}	Fit 10^{-14} Wcm^{-2} μ^{-1}	Residuals (%)
2.20	14.4 ±3.6%	13.58	+6.2
2.22	13.5 ±3.4%	13.18	+2.4
3.54	2.55 ±3.6%	2.539	+0.4
3.76	2.033 ±3.7%	2.035	–0.1
10.6	0.0373 ±3.8%	0.03835	–2.7
10.6	0.0381 ±7%	0.03835	–0.7
11.34	0.0291 ±8%	0.02940	–1
21.0	0.00257 +10%	0.002547	+0.9

$\chi^2 = 4$, reduced $\chi^2_\nu = 0.57$

Apparent 1ß random error = 2.6%

CO bands at 4.7 and 2.5 μm
Average profile scaled by $A_{co} = 0.22$

Beta Geminorum (Pollux)

Spectral Type: K0 III

T_{eff}: 4400 K

$$\phi(\lambda) = \frac{1.644 \times 10^{-11}}{\lambda^5 \left(\exp\left(\frac{4.431}{\lambda(1+18.06/\lambda)^{0.182}} \right) - 1 \right)}$$

Data, Fit, and Residuals for β Gem

Wavelength (μm)	Data 10^{-14} Wcm^{-2} μ^{-1}	Fit 10^{-14} Wcm^{-2} μ^{-1}	Residuals (%)
2.20	11.57 ±3.5%	11.24	+2.9
2.22	10.82 ±3.5%	10.89	–0.6
3.54	1.98 ±3.7%	2.023	–2.1
3.76	1.58 ±3.7%	1.616	–2.2
10.6	.0299 ±3%	0.02943	+1.6
10.6	.0305 ±7%	0.02943	+3.6
11.34	.0233 ±8%	0.02253	+3.4
21.0	.00195 ±10%	0.00194	+0.5

$\chi^2 = 2.1$, reduced $\chi^2_\nu = 0.30$

Apparent 1σ random error = 2.4%

CO bands at 4.7 and 2.5 μm
Strecker et al. [35]

Discrete Tabulation of CO Bands for Use in Integration Over Hands

β Gem CO band absorption at 2.5 μm

λ (μm)	1 – CO	λ (μm)	1-CO
2.22	0.990	2.74	0.967
2.26	0.982	2.78	0.975
2.28	0.977	2.82	0.981
2.30	0.966	2.86	0.983
2.32	0.958	2.90	0.980
2.34	0.954	2.94	0.983
2.36	0.937	2.98	0.981
2.38	0.930	3.02	0.986
2.40	0.933	3.06	0.985
2.42	0.929	3.10	0.988
2.44	0.933	3.14	0.994
2.46	0.937	3.18	0.991
2.48	0.942	3.22	0.992
2.50	0.941	3.26	0.987
2.52	0.934	3.30	0.994
2.54	0.938	3.34	0.995
2.56	0.945	3.38	0.997
2.58	0.948	3.42	0.997
2.60	0.951	3.46	0.995
2.62	0.954	3.50	1.00
2.64	0.956	3.54	0.997
2.66	0.957	3.58	1.00
2.68	0.958	3.62	1.00
2.70	0.958	3.66	

α Gem CO band absorption at 5 μm

3.90	1.00	6.4	0.977
4.0	0.985	6.5	0.980
4.1	0.950	6.6	0.982
4.2	0.930	6.7	0.984
4.3	0.905	6.8	0.988
4.4	0.890	6.9	0.989
4.5	0.883	7.0	0.991
4.6	0.864	7.1	0.995
4.7	0.870	7.2	0.995
4.8	0.888	7.3	0.998
4.9	0.898	7.4	0.998
5.0	0.890	7.5	0.999
5.1	0.892	7.6	0.999
5.2	0.917	7.7	1.00
5.3	0.927	7.8	1.00
5.4	0.928	8.0	
5.5	0.945	8.2	
5.6	0.939	8.4	
5.7	0.949	8.6	
5.8	0.957	8.8	
5.9	0.963	9.0	
6.0	0.965	9.2	
6.1	0.968	9.4	
6.2	0.972	9.6	
6.3	0.974	9.8	

See Figure B-6.

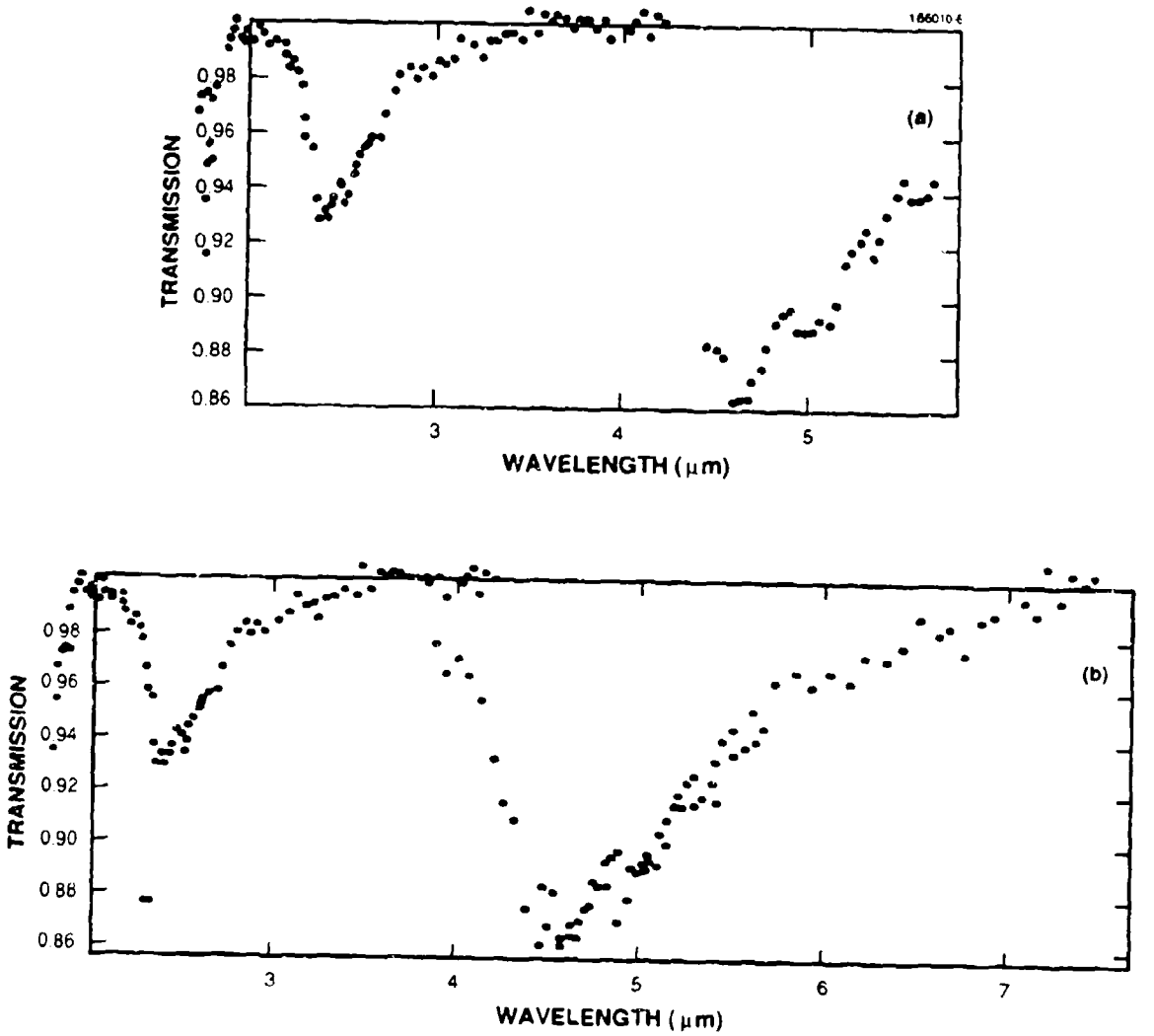

Figure B-6. Beta Geminorum CO bands: (a) Strecker et al. data and (b) same data and extension based on affine transformation of 2.2- to 3.5-μm region.

Eta Geminorum (Propus)

Spectral Type: M3 III

T_{eff}: 3410 K

$$\phi(\lambda) = \frac{3.359 \times 10^{-11}}{\lambda^5 \left(\exp\left(\frac{5.717}{\lambda(1 + 23.30/\lambda)^{0.182}} \right) - 1 \right)}$$

Data, Fit, and Residuals for η Gem

Wavelength (μm)	Data 10^{-14} $Wcm^{-2}\,\mu^{-1}$	Fit 10^{-14} $Wcm^{-2}\,\mu^{-1}$	Residuals (%)
2.20	14.3 ±6%	15.23	–6.1
2.22	13.4 ±5.8%	14.78	–9.3
3.54	2.97 ±4.4%	2.939	+1.1
3.76	2.37 ±4.5%	2.363	+0.3
10.6	0.0461 ±4%	0.04586	+0.5
10.6	0.0471 ±7%	0.04586	+2.7
11.34	0.0360 ±8%	0.03519	+2.3
21.0	0.00322 ±10.5%	0.003065	+5.1

$\chi^2 = 4.2$, reduced $\chi^2_\nu = 0.59$

Apparent 1β random error = 4.5%

CO bands at 4.7 and 2.5 μm

Average profile scaled by $A_{CO} = 0.30$

Muu Geminorum (Tejat Posterior)

Spectral Type: M3 III

T_{eff}: 3410 K

$$\phi(\lambda) = \frac{5.217 \times 10^{-11}}{\lambda^5 \left(\exp\left(\frac{5.717}{\lambda (1 + 23.30/\lambda)^{0.182}} \right) - 1 \right)}$$

Data, Fit, and Residuals for μ Gem

Wavelength (μm)	Data 10^{-14} $Wcm^{-2}\,\mu^{-1}$	Fit 10^{-14} $Wcm^{-2}\,\mu^{-1}$	Residuals (%)
2.20	24.6 ±3.8%	23.65	+4.0
2.22	22.98 ±3.6%	22.96	+0.1
3.54	4.34 ±4.5%	4.564	–4.9
3.76	3.46 ±4.5%	3.670	–5.7
10.6	0.0690 ±7%	0.07123	–3.1
10.6	0.0705 ±9%	0.07123	–1.0
11.34	0.0538 ±10%	0.05465	–1.6
21.0	0.00496 ±10%	0.004761	+4.2

$\chi^2 = 4.3$, reduced $\chi^2_\nu = 0.62$

Apparent 1σ random error = 3.6%

CO bands at 4.7 and 2.5 μm

Average profile scaled by $A_{CO} = 0.30$

Beta Gruis

Spectral Type: M3 II

T_{eff}: 3410 K

$$\phi(\lambda) = \frac{1.756 \times 10^{-10}}{\lambda^5 \left(\exp\left(\frac{5.717}{\lambda(1+23.30/\lambda)^{0.182}} \right) - 1 \right)}$$

Data, Fit, and Residuals for β Gru

Wavelength (μm)	Data 10^{-14} $Wcm^{-2}\ \mu^{-1}$	Fit 10^{-14} $Wcm^{-2}\ \mu^{-1}$	Residuals (%)
2.20	82.6 ±3.8%	79.60	+3.8
2.22	77.2 ±3.6%	77.26	–0.1
3.54	15.34 ±3.9%	15.36	–0.1
3.76	12.24 ±3.9%	12.35	–0.9
10.6	0.234 ±4%	0.2400	–2.5
10.6	0.239 ±7%	0.2400	–0.4
11.34	0.0183 ±8%	0.1839	–0.5
21.0	0.0162 ±10%	0.01602	+1.1

$\chi^2 = 1.5$, reduced $\chi^2_\nu = 0.21$

Apparent 1σ random error = 1.7%

CO bands at 4.7 and 2.5 μm
Average profile scaled by $A_{CO} = 0.30$

Alpha Herculis

Spectral Type: M5 I - II

T_{eff}: 3000 K

Variable with Circumstellar Dust

$$\phi(\lambda) = \frac{3.097 \times 10^{-10}}{\lambda^5 \left(\exp\left(\frac{6.72}{\lambda(1+27.4/\lambda)^{0.182}} \right) - 1 \right)}$$

Data, Fit, and Residuals for α Her

Wavelength (μm)	Data 10^{-14} $Wcm^{-2}\ \mu^{-1}$	Fit 10^{-14} $Wcm^{-2}\ \mu^{-1}$	Residuals (%)
2.20	106 ±3.8%	105.2	+0.8
2.22	99.4 ±3.9%	102.2	–2.7
3.54	21.3 ±3.7%	21.45	–0.7
3.76	17.0 ±3.7%	17.34	–2.0
10.6	0.362 ±3.9%	0.3542	+2.2
10.6	0.370 ±7%	0.3542	+4.5
11.34	0.283 ±8%	0.2723	+3.9
21.0	0.0295 ±10%	0.02395	+23.2*

* α Her shows excess emission from circumstellar material in the vicinity of 20 μm. (Do not use fit values above 12 μm.)

Excluding the 21-μm point:
$\chi^2 = 1.8$, reduced $\chi^2_\nu = 0.3$

Apparent 1σ random error = 2.7%

CO bands at 4.7 and 2.5 μm
Average profile scaled by $A_{co} = 0.32$

Alpha Hydrae (Alphard)

Spectral Type: K4 III

T_{eff}: 3900 K

$$\phi(\lambda) = \frac{2.233 \times 10^{-11}}{\lambda^5 \left(\exp\left(\frac{5.001}{\lambda(1+20.37/\lambda)^{0.182}} \right) - 1 \right)}$$

Data, Fit, and Residuals for α Hya

Wavelength (μm)	Data 10^{-14} Wcm^{-2} μ^{-1}	Fit 10^{-14} Wcm^{-2} μ^{-1}	Residuals (%)
2.20	13.0 ±3.3%	12.65	+2.8
2.22	12.2 ±3.2%	12.27	–0.6
3.54	2.31 ±3.6%	2.347	–1.6
3.76	1.84 ±3.7%	1.880	–2.1
10.6	0.0355 ±4.6%	0.03520	+0.9
10.6	0.0374 ±8%	0.03520	+6.3
11.34	0.0285 ±9%	0.02698	+5.6
21.0	0.00229 ±10%	0.002335	–1.9

$\chi^2 = 2.4$, reduced $\chi^2_\nu = 0.34$

Apparent 1σ random error = 3.4%

CO bands at 4.7 and 2.5 μm
Average profile scaled by $A_{CO} = 0.20$

Sigma Librae (Brachium)

Spectral Type: M4 III

T_{eff}: 3310 K

$$\phi(\lambda) = \frac{3.525 \times 10^{-11}}{\lambda^5 \left(\exp\left(\frac{5.890}{\lambda(1+24.00/\lambda)^{0.182}} \right) - 1 \right)}$$

Data, Fit, and Residuals for σ Lib

Wavelength (μm)	Data 10^{-14} $Wcm^{-2}\,\mu^{-1}$	Fit 10^{-14} $Wcm^{-2}\,\mu^{-1}$	Residuals (%)
2.20	15.7 ±3.8%	15.18	+3.4
2.22	14.7 ±3.6%	14.74	–0.3
3.54	2.93 ±3.7%	2.958	–0.9
3.76	2.33 ±3.9%	2.381	–2.1
10.6	0.0492 ±4.6%	0.04660	+5.6
10.6	0.0502 ±8%	0.04660	+7.7
11.34	0.0384 ±9%	0.03577	+7.4
21.0	0.00293 ±10%	0.003121	–6.1

$\chi^2 = 4.6$, reduced $\chi^2_\nu = 0.66$

Apparent 1σ random error = 5%

CO bands at 4.7 and 2.5 μm
Average profile scaled by $A_{co} = 0.32$

Alpha Lyrae (Vega)

Spectral Type: A0 V

T_{eff}: 9600K

t: 5881 K

$$\phi(\lambda) = \frac{3.952 \times 10^{-12}}{\lambda^5 \left(\exp\left(\frac{3.315}{\lambda(1+13.51/\lambda)^{0.182}} \right) - 1 \right)}$$

Data, Fit, and Residuals for α Lyr

Wavelength (μm)	Data 10^{-14} $Wcm^{-2}\ \mu^{-1}$	Fit 10^{-14} $Wcm^{-2}\ \mu^{-1}$	Residuals (%)
2.20	30.6 ±3.8%	30.00	+2
1.60	12.36 ±3%	12.72	−2.8
2.20	4.19 ±3%	4.10	+2.2
2.22	3.92 ±3.5%	3.97	−1.3
3.54	0.682 ±3.5%	0.696	−2.0
3.76	0.544 ±3%	0.553	−1.6
4.80	0.219 ±5%	0.216	+1.4
10.6	0.00965 ±3.5%	0.00956	+0.9
10.6	0.00986 ±7%	0.00956	+3.1
11.34	0.00753 ±8%	0.00731	+3.0
21.0	0.000773 ±10%	0.000624	+24 *

* α Lyr shows excess emission from surrounding dust at 20 μm and above. (Do not use fit values beyond 12 μm.)

Excluding the 21-μm point, $\chi^2 = 3.1$, reduced $\chi^2_\nu = 0.39$

Apparent 1σ random error = 2.2%

No CO bands

Alpha Orionis (Betelgeuse)

Spectral Type: M2 I

Variable with Circumstellar Dust

Below 8 μm,

$$\phi(\lambda) = \frac{5.207 \times 10^{-10}}{\lambda^5 \left(\exp\left(\frac{5.73}{\lambda(1 + 23.37/\lambda)^{0.182}} \right) - 1 \right)}$$

8- to 14-μm portion of a Ori spectrum

λ	Log(ϕ)	λ	Log(ϕ)
8.0	−13.673	10.00	−13.727
8.1	−13.695	10.25	−13.780
8.2	−13.706	10.50	−13.821
8.3	−13.724	10.75	−13.861
8.4	−13.739	11.00	−13.902
8.5	−13.751	11.25	−13.942
8.6	−13.761	11.50	−13.983
8.7	−13.765	11.75	−14.023
8.8	−13.761	12.00	−14.064
8.9	−13.768	12.25	−14.104
9.0	−13.761	12.50	−14.145
9.1	−13.761	12.75	−14.185
9.2	−13.761	13.00	−14.225
9.3	−13.761	13.25	−14.266
9.4	−13.753	13.50	−14.306
9.5	−13.748	13.75	−14.347
9.6	−13.732	14.00	−14.387
9.7	−13.717		

$A_{v} = 0.35$

16- to 32-μm portion of α Ori specrum

		21.50	−14.962	27.25	−15.368
16.00	−14.688	21.75	−14.980	27.50	−15.383
16.25	−14.671	22.00	−14.999	27.75	−15.402
16.50	−14.670	22.25	−15.019	28.00	−15.421
16.75	−14.670	22.50	−15.039	28.25	−15.440
17.00	−14.670	22.75	−15.063	28.50	−15.459
17.25	−14.671	23.00	−15.087	28.75	−15.473
17.50	−14.686	23.25	−15.101	29.00	−15.487
17.75	−14.682	23.50	−15.115	29.25	−15.505
18.00	−14.686	23.75	−15.137	29.50	−15.523
18.25	−14.713	24.00	−15.159	29.75	−15.538
18.50	−14.724	24.25	−15.175	30.00	−15.552
18.75	−14.754	24.50	−15.192	30.25	−15.572
19.00	−14.762	24.75	−15.211	30.50	−15.592
19.25	−14.781	25.00	−15.230	30.75	−15.607
19.50	−14.800	25.25	−15.244	31.00	−15.621
19.75	−14.816	25.50	−15.258	31.25	−15.640
20.00	−14.833	25.75	−15.273	31.50	−15.659
20.25	−14.855	26.00	−15.287	31.75	−15.678
20.50	−14.877	26.25	−15.306	32.00	−15.697
20.75	−14.896	26.50	−15.325		
21.00	−14.915	26.75	−15.339		
21.25	−14.938	27.00	−15.354		

See Figure B-7.

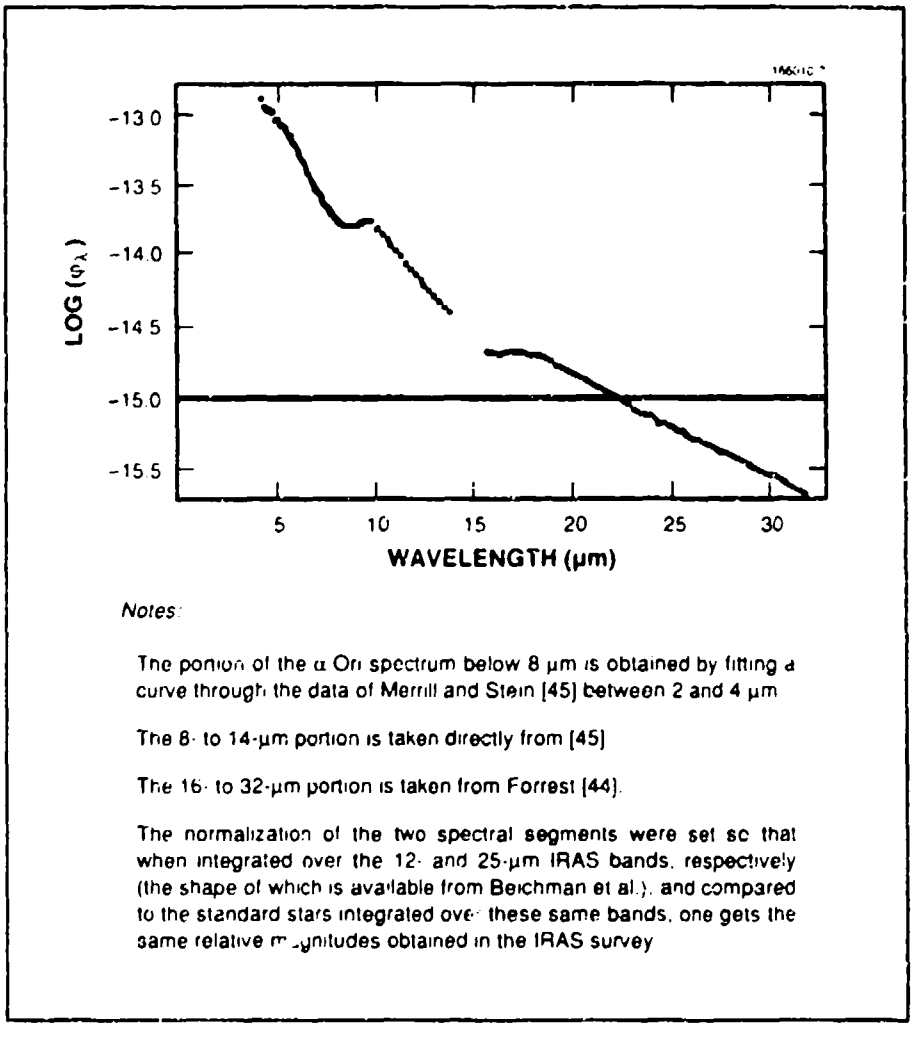

Notes:

The portion of the α Ori spectrum below 8 μm is obtained by fitting a curve through the data of Merrill and Stein [45] between 2 and 4 μm

The 8- to 14-μm portion is taken directly from [45]

The 16- to 32-μm portion is taken from Forrest [44].

The normalization of the two spectral segments were set so that when integrated over the 12- and 25-μm IRAS bands, respectively (the shape of which is available from Beichman et al.), and compared to the standard stars integrated over these same bands, one gets the same relative magnitudes obtained in the IRAS survey

Figure B-7. Spectrum of Alpha Orionis (Betelgeuse), M2-I supergiant with circumstellar dust.

Beta Pegasi (Scheat)

Spectral Type: M2.5 II to III

T_{eff}: 3470 K

$$\phi(\lambda) = \frac{6.933 \times 10^{-11}}{\lambda^5 \left(\exp\left(\frac{5.618}{\lambda(1 + 22.9/\lambda)^{0.182}} \right) - 1 \right)}$$

Data, Fit, and Residuals for β Peg

Wavelength (μm)	Data 10^{-14} $Wcm^{-2}\,\mu^{-1}$	Fit 10^{-14} $Wcm^{-2}\,\mu^{-1}$	Residuals (%)
2.20	32.90 ±3.5%	32.38	+1.6
2.22	30.76 ±3.5%	31.43	−2.1
3.54	6.112 ±3.9%	6.215	−1.7
3.76	4.875 ±4%	4.995	−2.4
10.6	0.09510 ±3.8%	0.0965	−1.5
10.6	0.1005 ±7%	0.0965	+4.1
11.34	0.0742 ±8%	0.0740	+0.3
21.0	0.00687 ±10%	0.00644	+6.7

$\chi^2 = 2.1$, reduced $\chi^2_\nu = 0.30$

Apparent 1σ random error = 3.2%

CO bands at 4.7 and 2.5 μm

Strecker et al. [35]

Discrete Tabulation of CO Bands for Use in Integration Over Bands

β Peg CO band absorption at 2.5 μm

λ (μm)	1 – CO	λ (μm)	1 – CO	λ (μm)	1 – CO
2.20	0.998	2.68	0.779	3.62	0.994
2.22	0.994	2.70	0.787	3.66	0.994
2.24	0.989	2.74	0.800	3.70	0.996
2.26	0.975	2.78	0.816	3.74	0.999
2.28	0.953	2.82	0.831	3.78	0.999
2.30	0.897	2.86	0.844	3.82	1.00
2.32	0.862	2.90	0.864		
2.34	0.828	2.94	0.883		
2.36	0.798	2.98	0.893		
2.38	0.786	3.02	0.906		
2.40	0.776	3.06	0.918		
2.42	0.764	3.10	0.922		
2.44	0.764	3.14	0.934		
2.46	0.759	3.18	0.938		
2.48	0.758	3.22	0.946		
2.50	0.755	3.26	0.953		
2.52	0.752	3.30	0.958		
2.54	0.758	3.34	0.963		
2.56	0.763	3.38	0.962		
2.58	0.768	3.42	0.974		
2.60	0.767	3.46	0.976		
2.62	0.771	3.5	0.983		
2.64	0.774	3.54	0.985		
2.66	0.777	3.58	0.989		

β Peg CO band absorption at 5 μm

3.90	0.996	6.4	0.909
4.0	0.982	6.5	0.917
4.1	0.938	6.6	0.930
4.2	0.892	6.7	0.937
4.3	0.822	6.8	0.946
4.4	0.774	6.9	0.952
4.5	0.727	7.0	0.956
4.6	0.714	7.1	0.971
4.7	0.716	7.2	0.975
4.8	0.720	7.3	0.983
4.9	0.723	7.4	0.988
5.0	0.716	7.5	0.993
5.1	0.721	7.6	1.00
5.2	0.734	7.7	
5.3	0.752		
5.4	0.773		
5.5	0.781		
5.6	0.791		
5.7	0.798		
5.8	0.809		
5.9	0.830		
6.0	0.852		
6.1	0.870		
6.2	0.883		
6.3	0.898		

See Figure B-8.

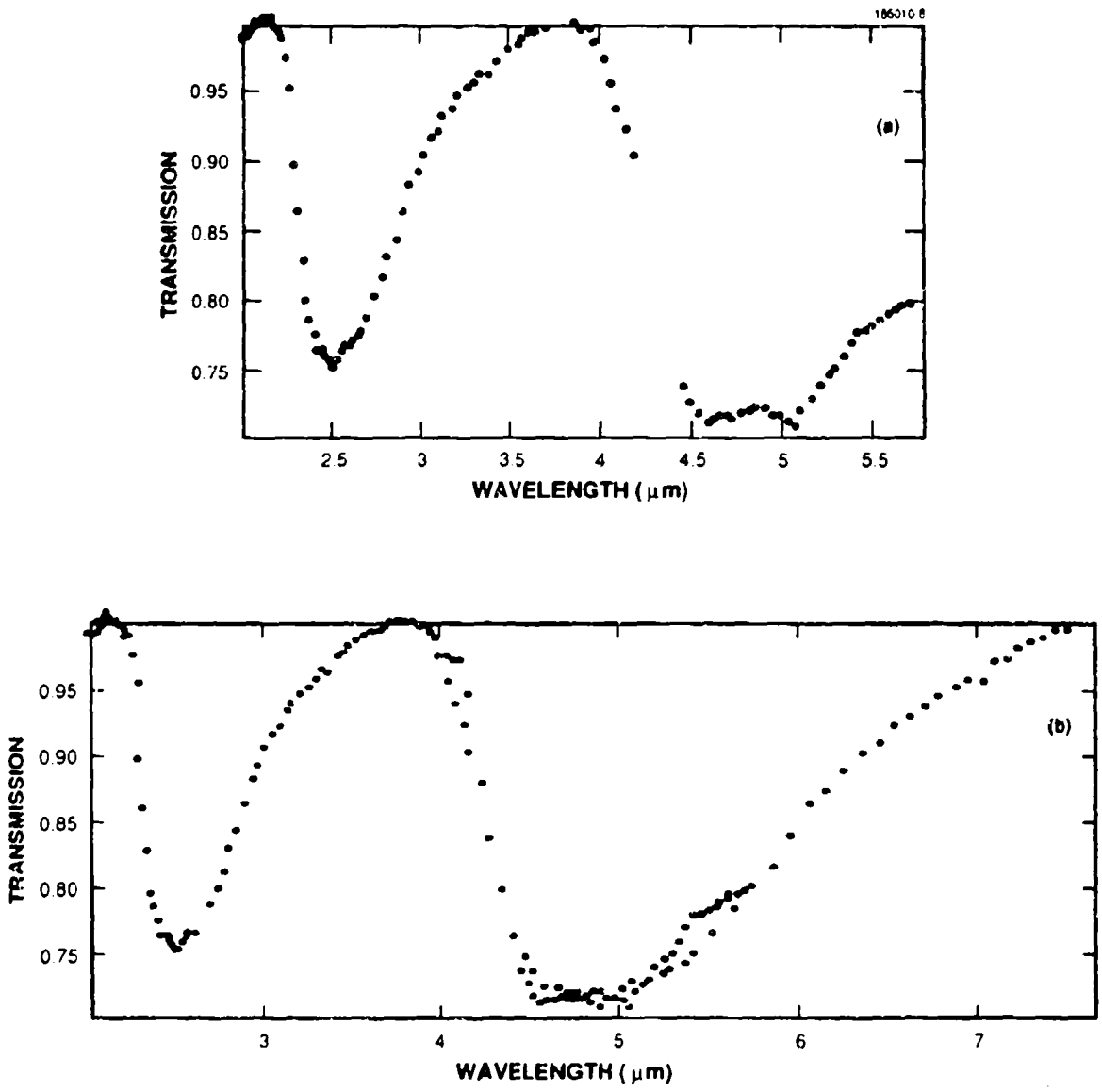

Figure B-8. Beta Pegasi CO bands: (a) Strecker et al. data and (b) same data and extension based on affine transformation of 2.2- to 3.5-μm region.

Rho Persei

Spectral Type: M4 II - III

T_{eff}: 3310 K

$$\phi(\lambda) = \frac{5.812 \times 10^{-11}}{\lambda^5 \left(\exp\left(\frac{5.890}{\lambda (1 + 24.0/\lambda)^{0.182}} \right) - 1 \right)}$$

Data, Fit, and Residuals for ρ Per

Wavelength (μm)	Data 10^{-14} $Wcm^{-2}\ \mu^{-1}$	Fit 10^{-14} $Wcm^{-2}\ \mu^{-1}$	Residuals (%)
2.20	32.90 ±3.5%	32.38	+1.6
2.22	23.7 ±3.6%	24.31	−2.5
3.54	4.74 ±4%	4.877	−2.8
3.76	3.78 ±4%	3.925	−3.7
10.6	0.0742 ±5%	0.07684	−3.4
10.6	0.0758 ±8%	0.07684	−1.4
11.34	0.0579 ±9%	0.05898	−1.8
21.0	0.00547 ±10%	0.005146	+6.3

$\chi^2 = 2.8$, reduced $\chi^2_\nu = 0.40$

Apparent 1σ random error = 3.3%

CO bands at 4.7 and 2.5 μm

Average profile scaled by $A_{CO} = 0.32$

Alpha Scorpii (Antares)

Spectral Type: M1 I

Variable with Circumstellar Dust

Below 6.9 μm,

$$\phi(\lambda) = \frac{3.66 \times 10^{-10}}{\lambda^5 \left(\exp\left(\frac{5.31}{\lambda(1 + 21.65/\lambda)^{0.182}} \right) - 1 \right)}$$

6.9- to 14-μm portion of α Sco spectrum

λ	Log(ϕ)	λ	Log(ϕ)	λ	Log(ϕ)
6.9	−13.573	9.3	−13.916		
7.0	−13.594	9.4	−13.911		
7.1	−13.613	9.5	−13.910		
7.2	−13.637	9.6	−13.900		
7.3	−13.652	9.7	−13.890		
7.4	−13.673				
7.5	−13.692	10.00	−13.906		
7.6	−13.712	10.25	−13.958		
7.7	−13.733	10.50	−13.998		
7.8	−13.754	10.75	−14.039		
7.9	−13.775	11.00	−14.079		
8.0	−13.796	11.25	−14.119		
8.1	−13.815	11.50	−14.159		
8.2	−13.829	11.75	−14.199		
8.3	−13.848	12.00	−14.239		
8.4	−13.863	12.25	−14.278		
8.5	−13.878	12.50	−14.319		
8.6	−13.889	12.75	−14.358		
8.7	−13.896	13.00	−14.397		
8.8	−13.897	13.25	−14.436		
8.9	−13.907	13.50	−14.475		
9.0	−13.905	13.75	−14.515		
9.1	−13.908	14.00	−14.553		
9.2	−13.912				

A_v = 0.30

16 - to 32-μm portion of α Sco spectrum

		21.50	−15.350	27.25	−15.759
16.00	−14.882	21.75	−15.369	27.50	−15.774
16.25	−14.904	22.00	−15.388	27.75	−15.791
16.50	−14.928	22.25	−15.408	28.00	−15.808
16.75	−14.974	22.50	−15.428	28.25	−15.825
17.00	−14.990	22.75	−15.449	28.50	−15.842
17.25	−15.014	23.00	−15.470	28.75	−15.857
17.50	−15.027	23.25	−15.487	29.00	−15.872
17.75	−15.040	23.50	−15.504	29.25	−15.888
18.00	−15.056	23.75	−15.524	29.50	−15.904
18.25	−15.081	24.00	−15.543	29.75	−15.921
18.50	−15.099	24.25	−15.560	30.00	−15.933
18.75	−15.125	24.50	−15.578	30.25	−15.950
19.00	−15.142	24.75	−15.596	30.50	−15.967
19.25	−15.163	25.00	−15.614	30.75	−13.981
19.50	−15.184	25.25	−15.630	31.00	−15.995
19.75	−15.203	25.50	−15.646	31.25	−16.011
20.00	−15.223	25.75	−15.662	31.50	−16.027
20.25	−15.245	26.00	−15.677	31.75	−16.043
20.50	−15.266	26.25	−15.695	32.00	−16.060
20.75	−15.286	26.50	−15.713		
21.00	−15.306	26.75	−15.728		
21.25	−15.328	27.00	−15.744		

See Figure B-9.

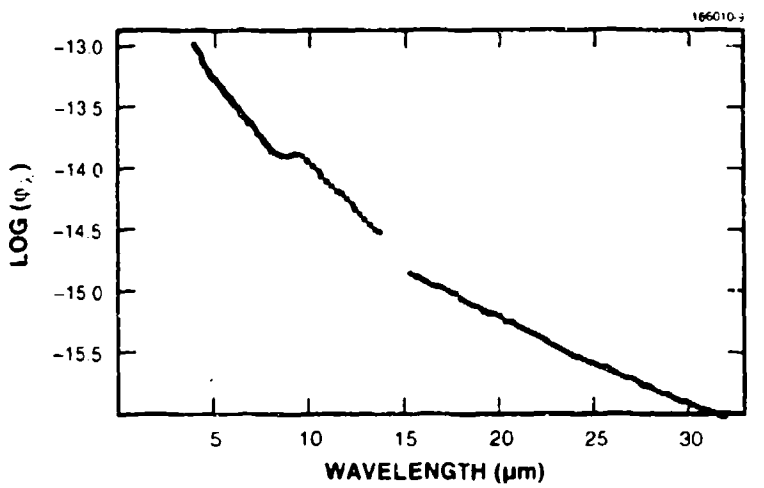

Notes:

The 8- to 14-μm portion of the spectrum was taken from Merrill and Stein [45].

The portion below 8 μm was estimated using a smooth spectral curve of the type used for stars with no circumstellar dust.

The portion beyond 15 μm was estimated by adding an excess with the same distribution as that observed in α Ori to the assumed underlying spectral curve. The amount of excess was chosen to give the correct IRAS magnitudes for α Sco.

Figure B-9. Spectrum of Alpha Scorpii (Antares), M1-I supergiant with circumstellar dust.

Alpha Tauri (Aldebaran)

Spectral Type: K5 III

T_{eff}: 3800 K

$$\phi(\lambda) = \frac{1.025 \times 10^{-10}}{\lambda^5 \left(\exp\left(\frac{5.131}{\lambda(1 + 20.9/\lambda)^{0.182}} \right) - 1 \right)}$$

Data, Fit, and Residuals for α Tau

Wavelength (μm)	Data 10^{-14} $Wcm^{-2}\,\mu^{-1}$	Fit 10^{-14} $Wcm^{-2}\,\mu^{-1}$	Residuals (%)
2.20	56.70 ±3.2%	55.66	+2.0
2.22	53.30 ±3.2%	53.98	−1.3
3.54	10.34 ±3.5%	10.40	−0.6
3.76	8.245 ±3.5%	8.339	−1.1
10.6	0.1567 ±3%	0.1571	−0.3
10.6	0.1601 ±7%	0.1571	+1.9
11.34	0.1223 ±8%	0.1205	+1.5
21.0	0.01068 ±10%	0.01044	+2.3

$\chi^2 = 0.9$, reduced $\chi^2_\nu = 0.12$

Apparent 1σ random error = 1.5%

CO bands at 4.7 and 2.5 μm
Strecker et al. [35]

Discrete Tabulation of CO Bands for Use in Integration Over Bands

α Tau CO band absorption at 2.5 μm

λ (μm)	1 – CO	λ (μm)	1 – CO
2.26	0.995	2.74	0.914
2.28	0.995	2.78	0.933
2.30	0.915	2.82	0.942
2.32	0.870	2.86	0.950
2.34	0.842	2.90	0.963
2.36	0.816	2.94	0.971
2.38	0.805	2.98	0.975
2.40	0.803	3.02	0.983
2.42	0.802	3.06	0.982
2.44	0.806	3.10	0.985
2.46	0.807	3.14	0.984
2.48	0.809	3.18	0.987
2.50	0.816	3.22	0.987
2.52	0.819	3.26	0.992
2.54	0.825	3.30	0.995
2.56	0.833	3.34	0.995
2.58	0.844	3.38	0.993
2.60	0.852	3.42	0.995
2.62	0.862	3.46	0.996
2.64	0.873	3.5	1.00
2.66	0.879		
2.68	0.886		
2.70	0.895		

α Tau CO band absorption at 5 μm

3.90	1.00	6.4	0.914
4.0	0.987	6.5	0.920
4.1	0.953	6.6	0.930
4.2	0.886	6.7	0.938
4.3	0.820	6.8	0.941
4.4	0.763	6.9	0.949
4.5	0.727	7.0	0.954
4.6	0.730	7.1	0.958
4.7	0.746	7.2	0.966
4.8	0.746	7.3	0.971
4.9	0.743	7.4	0.973
5.0	0.744	7.5	0.976
5.1	0.747	7.6	0.978
5.2	0.758	7.7	0.980
5.3	0.775	7.8	0.980
5.4	0.792	8.0	0.982
5.5	0.808	8.2	0.985
5.6	0.825	8.4	0.985
5.7	0.822	8.6	0.989
5.8	0.831	8.8	0.989
5.9	0.848	9.0	0.994
6.0	0.863	9.2	0.995
6.1	0.875	9.4	0.997
6.2	0.892	9.6	0.998
6.3	0.900	9.8	0.999

See Figure B-10.

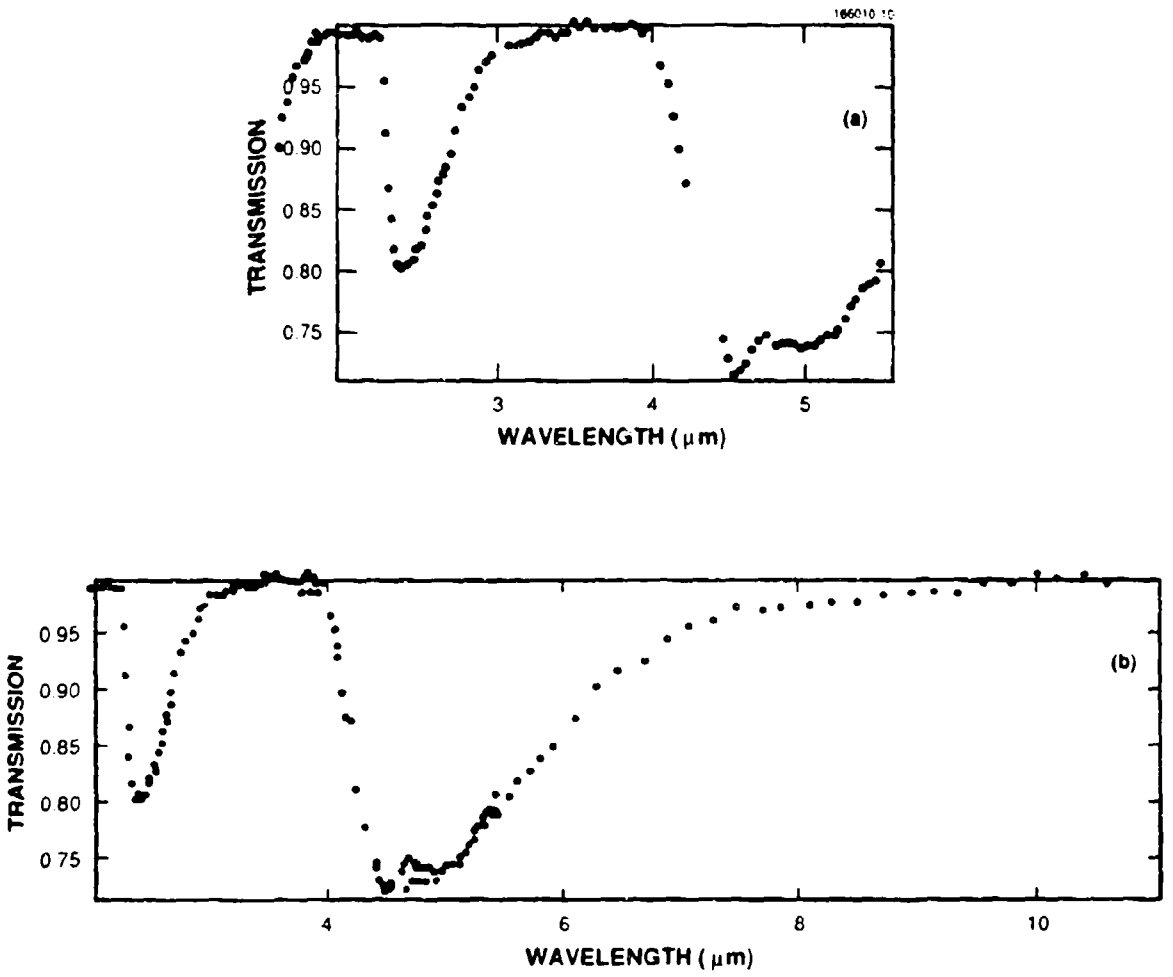

Figure B-10. Alpha Tauri CO bands: (a) Strecker et al. data on α Tau CO bands and (b) same data with postulated extension beyond 5.5 μm based on affine transformation of 2.5-μm band.

Muu Ursa Majoris

Spectral Type: M0 III

T_{eff}: 3730 K

$$\phi(\lambda) = \frac{1.720 \times 10^{-11}}{\lambda^5 \left(\exp\left(\frac{5.226}{\lambda (1 + 21.30/\lambda)^{0.182}} \right) - 1 \right)}$$

Data, Fit, and Residuals for μ Uma

Wavelength (μm)	Data 10^{-14} $Wcm^{-2}\,\mu^{-1}$	Fit 10^{-14} $Wcm^{-2}\,\mu^{-1}$	Residuals (%)
2.20	9.21 ±3.8%	9.062	+1.6
2.22	8.61 ± 3.6%	8.790	−2.0
3.54	1.676 ± 3.6%	1.703	−1.6
3.76	1.336 ± 3.7%	1.366	−2.2
10.6	0.0247 ±4.6%	0.02586	−4.4
10.6	0.0252 ±7.6%	0.02586	−2.6
11.34	0.01925 ±8.5%	0.01982	−2.9
21.0	0.001719 ±10%	0.001719	0.0

$\chi^2 = 2.2$, reduced $\chi^2_\nu = 0.31$

Apparent 1σ random error = 2.5%

CO bands at 4.7 and 2.5 μm
Average profile scaled by 0.24

Delta Virginis (Auva)

Spectral Type: M3 III

T_{eff}: 3410 K

$$\phi(\lambda) = \frac{2.811 \times 10^{-11}}{\lambda^5 \left(\exp\left(\frac{5.717}{\lambda(1 + 23.30/\lambda)^{0.182}} \right) - 1 \right)}$$

Data, Fit, and Residuals for δ Vir

Wavelength (μm)	Data 10^{-14} $Wcm^{-2}\,\mu^{-1}$	Fit 10^{-14} $Wcm^{-2}\,\mu^{-1}$	Residuals (%)
2.20	13.27 ±3.6%	12.74	+4.2
2.22	12.41 ±3.4%	12.37	+0.3
3.54	2.41 ±3.9%	2.459	−2.0
3.76	1.920 ±3.9%	1.978	−2.9
10.6	0.03927 ±5%	0.03838	+2.3
10.6	0.0401 ±8%	0.03838	+4.5
11.34	0.0306 ±9%	0.02945	+3.9
21.0	0.00276 ±10	0.002565	+7.6

$\chi^2 = 3.5$, reduced $\chi^2_\nu = 0.50$

Apparent 1σ random error = 4%

CO bands at 4.7 and 2.5 μm
Average profile scaled by $A_{CO} = 0.30$

REFERENCES

1. J.E. Vernazza, E.H. Avrett, and R. Loesser "Structure of the solar chromosphere. II. The underlying photosphere and temperature-minimum region," *Astrophys. J.* Suppl. **30,** 1 (1976).

2. C.A. Beichman, G. Neugebauer, H.J. Habing, P.E. Clegg, and T.J. Chester, *IRAS Explanatory Supplement*, Section VI, National Aeronautics and Space Administration, Washington, D.C. (1988).

3. C. Campins, G.H. Rieke, and M.J. Lebofsky, "Absolute calibration of photometry at 1 through 5 μm," *Astron. J.* **90** 896 (1985).

4. G.H. Rieke, M.J. Lebofsky, and F.J. Low, "An absolute photometric system at 10 and 20 μm." *Astron J.* **90,** 900 (1985).

5. D. Chambers and W. Bagnuolo, Aerospace Corp., private communication (1983).

6. G.H. Rieke, private communication (1988).

7. D. Engels, W.A. Sherwood, W. Wamsteker and G.V. Schultz, "Infrared observations of southern bright stars," *Astron. Astrophys.* **45,** 5 (1981).

8. J.A. Thomas, A.R. Hyland, G. Robinson, "Southern infrared standards and the absolute calibration of infrared photometry," *Mon. Not. R. Astr. Soc.* **165,** 201 (1973).

9. J.A. Frogel, S.E. Persson, M. Aaronson, and K. Mathews, "Photometry of composite stellar systems," *Astrophys. J.* **220,** 96 (1978).

10. H.L. Johnson, R.I. Mitchell, B. Iriarte, and W.Z. Wisniewiski, *Communications of the Lunar and Planetary Laboratory*, "Communications No. 63 UBVRIJKL, Photometry of the Bright Stars" Vol. 4, Part 3, Tucson: University of Arizona Press (1966).

11. J. Bergeat and M. Lunel, "IJHKL: Photometry of carbon stars," *Astron. Astrophys* **87,** 139 (1980).

12. R.D. Gehrz and N.J. Woolf, "Mass loss from M stars," *Astrophys. J.* **165,** 285 (1971).

13. R.D. Gehrz, "Infrared radiation from RV Tauri stars. I. An infrared survey of RV Tauri stars and related objects," *Astrophys. J.* **178,** 715 (1972).

14. R.D. Gehrz, J.A. Hackwell, and T.W. Jones, "Infrared observations of B stars from 2.3 to 19.5 microns," *Astrophys. J.* **191,** 675 (1974).

15. P. Persi, M. Ferrari-Toniolo, G. Spada, G. Conti, P. Di Benedetto, E.G. Tanzi, and M. Tarenghi, "Near-infrared photometry of HDE 245770 (A0535+26)," *Mon. Not. R. Astr. Soc.* **187,** 293 (1979).

16. F.J. Low and G.H. Rieke, in *Methods of Experimental Physics*, Vol. 12, Part A, N.Carleton (ed.) New York: Academic Press (1974), p. 456.

17. W.M. Sinton and W.C. Tittemore, "Photometric standard stars for L- and M-filter bands," *Astron. J.* **89**, 1366 (1984).

18. F.C. Gillet, K.M. Merril, and W.A. Stein, "Observations of infrared radiation from cool stars," *Astrophys. J.* **164**, 83 (1971).

19. A.T. Tokunaga, "A reevaluation of the 20-μm magnitude system," *Astron. J.* **89**, 172 (1984).

20. D. Morrison and T. Simon, "Broad-band 20-micron photometry of 76 stars," *Astrophys. J.* **186**, 193 (1973).

21. T. Simon, D. Morrison, and D.P. Cruikshank, "20-micron fluxes of bright stellar standards," *Astrophys. J.* **177**, L17 (1972).

22. K. Noguchi, K. Kwara, Y. Kobayashi, H. Okuda, and S. Sato, "Near-infrared photometry of carbon stars," *Publ. Astron. Soc. Japan* **33**, 373 (1981).

23. D.E. Blackwell, S.K. Leggett, A.D. Petford, C.M. Mountain, and M.J. Selby, "Absolute calibration of the infrared flux from Vega at 1.24, 2.20, 3.76, and 4.6 μm by comparison with a standard furnace," *Mon. Not. R. Astron. Soc.* **205**, 897 (1983).

24. S.C. Chase, J.L. Engel, H.W. Eyerly, H.H. Kieffer, F.D. Palluconi, and D. Schofield, "Viking infrared thermal mapper," *Appl. Opt.* **17**, 1243 (1978).

25. W.G. Mankin, in *The Solar Output and Its Variation*, O.R. White (ed.) Boulder: Colorado Associated University Press (1977), p. 151.

26. D.F. Carbon and O. Gingerich, in *Proc. Third Harvard-Smithsonian Conference on Stellar Atmospheres*, "The grid model of stellar atmospheres from 4000 K to 10,000 K," Cambridge, Mass.: MIT Press, (1969), p. 377.

27. H.R. Johnson, J.G. Collins, and B. Krupp, "The line blanketing and structure of the atmosphere of Arcturus," *Astrophys. J.* **212**, 760 (1977).

28. C.W. Allen, *Astrophysical Quantities*, 3rd ed., London: Athlone, (1973), pp. 99–102.

29. J.R. Baldwin, J.A. Frogel, and S.E. Persson, "The strengths of infrared CO and H_2O bands in late-type stars," *Astrophys. J.* **184**, 427 (1973).

30. A. Manduca, R.A. Bell, and B. Gustafsson, "The analysis of infrared fluxes of some late-type stars," *Astrophys. J.* **243**, 883 (1981).

31. P.R. Bevington, *Data Reduction and Error Analysis for the Physical Sciences*, New York: McGraw-Hill (1969), p. 314.

32. D.F. Gray, *Lectures on Spectral-Line Analysis: F, G, and K Stars*, Ontario: Aylmer Express Ltd. (1988), pp. B1-B4.

33. G.C. Augason, B.J. Taylor, D.W. Strecker, E.F. Erickson, and F.C. Witteborn, "Comparison of predicted and observed spectral energy distribution of K and M stars. I. Alpha Bootis," *Astrophys. J.* **235,** 138 (1980).

34. S.K. Leggett, "The flux distribution of Vega for 10 μm ≤ λ ≤ 100 μm, and the calibration of IRAS at 12 μm and 25 μm," *Astron. Astrophys.* **153,** 273 (1985).

35. D.W. Strecker, E.F. Erickson and F.C. Witteborn, "Airborne stellar spectro-photometry from 1.2 to 5.5 microns: Absolute calibration and spectra of stars earlier than M3," *Astron J. Suppl.* **41,** 501 (1979).

36. J.A. Hackwell and R.D. Gehrz, "Infrared photometry of high-luminosity supergiants earlier than M and the interstellar extinction law," *Astrophys. J.* **194,** 49 (1974).

37. R. Schild, D.M. Peterson, and J.B. Oke, "Effective temperature of B- and A-type stars," *Astrophys. J.* **166,** 95 (1971).

38. J.M. Saari and R.W. Shorthill, "The sunlit lunar surface: I. Albedo studies and fullmoon temperature distribution," Dordrecht-Holland: D. Reidel, *The Moon 5*, 179 (1972).

39. P.E. Johnson, J.C. Kemp, M.J. Lebofsky and G.H. Rieke, "10-μm polarimetry of Ceres" *Icarus* **56,** 387 (1983).

40. C.W. Engelke, private communication (1989).

41. L.B.F.M. Waters, J. Cote, and H.H. Aumann "IRAS far-infrared colours of normal stars," *Astron. Astrophys.* **172,** 225 (1987).

42. R.W. Russell, B T. Soifer, and W.J. Forrest, "Spectrophotometric observations of Mu Cephei and the Moon from 4 to 8 μm," *Astrophys. J.* **198,** L41 (1975).

43. F.H. Murkray, D.G. Murkray, and W.J. Williams, "Inrfared Emissivity of lunar surface features: 1. Balloon-borne observations," J. *Geophys. Res.* **75,** 2662 (1970).

44. W.J. Forrest, J.F. McCarthy, and J.R. Houck, "16-39 micron spectroscopy of oxygen-rich stars," *Astrophys. J.* **233,** 611 (1979).

45. K.M. Merrill and W.A. Stein, "2-14 μm stellar spectrophotometry I. Stars of the conventional spectral sequence," *Pub. Astron. Soc. Pac.* **88,** 285 (1976).

REPORT DOCUMENTATION PAGE

Form Approved
OMB No. 0704-0188

1. AGENCY USE ONLY (*Leave blank*)	2. REPORT DATE	3. REPORT TYPE AND DATES COVERED
	10 April 1991	Technical Report

4. TITLE AND SUBTITLE

LWIR Stellar Calibration: Infrared Spectral Curves for 30 Standard Stars

5. FUNDING NUMBERS

C — F19628-90-C-0002
PR — 34

6. AUTHOR(S)

Charles W. Engelke

7. PERFORMING ORGANIZATION NAME(S) AND ADDRESS(ES)

Lincoln Laboratory, MIT
P.O. Box 73
Lexington, MA 02173-9108

8. PERFORMING ORGANIZATION REPORT NUMBER

TR-908

9. SPONSORING/MONITORING AGENCY NAME(S) AND ADDRESS(ES)

USASDC/CSSD-SD-D
P.O. Box 1500
Huntsville, AL 35807-3801

10. SPONSORING/MONITORING AGENCY REPORT NUMBER

ESD-TR-90-143

11. SUPPLEMENTARY NOTES

None

12a. DISTRIBUTION/AVAILABILITY STATEMENT

Approved for public release; distribution is unlimited.

12b. DISTRIBUTION CODE

13. ABSTRACT (*Maximum 200 words*)

Best estimate spectral energy distributions are created for approximately 30 stars by fitting theoretically expected spectral curves to the available empirical flux data on the stars at a variety of wavelengths. The curves can be integrated over the band response profiles for a given sensor in order to produce broadband power predictions against which to calibrate.

14. SUBJECT TERMS

long wavelength infrared (LWIR) calibration
stellar spectral curves (infrared)
stellar spectral models (infrared)
infrared calibration
stellar calibration
stellar flux densities
stellar flux densities (infrared)
wideband calibration (infrared)
angular size of stars

15. NUMBER OF PAGES
134

16. PRICE CODE

17. SECURITY CLASSIFICATION OF REPORT	18. SECURITY CLASSIFICATION OF THIS PAGE	19. SECURITY CLASSIFICATION OF ABSTRACT	20. LIMITATION OF ABSTRACT
Unclassified	Unclassified	Unclassified	SAR